



A Novel strategy for controlling Forklift's Mast Vibration

BY
Siavash Esmaeili

Department of Mechanical, Aerospace and Civil Engineering College of Engineering,
Design and Physical Sciences

A Thesis submitted for the Degree of Doctor of Philosophy

August 2019

Abstract

Material handling lift trucks, most commonly known as forklift trucks, have enhanced significantly both in the safety and comfort aspects in the past three decades. However, there are still some rooms for improvement in terms of control, efficiency, user experience, productivity, and the safety of the forklifts. Besides, the efficiency of the equipment is important for the industry; as this can assist in increasing the productivity and business profits. Forklifts are designed to be compact; however, while loading, carrying and offloading heavy loads, they can be unstable at times, causing safety matters. The tilting of the mast can consequently cause the forklift to tip over; therefore, forklifts should not be maneuvered when parts are moving or with the mast raised. Currently, the operator must wait until the vibration of the mast is damped before moving. Therefore, the mast vibration must be dampened with the new strategy that works efficiently and economically. Previous studies carried out in this area were mainly concerned with vibrations in driver cabins, and their main idea was mostly to reduce these vibrations through implementing active damping systems which was not economical for manufacturers. There are a few types of research that are specifically trying to reduce the vibration of mast unit with an active control system or passive control system to base or mast, however manufacturers did not welcome the ideas because of complications of the systems and costs involved. Also it has been found that these mass-dampers are always adjusted to operate in certain frequency and when natural frequency of structure is changed the mass-damper becomes less effective and can even increase the vibration of mast.

In the current research, it has been strived to control the vibrations of the forklift's mast unit with a novel strategy that dampens the vibration of the mast with the semi-active control system and without adding any extra mechanical component to the system. In order to achieve this aim, a numerical model based on a simplified system and the degree of freedom associated with the mast unit oscillations is presented. This research introduced and implemented two methods of second-order linear control (i.e. LQR and SMC) to control the cylinders of the forklift. Then, in order to achieve the maximum force for the cylinders, a PID control method is presented based on flow control of servo-hydraulic valves of the forklift. By comparison with real results, the newly designed controllers have been successful to achieve between 13.6% to 36 % reduction in vibration of forklift's mast with different loads on the mast unit.

Acknowledgments

It was the grace of God that gave me the strength to continue the work that concluded in this research; I wish to sincerely thank all those who have contributed in oneway or another to this research.

Words can only inadequately express my sincere appreciation to my Supervisor, **Prof. Ibrahim Esat**, for his meticulous care, kindness, and generosity. His fruitful comments and insightful suggestions have been a crucial formative influence on the present research.it has been my great fortune and privilege to be working with him.

Dr Jie Chen is also greatly acknowledged as the second supervisor for all his expert advice and support from the very beginning of the research.

The College of Engineering, Design and Physical Sciences, in specific **Prof. Tassos Karayiannis** and **Dr. Philip Collins** of Brunel University, are acknowledged for their financial support and motivations through the course of this research.

I would like to acknowledge the industrial partner of this project **Hyster-Yale Group** and in specific **Malclm Cole**, the Test Engineering Manager, for his constant motivation, expert guidance, invaluable suggestions. Grateful acknowledgments are also due to **Phil Mean**, Mechanical Engineer for his valuable suggestions and kind assistance on this project.

Finally, I would like to give profound thanks and gratitude to my lovely wife, **Mrs. Elmira Afshar**, My little daughter **Melorin** and my Parents **Mr. MohammadMehdi Esmaeili** and **Mrs. Narges Zolfaghar** for their unlimited love and moral support. Without them, it was impossible to complete this research.

Declaration

I hereby declare that this Ph.D. thesis entitled A Novel strategy for controlling forklift's mast vibration I have submitted to the office of the Engineering and Design, Brunel University London, is entirely my original work prepared under the supervision of Prof. Ibrahim Esat. I have duly acknowledged all the sources of information which have been used in the thesis. The results of this dissertation have not been presented or submitted anywhere else for the award of any degree or other purposes.

Table of Contents

Abstract	I
Acknowledgments	II
Declaration.....	III
List of Figures	VII
List of Tables	IX
Abberivation	X
List of Symbols	XI
Chapter 1 Introduction	0
1.1) Background	1
1.2) Different types of forklifts.....	2
1.3) Stability	4
1.4) Forklift control	5
1.5) Definition of vibration.....	6
1.6) Dynamic of the vibrating system	7
1.6.1) Mass	7
1.6.2) Stiffness.....	8
1.6.3) Damping	8
1.7) Type of vibration.....	8
1.8) Forklift's Mast Vibration	9
1.9) Novel contributions	11
1.11) Thesis structure	12
Chapter 2 Literature Review	13
2.1) Vibration control methods for structures	14
2.1.1) Passive control systems	15
2.1.2) Active control systems	16
2.1.3) Hybrid Control Systems.....	16
2.1.4) Semi-active control systems.....	17
2.2) Systems control methods.....	18
2.2.1) Optimal controller.....	19
2.2.2) PI, PD & PID Controllers.....	19
2.2.3) Sliding mode controller (SMC).....	23
2.3) Forklift vibration	23
2.3.1) Control of forklift trucks	23
2.3.2) Vibrations of the forklift body	25

2.4) Controlling vibrations of the beam.....	27
2.4.1) Modelling smart structures	28
2.4.2) Controlling piezoelectric based vibrations	29
2.4.3) Memory alloy based controlling of vibrations.....	30
2.4.4) Beam controlling systems	31
2.5) Forklift body and mast vibration	34
2.6) Comparative analysis of the previous studies.....	42
Chapter 3 Numerical analysis.....	45
3.1) The system movement equations	46
3.1.1) Energy method	46
3.1.2) Virtual work principle.....	47
3.2) Modelling of a forklift system	49
3.2.1) The kinetic energy of the system.....	51
3.2.2) System potential energy:	53
3.3) Equations of the system movements	53
3.4) A linear model around the operating point	57
3.5) Equations of the system with one degree of freedom	58
3.5) Space state equations of the system	60
3.6) System control.....	60
3.6.1) LQR controller.....	61
3.6.2) Sliding mode controller	63
3.6.3) PID controller.....	70
3.7) Chapter Conclusion.....	76
Chapter 4 Experimental setup	77
4.1) Forklift Body	78
4.3) Design	80
4.3.1) Base.....	80
4.3.2) Pivot	80
4.3.3) Mast	80
4.3.4) Forks.....	81
4.3.5) Tilt Cylinder.....	81
4.3.6) Electro-Hydraulic Control Valve.....	81
4.3.7) Flexible hose, pipe fittings and seal materials.....	82
4.4) Hydraulic Power Unit.....	84
4.4.1) Hydraulic system circuit and operation	84

4.5) Control system equipment.....	85
4.5.1) CompactRIO with Chassis.....	85
4.5.2) NI 9234 - 4-Channel, ± 5 V.....	85
4.5.3) NI 9472 - 8-Channel, ± 24 V.....	86
4.5.4) Accelerometer	86
4.5.5) LabVIEW	86
4.6) Rig Setup	88
4.6.1) Preliminary experiment – pluck test.....	88
4.6.2) Calibration test	89
4.7) Control system tests on Rig.....	89
4.7.1) PID controller.....	89
4.7.2) LQR controller.....	99
4.7.3) Sliding mode controller (SMC).....	100
4.8) Chapter Conclusion.....	102
Chapter 5 Results and Discussion	103
5.1) Numerical model’s results.....	104
5.1.1) Simulation.....	105
5.1.2) Controllers section	106
5.1.3) LQR controller.....	106
5.1.4) Sliding mode controller	109
5.2) Experimental Results	113
5.2.1) LQR_PID controller.....	115
5.2.2)SMC-PID controller	116
5.3) A Comparison of control methods	119
5.4)Chapter Conclusion.....	124
Chapter 6 Conclusion.....	126
6.1) LQR-PID controller	127
6.2)SMC-PID controller	127
6.4) Overall outcome	128
6.5) Future work	128
References	130
Appendices.....	137

List of Figures

Figure 1: 1920's Yale Forklift Truck.....	1
Figure 2: Yale's VL Series in operation	4
Figure 3: the stability factors	4
Figure 4: Basic forklift hydraulic system	5
Figure 5: vibration system	7
Figure 6: A lumped system with 4 factors	8
Figure 7: Sinusoidal graph from the Hyster Yale pluck test experiment	10
Figure 8: An example of active damper used in structures to reduce vibrations	16
Figure 9: Smart damper used in vehicles and various dynamic systems	17
Figure 10 :Block diagram for a PI Controller with the three aforementioned domains	21
Figure 11: Block diagram for a PD Controller with the three aforementioned domains	22
Figure 12 : An autonomous forklift and block diagram of its control system	24
Figure 13: Structure of the hydraulic part of the forklift	25
Figure 14: Bump accelerometer sensor (left) and bump positioning (right)	26
Figure 15: Results of the acceleration output entered into the left side front	26
Figure 16: Piezoelectric-based vibration control	27
Figure 17: The beam used in for shape control	31
Figure 18: Control system schema based on neuro-fuzzy feedback controller	33
Figure 19: Schematic representation of experimental test	33
Figure 20: Forklift system model forms in two modes of full loading and semi-loading.....	34
Figure 21: simplified model and loaded force changes diagram in terms of time.....	35
Figure 22: Changes in the forces brought into the front and rear of the forklift system.....	35
Figure 23: The realistic model of the flexible link and its schematic of rotary motor.....	36
Figure 24: Block diagram of state feedback control and LQR.....	36
Figure 25: System responses based on LQR and state feedback controllers	37
Figure 26: Schematic of the forklift system and location of the strain gauge sensor	37
Figure 27: Block diagram of the feedback and feedforward controllers	38
Figure 28: Deflection diagram of the forklift mast unit without braking (left side figure).....	38
Figure 29: Control system performance based on the output of forklift's longitudinal speed and input of control system	38
Figure 30: Simulation results of the process for the forklift mast unit optimization.	39
Figure 31: Three lowest natural frequencies that can be generated in the mast structure.....	40
Figure 32: Mast vibration reduction method based on the research	41
Figure 33: Passive control of mast vibration a (left) and	42
Figure 34: A forklift system produced by the Yale Corp.....	49
Figure 35: A schematic model of the forklift system during load movement.....	50
Figure 36: Simplified schematic model of the forklift mast.....	50
Figure 37: Simplified model of the movement of the forklift mast.....	51
Figure 38: Block diagram of a two-degree freedom vibrational model from the movement of the forklift mast system in the Simulink / MATLAB software	57

Figure 39: simplified schematic model with one degree of freedom to extract the dynamic equations of the system	58
Figure 40: Block diagram of the LQR controller based on the vibration model	62
Figure 41: Sliding mode controller diagram block based on a vibration model	70
Figure 42: Schematic model of a dual-channel cylinder and its simplified model.....	71
Figure 43: Schematic model of a two-channel cylinder in extension stroke.....	71
Figure 44: Schematic model of a two-channel cylinder in pressure mode	72
Figure 45: cylinder position and the connections of the inlet and outlet valves.....	74
Figure 46: Block diagram related to a dual-channel hydraulic valves operator	75
Figure 47: Block diagram for the final control method of the system	75
Figure 48: 2D drawing of the rubber bumper.....	79
Figure 49: Electro-Hydraulic Control Valve.....	82
Figure 50: Optimised Design of the forklift test rig	83
Figure 51: Hydraulic Power Unit.....	84
Figure 52: Hydraulic system circuit for scale down forklift	84
Figure 53: NI-9024 cRIO with NI-9114 chassis.....	85
Figure 54: A low pass filter and its circuit	87
Figure 55: Filter used to cancel the noise.....	87
Figure 56: Equipment set-up for tests	88
Figure 57: Calibration Test Amplitude vs. Time Results.....	89
Figure 58: PID block Diagram	90
Figure 59 : (A) Gain Schedule (B) Indirect Method (C) Process Dynamics.....	91
Figure 60: VI to find optimum gains via the Zeigler Nichols method.....	94
Figure 61: 50% and 25% Duty Cycle Respectively.....	95
Figure 62: PWM signal generator.....	96
Figure 63:PID & PWM Combined Control	96
Figure 64; Input elements of PID controller.....	97
Figure 65: Output elements of PID controller	98
Figure 66 : Complete VI program using PID controller for valves operation.....	98
Figure 67: LQR structure	99
Figure 68 : LQR Labview block diagram for cylinder	100
Figure 69: displacement conversion code in Labview	101
Figure 70: Implemented SMC equations in Labview via mathscript	101
Figure 71: Vibrational response of acceleration domain and angular displacement	105
Figure 72: The acceleration domain of the forklift mast while carrying a load of 10 kg	106
Figure 73: Angular displacement range of the mast while carrying a load of 10 kg.....	107
Figure 74: The acceleration domain of the mast part while carrying a load of 30 kg	107
Figure 75:Angular displacement range of the mast while carrying a load of 30 kg.....	108
Figure 76: changes in time for LQR controller cost function while carrying a 10kg load ...	109
Figure 77: Comparison of the output of the acceleration domain with a load of 10kg	110
Figure 78: Comparison of Angular Displacement Range Output with load of 10kg	110
Figure 79: Comparison of the output of the acceleration domain with load of 30 kg	111
Figure 80: Comparison of Angular Displacement Range Output with load of 30kg	111
Figure 81: Comparison of Forces in Operating Cylinders Based on SMC and LQR Controllers while Carrying a Load of 10 kg.....	112

Figure 82: Comparison of Forces in Operating Cylinders Based on SMC and LQR
Controllers while Carrying a Load of 30 kg..... 112

Figure 83: Vibrational Response of the Mast with Different Loads: A: Acceleration Domain
B: Angular Displacement Range 114

Figure 84:LQR Controller's Cost Function Changes While Carrying a Load of 10kg..... 116

Figure 85: Acceleration Domain while Carrying a Load of 10kg 117

Figure 86: Angular Displacement while Carrying a Load of 10kg 117

Figure 87: Acceleration domain while carrying a Load of 30kg..... 118

Figure 88: Angular displacement range while carrying a Load of 30kg..... 118

Figure 89: Comparison of Voltage Variations of Operating Cylinder Valves for Platform
Model of Forklift Mast 119

Figure 90: Acceleration domain while carrying a load of 10kg in 2m height..... 120

Figure 91: Angular displacement while carrying a load of 10kg in 2m height 120

Figure 92: Acceleration Domain while Carrying a Load of 30kg in 1m Height..... 121

Figure 93:Angular displacement range while Carrying a Load of 30kg in 1m Height 121

Figure 94: Comparison of Input Voltage of Dual- Cylinder Valves 2m Height 122

List of Tables

Table 1:Different Types of forklifts..... 3

Table 2: Comparison of alternative Materials 78

Table 3:Specifications of the rubber bumper 79

Table 4:The specific parameters and the supporting dimensions 81

Table 5: The specifications of the hoses 82

Table 6: Effect of Action Parameters on a System's Dynamics..... 93

Table 7 : Zeigler Nichols parameters 94

Table 8..... 104

Table 9: Comparison of Maximum Acceleration Domain and Angular Displacement
Variables Based on Different Weights in Numerical Model..... 113

Table 10: Comparison of RMS Value of Numerical Model Results and Experimental Test
results for Weights of 10, 20 and 30 Kg 115

Table 11: Maximum acceleration domain based on positioning at 1 meter..... 123

Table 12: Maximum angular displacement based on positioning at 1 meter 123

Table 13: Maximum acceleration domain based on positioning at 2 meters 123

Table 14: Maximum angular displacement based on positioning at 2 meters height..... 123

Table 15: Results for Maximum Reduction Rate of Acceleration Domain and Angular
Displacement Variables Based on Placing The Load in 1 m Height in Platform Model..... 124

Table 16: Results for Maximum Reduction Rate of Acceleration Domain and Angular
Displacement Variables Based on Placing The Load in 2 m Height in Platform Model..... 125

Abberivation

AC	Alternating Current
API	Application Programming Interface
AO	Analogue Output
BS	British Standard
CAD	Computer Aided Design
cRIO	CompactRIO
CNC	Computer Numerically Controlled
DAQ	Data Acquisition
DC	Direct Current
DMA	Direct Memory Access
DO	Digital Output
DOF	Degree of Freedom
DO	Digital Output
DSUB	D-sub Miniature
ER	Electro Rheological
FIFO	First In First Out
FPGA	Field Programmable Gate Array
GUI	General User Interface
HP	High Power
I/O	Input/ Output
IP	Internet Protocol
LabVIEW	Laboratory Virtual Instrument Engineering Workbench
LVDT	Linear Voltage Differential Transducer
MAX	Measurement & Automation Explorer
MR	Magnetorheological
NI or N.I.	National instrument
NVH	Noise, Vibration and Harshness
ODE	Ordinary Differential Equation
OS	Operating System
PID	Proportional Integral Derivative
RMS	Root Mean Square
RTOS	Real-Time Operating System
SAS	System of Active Stability
VI	Visual Interface
.vi	Visual Interface file –LabVIEW
WBV	Whole Body Vibration
ODE	Ordinary Differential Equation
PC	Personal Computer
PPC	POWER Performance Computing
PSD	Power Spectral Density
RFC	Relative Feedback Control
SDoF	Single Degree of Freedom
SISO	Single-Input Single-Output
TF	Transfer Function
THD	Total Harmonic Distortion
VFC	Velocity Feedback Controller

List of Symbols

A	Amplitude
AC	Alternating Current
C	Damping Coefficient
d	Wire Diameter
DC	Direct Current
D	Derivative
Dc	Duty Cycle
DO	Digital Output
b	Damping Constant
e	Steady State Error
ER	Electro Rheological
F	Force
f	Excitation Frequency
f_n	Natural Frequency
fHZ	Frequency (cycles per second);
G	Modulus of Rigidity
g	Gravity
h	Height
I/O	Input/ Output
IC	Current
k	Spring Stiffness
l	Length
m	Mass
n	Number of Active Coils
ω (Omega)	One rotation in radians per second
ω_0 (Omega)	Gravitational Force
P	Proportional
Pw	Power
R	Mean of the Internal Radius of a Coil
R_Ω	Resistance
s	Displacement due to time (function of time)
s	Seconds
t	Time
T	Time of one cycle duration per second
V	Voltage
w	Width
x	Displacement

Chapter 1 Introduction

Highlights:

- ❖ History of forklifts operation
- ❖ Different types of forklifts, the stability of forklift
- ❖ Vibration types, control system, and its characteristics
- ❖ Novel contributions

This chapter provides general background on the research field and states the overall goals of the project. It also discusses the challenges to be addressed combined with the strategies adopted for tackling these challenges. In the process of achieving the aims and objectives of the project, several novel contributions have been made, which are listed in this chapter.

1.1) Background

In the majority of wholesale distributor operations; bundles and stacks of material in various shapes and sizes are transferred to different locations. Manual material handling increases the risk of injuries and incurs costs to have a greater manual workforce [1]; thus, the use of forklifts was introduced. Forklift trucks have been a significant part of the construction and wholesale industry since their introduction, nearly a century ago. Forklifts have been developed and enhanced in the past decades to improve the operator's experience, their health and safety aspects, and productivity. Nonetheless, there are still concerns and issues that need to be addressed to enhance the use of forklifts.

Material handling lift trucks most commonly known as Forklift trucks are power-driven industrial trucks used to lift and transport heavy loads and materials. Clark is recognised with the concept of the seated counterbalanced truck in 1917 [2]. However, the first electric forklift truck with raising forks and elevating mast was invented by Yale (Figure 1) in the early 1920s [3];



Figure 1:1920's Yale Forklift Truck

Nowadays, forklift trucks are more sophisticated with complex electronics and hydraulic systems, comfort for the user, high visibility masts and consideration for safety. These can be powered by an internal combustion engine running on petrol, diesel, or electric motors [4]. Thus, forklifts are utilised for various applications in many warehouses, construction sites, and manufacturing facilities. Forklift trucks are always been developed with new concepts and designs to improve the user experience and to reduce the time cycle and risks. This makes the current project very important for the industry; hence the involvement of a prominent industry name, Hyster Yale Group, in the project.

1.2) Different types of forklifts

There is a vast range of forklift trucks to suit the needs of various applications. Majority of forklifts are designed for a specific operation; however, there are some multi-use forklifts available too [5]. Forklifts are classified into seven groups that define its engine type, working environment, operator, and equipment characteristics such as tyre type and maximum grade [6]. Few types of different forklifts compared below.

‘Internal combustion cushion tyre forklift’ are designed for indoor use associating with applications such as manufacturing, warehousing and trucking. These trucks can be gasoline or diesel powered; powered solely through the engine. ‘Internal combustion pneumatic tyre forklift’ are primarily designed for outdoor use where the surface is deemed to be uneven. These trucks utilise large tyres are filled with air (pneumatic). Even though the forklift is designed for outdoor use; they still find it difficult to work in sand or loose gravel.

A versatile forklift used in the industry is known as the ‘truck mounted forklift’ that can be mounted to be the back of a truck and carried to worksite. A very noticeable and in some sense unique feature of this forklift is the lift cylinder is normally a double acting cylinder. Another type of forklift is the ‘rough terrain forklift’ that are built for carrying material over terrain, something a normal pneumatic tyre forklift will not be able to achieve. These forklifts have oversized tyres so they do not get trapped in soft surface.

There are also the ‘narrow aisle trucks’ and the ‘order selector’. The narrow aisle trucks are made to be used in warehouses that have small aisles. The operator in these trucks stands up to conduct operations, this is so the truck can be made fairly compact for the aisles. These trucks can rise up to 15m. The order selector trucks have the operator riding on the platform so that the user’s feet are at the same height as the forks at any given time. These trucks are used in warehouses to physically pick out the order for customers.

Finally, there is the ‘electric sit down rider forklift’ that is powered by large industrial battery. The functions of these forklifts are controlled with an electric motor. The latest and most supreme forklifts are engine-powered counterbalance with the capacities to lift loads from 1.5-8 tonnes. Furthermore, Toyota forklifts have added developments for faster acceleration and higher lift speeds to enhance productivity.

A quick summary of all types of forklifts is illustrated in Table 1.

Table 1: Different Types of forklifts

Types of Forklift	Description
Class I forklift	Rider trucks with an electric motor, stand-up operator or three-wheel seated. Usually counterbalanced with a cushion or pneumatic wheels.
Class II forklift	Include electric motor vehicles use in the narrow aisle; they may include extra reach or swing mast options.
Class III forklift	Have a walk-behind or standing rider controller and have an electric motor. Commonly pallet-lift trucks and high lift models.
Class IV forklift	Equipped with cabs and seated controls for the operator and have an internal combustion engine.
Class V forklift	Equipped with cabs and seated controls for the operator and have an internal combustion engine.
Manual drive forklifts	Used to manually move the load and usually have an operator walking behind it.
Motorised drive forklifts	Include a seat for the driver to operate the truck while riding in it.
Narrow Aisle trucks	Designed for narrow places and operate in aisles typically 8 to 10 feet clear.
Pallet trucks	Commonly used with pallets in the warehouse or manufacturing
Platform trucks	Have a load platform intended to pick up and deposit a specific
Side loads	Equipped to reach forwards to pick or deposit heavy loads, pallets; furthermore, they are able to operate in very narrow

This research is based on Yale's VL Series, electric counterbalance forklift truck, which has a load capacity range of 2200kg – 3500kg and is considered as a mid-range forklift [7]. Yale's VL Series is one of the most enhanced mid-range forklifts with AC technology and continuous stability enhancement. Also, an AC motor is interlinked with the hydraulic pump and steering, eliminating the need for a separate steering motor. The masts on the VL series are designed to maximise visibility for the operator, with added lift chains and main lift cylinder [7]. Moreover, the VL series is designed to be used indoor or outdoor. Therefore, it has weather protection.



Figure 2: Yale's VL Series in operation[7]

1.3) Stability

Stability is essential to the safety of a forklift; hence, during the manufacture of forklift trucks, standard laid down tests are done by the manufacturers. As illustrated in Figure 2, the load is carried close to the drive axle; however, the distance to the counterweight at the back is longer. This offers the ability for the counterweight to balance the load with a safety factor.[8]

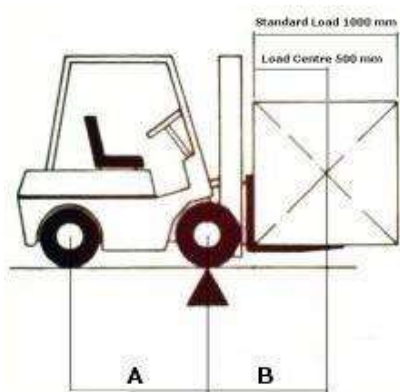


Figure 3: the stability factors[8]

In the same respect, Toyota introduced SAS ‘System of Active Stability’, which is patented to the company comprising ten sensors, 3 actuators, and a controller. SAS is an advanced technology that monitors the forklift operations, and when it senses factors that could lead to instability, it takes corrective action [9].

1.4) Forklift control

Initially, the standard technique to control the forklift was to arrange a combination of resistors and contactors to control the speed. The passage of the electricity would be resisted by the resistor, turning it into heat. The contactor would be a big switch; turning the supply on and off [10]. Although, this technique still exists in small trucks, it has largely been replaced by Thyristor control systems and AC systems. In the modern era, the forklifts have a refined hydraulic system that is usually controlled electronically in the same way as the traction systems.

Furthermore, traction or motive power lead-acid batteries are often the power source used for electric vehicles such as Forklifts [11]. These batteries range from 24 to 80 volts and are compatible with small or large Forklift trucks [12]. Figure 3 illustrates a basic hydraulic system used in a forklift formed of a control valve, filter, pump, and oil tank.

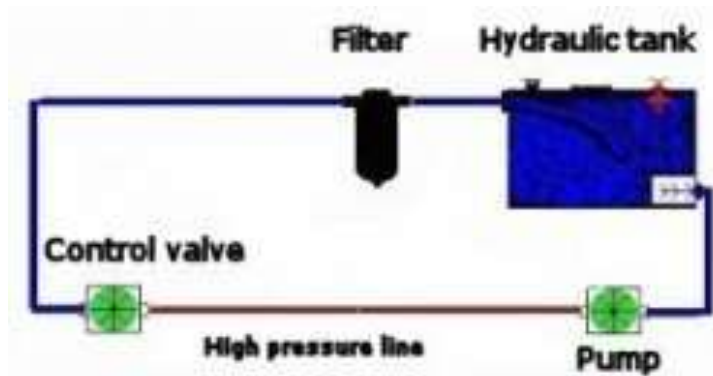


Figure 4: Basic forklift hydraulic system[12]

Forklifts have developed significantly in the past two to three decades; enhancing both safety and comfort aspects, in addition to control and accessibility. However, there are still concerns that can be improved to enhance the control, efficiency, user experience and the safety of the driver. Some stats illustrate that every year nearly 100 workers are killed and 20,000 seriously injured in forklift-related incidents [1].

The current concerns with the forklifts can be sectioned into health and safety and the efficiency of the product. Forklift operators perform diverse tasks; therefore, have the potential to be exposed to different types of injuries. The efficiency of the equipment is as important for

the industry; as this can assist in reducing the costs and increasing the business profits. In addition, the safety has been a tough challenge for the construction industry

Forklifts are designed to be compact; however, whilst carrying heavy loads, they can be unstable at times causing safety matters for the operator, pedestrians and general public. The forklift is not just a risk to the operator but also other employees or nearby pedestrians as they can be injured if the correct procedures of safety are not followed. Furthermore, the stability of a forklift is extremely low and they work in non-controlled traffic conditions so there are many incidents; thus, so much work has been done and still on-going to improve the forklifts.

The operators of the forklift are also in risk of many health problems. Some health threats among the operators of the manufacture equipment such as forklift are: whole body vibration, awkward posture due to limited shock absorption from wheels the vibrations from mast cause operators these vibrations which can subsequently result in health problems, including lower back pain. There are also issues of dust, noise and so forth. The whole body vibration and the awkward posture are issues that can be dealt with through improvements to the forklift. [13]

The tilting of the mast can consequently cause the forklift to tip over, therefore, forklifts should not be manoeuvred with the mast raised or when parts are moving; moreover, the load should be carried near the ground to reduce the risk of safety hazards. The loaded, raised forks cause vibration when tilted backwards and/or forwards so the operator must wait till the vibration is damped before moving the forks lower to ground and driving away. This precaution is taken to reduce risks; however, doing so also increases the time cycle and makes the workload less efficient. Therefore, the mast vibration is a huge element to the forklift industry; thus, to reduce the health issues, increase the productivity and not to compromise the safety, the mast vibration must be dampened. [13]

1.5) Definition of vibration

Vibration is a mechanical phenomenon which accrues with a dynamic force and causes oscillation at specific point. To control or dampen the vibration of the mast, it is essential to understand the concept of vibrations and how it is related to the forklift. The oscillation or the repetitive motion of a body or system (forklift's mast) around an equilibrium position can be regarded as vibrations [14]. This type of vibration is also known as 'whole body motion'; because all parts of the body (system) are moving in the same direction at any one time.

As illustrated in figure 4, the vertical movement of the mass attached to the spring is the most basic model of vibration where there is not any external force in position 1 and deflection, known as static deflection, is happened because of the mass. When external force applies and takes the system to position 2 and released by an elastic force of spring, the M will go to the position three, which is at its highest. By then there is no velocity in system and the mass starts to go back because of gravity. This oscillation can be continued indefinitely unless there is some resistance to dampen the amplitude.

As figure 4 shows, line 1 can present the oscillation without the presence of any resistance or friction. Also, the amplitude can be seen from the gap between the middle line to the lowest point or highest point of the graph. The time between A_1 and A_2 , which represent two consecutive minimum points, can be considered as one cycle (1HZ). The behaviour of this system and objects is more understandable by knowing the dynamic of vibration and oscillation, which will be covered in the next section.

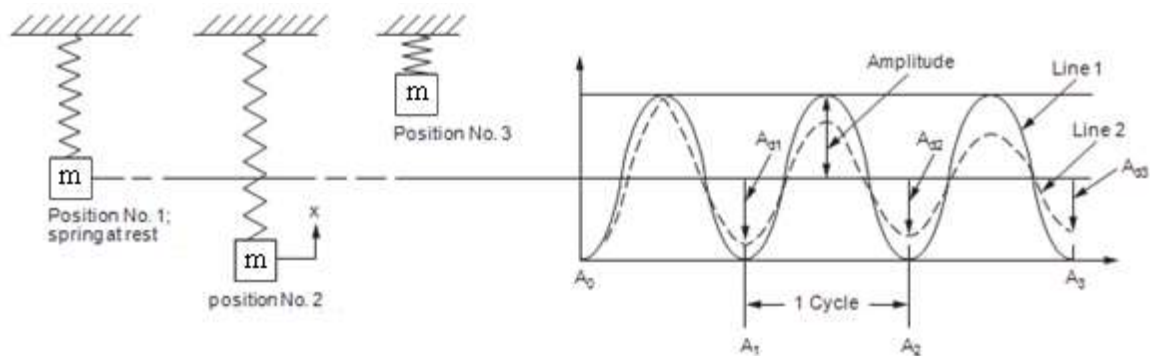


Figure 5: vibration system[14]

1.6) Dynamic of the vibrating system

Every vibrating system is made of 4 factors, namely mass, stiffness, damping, and degree of freedom, which can make a different system based on the level of their involvement in the system.

1.6.1) Mass:

Mass can be defined as the property of a system that resists against the external forces in a dynamic system. As mass increases through the system, it needs greater force to accelerate the whole system. Real systems are the continuous distributed mass systems. However a system with continuous mass displacement can be described as a superposition of modal

displacements, each with its own typical shape and natural frequency, which can be described as a system with multi-degree of freedom.

1.6.2) Stiffness

Stiffness is the resistance of the body when the body deforms by an applied force. In a real system, the mass and stiffness are distributed throughout the system; however, in a lumped system, as shown in figure 6, this can be presented by a spring between the lumped mass and its footing.

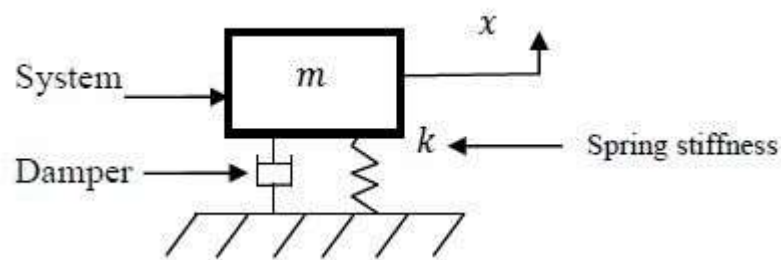


Figure 6:A lumped system with 4 factors

1.6.3) Damping

Damping effect is to reduce the velocity of the oscillatory system by restricting its oscillation. In particular, it transforms the kinetic energy into heat in order to dissipate energy from a system. There are three different damping types, namely viscous, structural, and coulomb damping. Viscous damping is caused by energy and movement velocity; structural damping is caused by the resistance happening because of internal friction of materials; and coulomb damping is a type of damping where energy is absorbed via sliding friction of two surfaces. All continuous vibration systems have a kind of damping effect, which can be considered as structural damping. These type of damping effects apply to systems all the time, whilst having a different ratio in different materials.

1.7) Type of vibration

There are three types of mechanical vibrations; free vibration, forced vibration and self- excited vibration. A figure that illustrates the exact criteria, resulting from motion and the characteristics of each of the damping effects can be found in appendix 1.

In general, in any systems that vibrations take place without any external forces, that fluctuation is called free vibration. The primary interest for such vibrations is the natural frequency [15]. Forced vibration occurs when a system or body is exposed to a repeated

external force; the resultant vibration is called the forced vibration. Furthermore, if the oscillation of the external force agrees with any of the natural frequencies of the body, resonance occurs; thus the body experiences dangerously large vibrations. Occurrences of resonance have been associated with the failure of building structures, bridges, turbines, and airplane wings [16]. The third type of mechanical vibration is known as self-excited vibration. When objects or systems commence vibrating on their own accord unexpectedly, there is an increase in amplitude until a nonlinear effect limits any further increase in vibration [17]. ‘Chatter’ in the machining process is a good example of self-excited vibration.

1.8) Forklift’s Mast Vibration

Forklift’s mast vibrations are transmitted through the seat of the operators who drive the machines over rough and even surfaces. This vibration can cause health risks, including back-pains; hence becoming a hot topic especially after the introduction of the European Directive 2002/44/EC, The Directive distinguishes between vibration affecting the hand-arm-system and vibration being transmitted to the whole body [18].

The mast contributes significantly towards the production of forklifts. Therefore new technologies [19] and research studies to improve the mast’s vibration problem have been highlighted by many industries [20]. Whilst it is crucial for these industries to increase productivity, they must not compromise the safety of the operator or the other workers. Thus, improving the mast gives the edge as productivity is improved without any compromises.

In same respect, CESAB utilised hydraulic brake effect for lifting and lowering end stroke for smoother movements. The two-cylinder design reduced vibration in comparison to one cylinder. Furthermore, it improved the safety, stability, and contributed to the less fatiguing working environment [21]. A figure that illustrates the two-cylinder design for the forklift’s mast can be found in appendix 2.

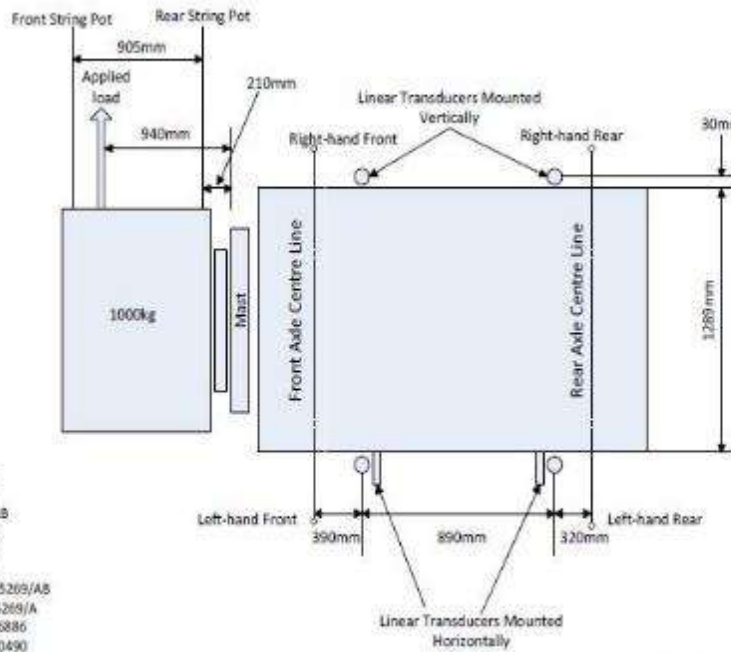
Hyster Yale Group investigated the vibrations of the mast by doing a simple pluck test on a loaded, raised forklift’s mast (Figure 7). The findings showed that it takes approximately 30 seconds for the vibration to thoroughly dampen; hence losing time and decreasing productivity. This was the basis for the current study, suggesting that if the mast vibration can be dampened or controlled, it can improve productivity. The research conducted by Hyster-Yale supports the importance of this project to the forklift truck industry. Figure 7 illustrates the sinusoidal graph from the Hyster Yale pluck test experiment.

TRUCK DETAILS
 Type: Yale ERP23VL
 Serial No: A976801301F
 Wheelbase: 3606mm
 Front Track: 1054mm
 Rear Track: 992mm
 Front Tyres: 23x10-12 Master Solid SE
 Rear Tyres: 18x7-8 Master Solid SE
 Battery: Hawker 4P23560 B545659
 Volts: 80 Ah: 560 Weight: 1490kg
 Unladen Truck Weight: TBA

MAST DETAILS
 Type: Full Free Lift Triple
 Lift Height: 4800mm
 Closed Height: 2290mm
 Fitted with an integral sideshift.

TEST DETAILS
 Test Load: 1000kg
 Horizontal Load Centre: 500mm
 Vertical Load Centre: 55mm
 Applied Load: 200kg
 Test Height: 4800mm Mast Vertical

INSTRUMENTATION
 2.54m Front String Pot Transducer J2308712C
 2.54m Rear String Pot Transducer TBA
 100mm R/H Front Linear Transducer 105269/AB
 100mm R/H Rear Linear Transducer 105269/A
 100mm L/H Front Linear Transducer 106773/A
 100mm L/H Rear Linear Transducer 092797/A
 100mm L/H Front Lateral Linear Transducer 105269/AB
 100mm L/H Rear Lateral Linear Transducer 105269/A
 500kg Tension/Compression Load Cell M2A026886
 LogMessage Data Acquisition Instrument 31120490



PLUCK TEST - TRUCK AND INSTRUMENTATION DETAILS

G L Gould
 2nd March 2012
 Not to scale

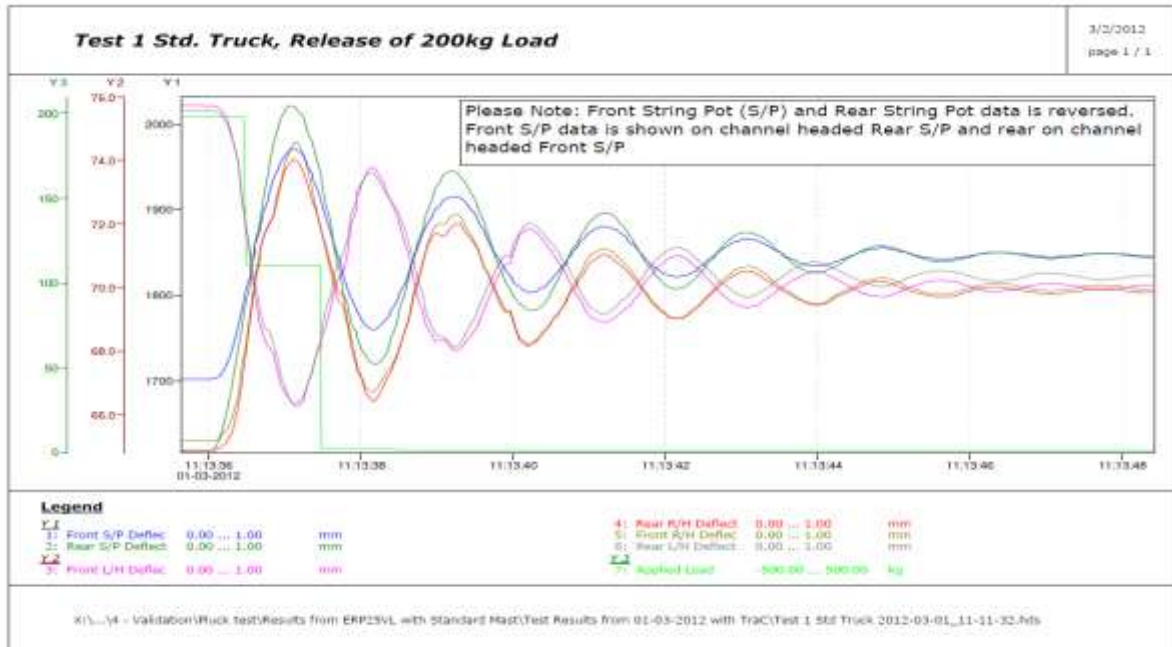


Figure 7: Sinusoidal graph from the Hyster Yale pluck test experiment[14]

1.9) Novel contributions

According to the analyses carried out on previous studies in the literature review chapter, it is conceivable that a little number of studies considered the forklift's mast system's vibrations.

In few studies, active control systems and passive control systems have been used for the reduction of vibrations related to the mast unit, which caused an increase in expenses of producing forklifts for both producers and consumers.

The main aim of this research relates to a method and arrangement for dampening vibration of the mast unit without adding any extra mechanical components to it. The critical characteristics of mast and cylinder are measured by sensors and are fed into computing systems. The order for movements is received from driver or master system. The critical characteristics of mast and cylinders are measured again after it reached final destination and are fed into the computing system. The controller system designed for cylinders, which are responsible for moving the mast, will try to bring the system to a desired error level set on them. In order to achieve this, the following **objectives** are set out for this research:

- To extract nonlinear relationships concerning with the vibration of the forklift's mast unit based on multi-member dynamical methods.
- To design a robust controller (based on the existence of uncertainties) in order to reduce the fluctuations of the forklift's mast unit for the first time based on its dynamic relationships. (Controlling cylinders)
- To reduce fluctuations of the forklift's mast unit through designing a PID controller that controls fluid flow (Controlling valves).
- To implement the two control systems for the first time based on the model made of the forklift's mast section

In order to achieve above aims, a numerical model based on a simplified system and the degree of freedom associated with the mast unit oscillations is presented. This research introduced and implemented two methods of second-order linear control (i.e. LQR and SMC) to control the cylinders of the forklift. Then, in order to achieve the maximum force for the cylinders, a PID control method is presented based on flow control of servo-hydraulic valves of the forklift. By comparison with real results, the newly designed controllers have been successful to achieve between **13.6% to 36 % reduction in vibration of forklift's mast** with different loads on the mast unit.

1.11) Thesis structure

The current thesis is organised in six chapters. In **Chapter 1** current concerns in the forklift industry is discussed. Also, an analysis of different types of vibrations and their effects on forklift's mast system and the stability of the forklift is dealt with. **Chapter 2** is devoted to the literature in the field of vibrations and stability of forklift systems and other similar dynamic systems. Furthermore, different controlling methods and the pros and cons are discussed. Finally, the selected controlling system in this research is presented based on an overall comparison of previous studies. **Chapter 3** is dealt with experimental methods based on a 3-D model of the forklift system, governing dynamic equations, and instruments needed to implement the controlling system. **Chapter 4** is a mixture of methodologies, and experimental setup to carrying out tests mentioned above, some essential equipments and design process explained followed by experimental tests and how they are performed in Lab-view. In **Chapter 5**, the simulation results based on the designed controller, and the results of experimental tests on the designed forklift unit are presented. In **Chapter 6**, the results related to the numerical model and experimental tests, along with the performance of the controlling system, are discussed. Finally, the concluding remarks and future research possibilities regarding decreasing vibrations of the forklift mechanism are presented.

Chapter 2 Literature Review

Highlights:

- ❖ Vibration Control Methods
- ❖ Different types of controllers
- ❖ Vibration of the forklift body and mast
- ❖ Beam control systems
- ❖ Detailed discussion of previous studies

This chapter consists of several sections to understand the control science and to identify the gaps in the research field for subsequent mast vibration. The key to successful research is an extensive review, providing the foundations of knowledge by covering vast but detailed aspects of the research field.

Reducing the vibrations of structures and dynamical systems has long been discussed as an important challenge. Reducing system vibrations will improve their performance. For example, successful damping of the vibrations and rattles of a vehicle will improve the service life of the vehicle components, passenger comfort and steering stability. It is also important to reduce the vibrations of long structures and bridges. The largest share of research in this field is focused on the use of passive and semi-active control systems based on different dampers, including electromagnetic ones.

One of the most important dynamical systems in the factories is load carrying forklifts, different types of which are used by industrial plants according to their needs. The use of these forklifts to carry heavy loads has contributed greatly to the reduced manpower and production cycle in industrial plants. Due to the constant movement of this system, the vibration in each section can lead to financial losses and casualties, so that by transferring the vibrations into the driver's cabin, the driver can be irritated based on the noise generated by these vibrations.

The presence of vibration in the body of the forklift's mast is very important, in a sense that the fluctuation in this section leads to a decrease in the service life of the forklift system. Furthermore, due to fluctuations in the forklift's mast and the possibility of the system instability, the driver is forced to move at a low speed when raising loads. To avoid this, various methods and control systems are considered in this section and their pros and cons are discussed. Previous studies on various control systems used in the forklift trucks are examined. Further studies on the reduction of vibration of the forklift system (both in the driver's cabin and forklift's mast) and similar systems are also looked at. Finally, by presenting a summary, the challenges ahead in the field of vibration of the forklift's mast systems are discussed.

2.1) Vibration control methods for structures

Different methods are used to reduce the vibration of structures and dynamic systems. Controllable equipment, computerised control systems, sensors, and maintenance semi-active systems are more effective than passive ones. On the other hand, the cost of running and maintaining passive systems is very low. Accordingly, a hybrid system could be highly justifiable. In the following, each control system is discussed thoroughly.

Vibration reduction tools are divided into several groups based on their system requirements, including passive control systems, active control systems, hybrid control systems, and semi-active systems. Passive control systems have problems such as dependency on the frequency of external forces and environmental conditions, whilst the active control of the structure,

despite its effectiveness, has problems such as the need for a lot of external power, like electricity. Furthermore, active systems incur additional costs.

2.1.1) Passive control systems

A passive control system is the one that modifies the stiffness or damping of the structure appropriately and without the need for an external power source and loading in the system.

In a passive control system, external power is not required to operate the control system, and the system thus creates control forces by using the movement of the structure. Control forces are created as a function of the structure response at the point of the passive control system [22]. In the case of installing this system in structures, there is no longer the possibility of making abrupt changes. For the effectiveness of this control system, there is always a need for a reliable forecast of loads design and a precise numerical model of the physical system. Usually, in this control system, it is not possible to locally improve the responses. It should be noted that the use of passive control systems is very common in engineering structures due to the ease of installation and low maintenance costs. An example of these control systems can be found in Base Isolation, which reduces the energy transfer rate due to flexibility.

On the other hand, these systems have advantages, including simplicity of design compared to other structural control systems, no need for external power such as electricity and low maintenance costs. Also, the disadvantages of these systems include non-compliance with environmental conditions and dependence on external stimulation. In the following, various types of passive control systems are mentioned.

a) Separators: They include two sub-groups, namely seismic separators and aerodynamic separators. In seismic separators, the structures are separated from the place of load and reduce the response of the structure. Their application is limited to structures with an average height. On the other hand, aerodynamic separators have a shape that can reduce wind force into the structure.

b) Energy dissipaters: They increase the damping and stiffness of the structure, and reduce the structure's response. Various sub-types of these systems include frictional dampers, viscous dampers, and metal dampers.

c) Dynamic vibration absorbers: These systems change the structure's dynamic properties, such as the natural frequency and damping, through which it will reduce the structure's response. They include three sub-types, namely three tuned mass damper (TMD), tuned liquid damper (TLD, TCLD) , and tuned roller damper (TRD).

2.1.2) Active control systems

An active control system is the one in which an external source provides energy to one or more of the stimulators of the control system, and these actuators impose forces in accordance with predefined states of the structure. These forces may be used to add or dissipate the energy of the structure.

Control forces are created based on the feedback received from sensors measuring the response of the structure or stimulation applied to it [23]. Since active control systems require an external source of energy to operate, in order not to affect the integrity of the structure and its function, it is necessary that this energy source remains unchanged and safe at the time of severe events. Along with this, there is a possibility that the active control systems cause additional mechanical stress to the structure which results in its instability. Therefore, active control systems are basically used as a supplement to passive control systems in engineering structures. As an example of the application of these controllers, the role of active mass dumpers in reducing the vibrations of buildings in severe winds and moderate earthquakes can be mentioned, which increase the comfort and convenience of residents in buildings [24]. In Figure 7, an example of the active damper is shown as a vibration damper for structures.



Figure 8: An example of active damper used in structures to reduce vibrations [25].

2.1.3) Hybrid Control Systems

The common sense of the word “**Hybrid** control” explicitly implies the concept that this system is a combination of active and passive control systems. In a hybrid system, an active control system may be used as a complement to improve the efficiency of the passive control system or vice versa. For example, a construction with a series of viscoelastic dampers and an active mass damper that is located on top of it can be mentioned. It should be noted that the only

major difference between active and hybrid systems is the amount of external energy required by the system. Thus, it can be said that hybrid control systems reduce some of the limitations of each of the main control systems [26]. As a result, these systems have a higher level of performance. In addition, if some sources of energy are encountering a problem, the passive component of the hybrid system still performs its task and protects the structure.

2.1.4) Semi-active control systems

Semi-active control systems are a series of structural control systems in which external energy is used to change the mechanical properties of the device. These systems are primarily passive control systems that are capable of changing and adjusting the mechanical properties of the system, and for this reason, often referred to as Controllable Passive Devices. The mechanical properties of these systems are based on feedback received from the structure response. In a semi-active control plan, a control system (a computer) measures the feedback and, based on the predetermined control algorithm, sends the signal to adjust the function of the semi-active devices. The control forces are produced as a result of the structure's movement and the adjustment of the mechanical properties of the semi-active control system. Moreover, since the control forces act in the majority of semi-active control systems in the opposite direction of the structure, they cause the overall stability of the structure. Semi-active control systems have different types of structures, including Magneto-Rheological Dampers, semi-active stiffness dampers, piezoelectric dampers, semi-active tuned liquid column damper and semi-active tuned mass dampers [27]. In Figure 8, an example of a smart damper is shown that is used in vehicles and various dynamic systems as a vibration absorber.



Figure 9: Smart damper used in vehicles and various dynamic systems [28]

On the other hand, semi-active control systems inherently have a nonlinear behaviour and include many benefits of active control systems without the need for a large energy source. Semi-active control devices do not provide any mechanical energy to the structure and also require very little energy (often with a small number of batteries) to set up and modify mechanical systems for controlling the device's behaviour (e.g., an electric control valve). In addition, the control power generated by a semi-active device always depends on the relative speed and displacement of the device.

2.2) Systems control methods

In order to maintain and improve the behaviour of time-varying dynamic systems, different control methods can be used. These methods can be categorised according to linear and nonlinear control methods.

Basically, the design of linear control systems can be considered as the problem of sorting the position of poles and the zeros of the closed-loop transfer function, so that the behaviour of the system is in accordance with the desired behaviour. Design methods are based on the basic assumption of performance in a small range for the linear model. When the range of performance requires a wide range of frequencies, the linear controller will perform poorly because it cannot compensate for the nonlinear effects of the system. Another assumption about linear controllers is that the system model is linear and free from uncertainties.

However, nonlinear control methods are used to control nonlinear systems. In this case, due to the nonlinearity of the system, we study the behaviour of the system around its equilibrium point, and its stability is determined based on locating the working equilibrium points. Some examples of Nonlinear control methods include phase plane method, Lyapunov stability analysis, Singular perturbation method, the Popov criterion, Centre manifold theorem, and Small-gain theorem.

control methods can be classified based on their properties, such as resistance to uncertainties and noise, as well as their comparative behaviour. Robust control is one of the design strategies of control systems, which emphasizes the stability and performance of the control system against changes and uncertainties. The purpose of the design is to create a control system that minimizes the effects on system output in the presence of changes in system conditions.. In particular, providing proper performance or sustainability in the presence of uncertainties, unmodified dynamics or disturbing agents such as shock is one of the main goals in designing

robust control systems.

There are various approaches to designing a robust controller, including H_∞ , H_2 , two and infinity norms (Mix H_∞ / H_2), and μ -Synthesis. Of course, the concept of robustness is not complete, and each controller structure is robust to some extent. Therefore, many well-known control methods, such as the PID controller or sliding mode control (SMC) are found to be robust only to some degrees. Here are some examples of these controllers.

2.2.1) Optimal controller

Optimal control systems are an important category of methods that, along with technical and industrial applications, have many applications in different areas of management, economics, and finance. In designing optimal control systems, in addition to the accuracy of the control system's performance, its rate of optimality in satisfying the requirements of the designers is important too. It means that not only reaching the goal but also how to achieve it is crucial. In this regard, the performance of an optimal control system does not just meet the basic and rudimentary requirements of a system, but it is also interested in performance optimization. Often in the design of optimal control systems, criteria are defined in the form of a performance index or cost function, which is ultimately translated into the satisfaction and optimization of their value systems with the best response time or the least amount of energy or the least amount of error regarding a reference signal [29]. On the other hand, the topics of optimal control, ultimately, find a very close relationship with reinforcement learning methods, and from another perspective, it can be considered as a loop between machine learning and control engineering science.

2.2.2) PI, PD & PID Controllers

The control applied to a system is determined by the system requirements; this can vary between the full embodiment of a PID controller for systems with different dynamic magnitudes for a constant time or necessitating high-order dynamics. A PI controller differs from PID in that they are applicable to first-order dynamic systems and the systems that do not need stringent control. These systems only require proportional actions to diminish error and integral actions for removal of the steady-state error. Alternatively, PD controllers can be employed when a system requires stabilisation only or an improvement in the prediction of errors.

2.2.2.1) PI Controllers

There are three main domains in which a PI controller can be portrayed; these are termed Frequency, Time and, S domains.

Where the frequency domain is expressed through the equation:

$$G_c = K_p + \frac{K_i}{j\omega} \quad \text{Equation 1}$$

PI controllers are considered to be a low pass filter, supplying a suppression of noise for noises at high frequency. The cause of this can be found in following Equation, as $|j\omega|$ reduces in size with higher frequency, (ω).

The time domain is comprised of an additional zero-point attained from the S-Domain, which denotes an open-loop transfer function that increases once. This restricts the actions for the transient state while still providing aid in removing the steady-state error.

Alternatively, within the S – Domain the PI Controller includes an additional zero-point along with a pole. This occurs when $S=0$ and $s= KI/KP$ in an open-loop transfer function. The system will be more influenced due to the new additional pole being positioned closer to the imaginary axis, resulting in the stability of the system becoming either unstable in particular gains or entirely reduced.

The corresponding block diagram for a PI Controller with the three aforementioned domains can be seen in Figure 10:

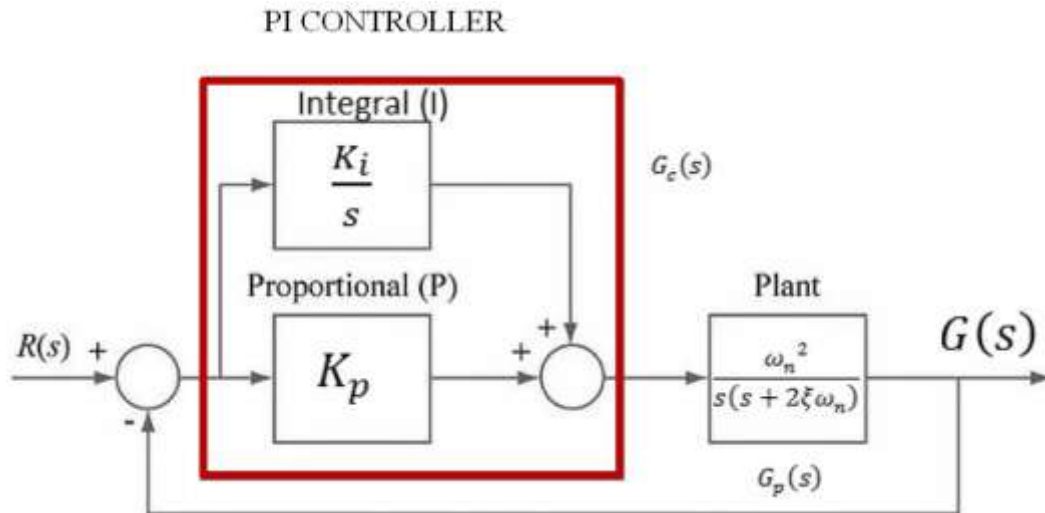


Figure 10 :Block diagram for a PI Controller with the three aforementioned domains[29]

From the above block diagram, the second order system transfer function for a PI controller can be represented through the following equation:[29]

$$G_s(S) = G_c(S)G_p(S) \equiv \left(K_p + \frac{K_i}{s} \right) (G_p(S)) \equiv \frac{\omega_n^2(K_p s + K_i)}{S^2(S + 2\xi\omega_n)} \quad \text{Equation 2}$$

In PI Controllers, steady state error can be eliminated; however, a PI controller cannot improve the transient response. This is due to the effect of the ‘I’ term increasing proportionally to the duration in which the system acts. This makes the PI controller envisaged as a memory-type controller.

2.2.2.2) PD Controller

Similar to the PI controller, a PD controller can also be characterised by the three main aspects of Frequency, Time, and S domains. However, they slightly differ in their attributes.

As for the frequency domain, where $(j\omega)=KP+j\omega KD$, with high frequencies $|Gc(j\omega)|$ responds correspondingly, As a result, a PD controller is easily influenced by high-frequency noise; hence referred to as high pass filter.

Initially within the time domain, due to the high presence of error and small t , the ‘D’ term provides a larger effect. This enables the provision of a rapid transient response. Conversely, the ‘D’ term is found to occur lesser in the steady-state systems due to t reducing significantly. In contrast to the zero-point added within a PI controller, the PD controller includes a nonzero-point, realigning the trajectory and subsequently improving the stability of the closed-loop system.

The corresponding block diagram for a PD Controller with the three aforementioned domains can be seen in Figure 11 below:

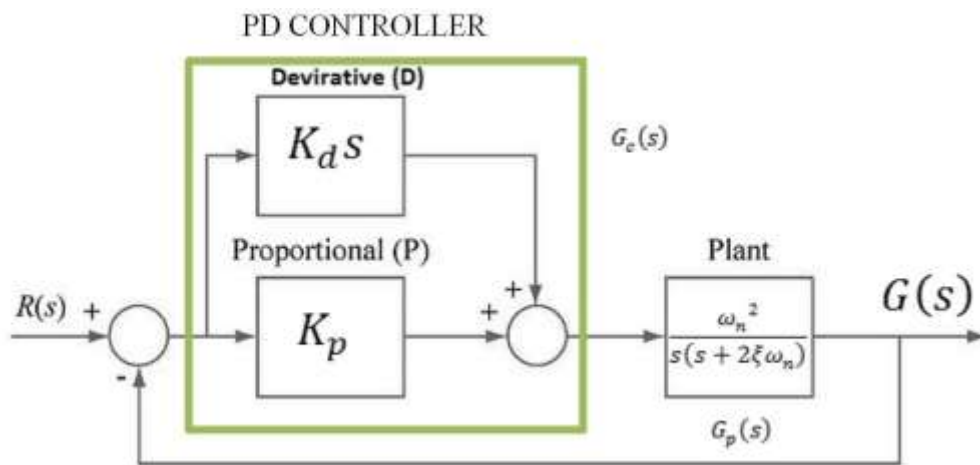


Figure 11: Block diagram for a PD Controller with the three aforementioned domains

From the PD controllers block diagram and expressed domains, the corresponding second order system transfer function for a PI controller can be represented through the following equation:

$$G_s(S) = G_c(S)G_p(S) \equiv (K_p + j\omega K_d)(G_p(S)) \equiv \frac{\omega_n^2(K_p s + K_d)}{S^2(S + 2\xi\omega_n)} \quad \text{Equation 3}$$

In this case, the ‘D’ term provides a necessary response prior to the occurrence of any overshoot [30]. As a result, a PD controller is considered as an anticipatory controller type.

A PID controller is an amalgamation of the properties exhibited by a Proportional controller (P), the integral controller (PI), and derivative controller (PD) to achieve a fast response while maintaining accurate control; hence representing a superior control system.

2.2.2.3) Gain and auto-tuning of PID Controllers

The assignment of parameters for each term is defined as tuning. There are two focal methods of setting PID gains; namely the Ziegler Nichols and ‘trial and error’ method [31]. Auto-tuning is a commanding procedure for tuning PID gain, which is applied only when processes act

conditionally or vary with time. If the process changes are predictable, the control system can be altered through the use of a gain schedule. Alternatively, an adaptive controller could be used to adjust the PID gain, to manage erratic variations. While adaptive controllers provide a general range of dissimilar situations, gain scheduling is operated to construct a table that contains numerous parameter sets for diverse conditions. Retracting distinct corresponding parameters can be implemented to modify the PID gains when process requirements change.

2.2.3) Sliding mode controller (SMC)

Sliding mode controller uses a robust control method. This controller is utterly resistant to disturbances and changes in parameters as well as intrusive noise. The reason for the high efficiency of this method is the simplicity of its design and implementation. This method is widely used in various nonlinear systems. The sliding mode controller approach consists of two steps. First is the selection of a path in the state space, which forces the state paths to stay in that space. The second is the design of discontinuous state-feedback that can bring the system to the state on the path in a limited time. However, the weakness of this control method is the presence of the chattering effect due to the switching frequency of the control [32]. High-frequency components of a control system that are not modified for a fast response cause unwanted fluctuations. This situation can reduce system performance and lead to instability. SMC, in fact, is a compromise between modelling and proper performance with inaccurate design [33]. The presence of chattering will increase the control effort and may stimulate high-frequency dynamics that are neglected in modelling.

2.3) Forklift vibration

2.3.1) Control of forklift trucks

With smart motion systems, especially in vehicles, control systems have progressed vastly. This has helped many companies to devise control systems that control various types of robots, cars, aircraft, etc.

Similarly the use of smart forklift systems has increased along with the advent of smart factories and production lines. The guidance and control of these systems are of high importance due to their limited workspace in the factories, and it is also important to control and guide them along their paths. In the following, some studies regarding the control of these systems are reviewed.

(Tamba et al) have studied the path control of an autonomous forklift system. In this study, the system is guided on a specific path based on the kinematics of the movement of the system and the implementation of the rules state feedback control method [34]. In Figure 12, the forklift system and the block diagram of the control method used in this study are shown.

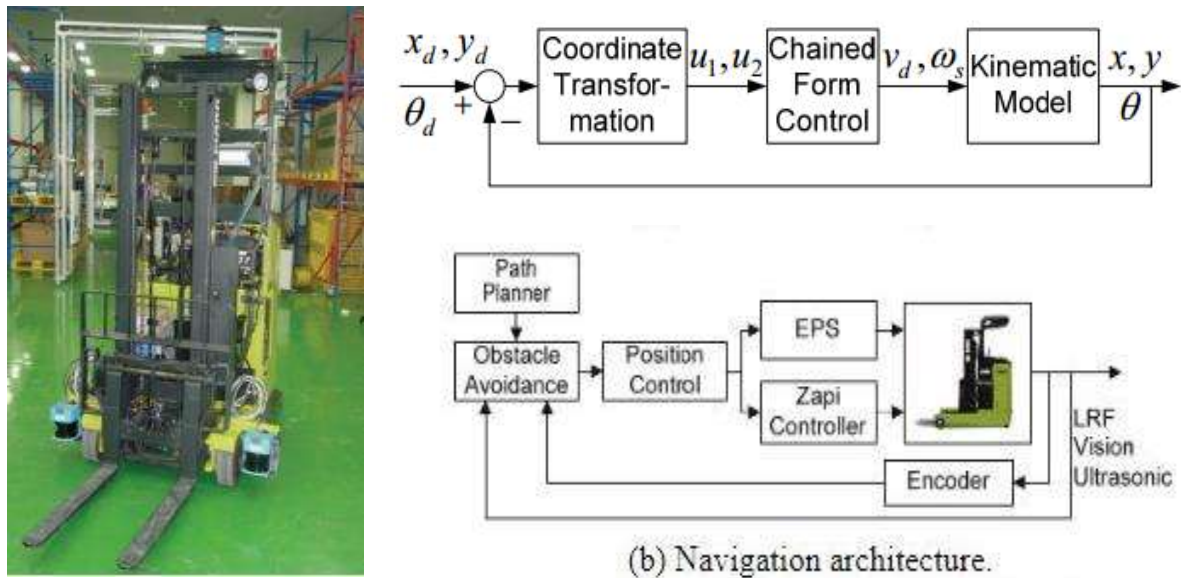


Figure 12 : An autonomous forklift and block diagram of its control system [34]

In another research, (Minav et al.) have designed a control system based on direct torque control using electric servomotors as well as hydraulic pumps in order to control the position of the forklift system [35]. In Figure 13, the overall software and hardware structure used in this study to control position and speed is shown.

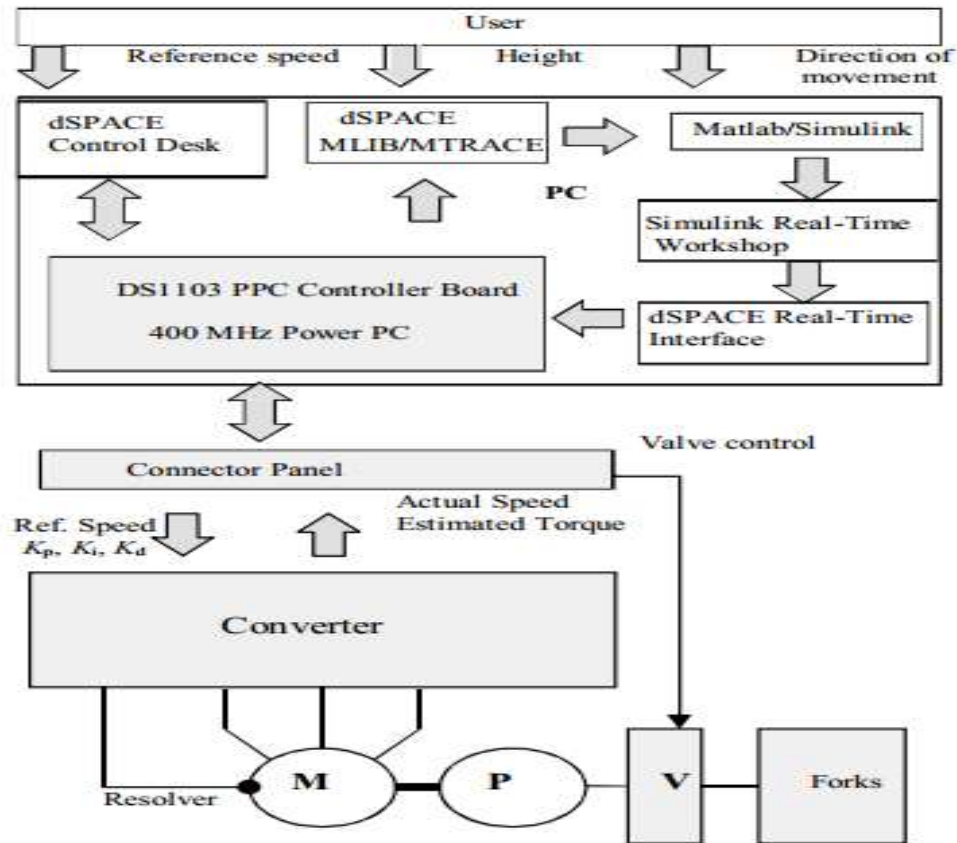


Figure 13: Structure of the software and hardware (speed, position) control of the hydraulic part of the forklift [35].

2.3.2) Vibrations of the forklift body

In a research conducted by (Ventura et al.), they developed modelling of a forklift system based on the multi-component dynamics method using Adams software. In this study, using accelerometer sensors placed on the wheel hub of the forklift, the vibrations on the forklift body were measured. The test is carried out on a bump, whilst the acceleration of the forklift with a constant speed on this bump is measured in different locations and directions. The results of this research indicate that the Adams software model is compatible with experimental results. In figure 14 the position of the accelerometer sensor and the bump are shown.[36]



Figure 14: Bump accelerometer sensor (left) and bump positioning (right) in the experimental test [36]

The results of the acceleration output entered into the left side front wheel of the forklift based on the numerical model (Adams software) and experimental test are shown in figure 14.

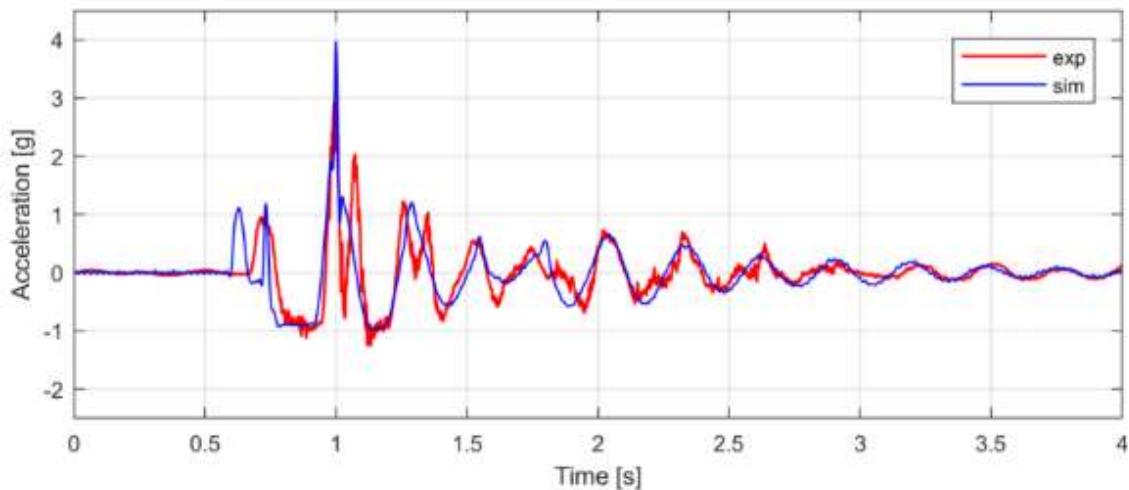


Figure 15: Results of the acceleration output entered into the left side front wheel of the forklift [36]

In another study, (Blood et al.), analysed the vibrations entered into the entire body of the forklift system based on changes in the seat suspension system. Two accelerometer sensors on the floor of the cabin and on the base of the seat measured the vibrations entered in different working conditions. In this study, considering two mechanical and air suspension systems, the impact of these two mechanisms on the vibration entered into the driver's body has been

addressed. The results of this research proved the positive performance of the air suspension system, with a 20% reduction in the RMS value of the acceleration entered in different situations [37]

2.4) Controlling vibrations of the beam

Active control of vibrations is important in structures. One of the ways to overcome this problem is creating a purposeful, smart, adaptive, self-controlling structure. The need for these smart structures is perceived due to their high performance.

(Dean and its colleagues.) published their work on active suppression and shape control regarding the development of smart structures. In their analysis, particular emphasis is placed on various methods adopted by a number of researchers to achieve the shape control and active vibration control in a smart structure. The focus of this study is on two technologies: piezoelectric based actuation and shape memory alloy-based actuation. Other methods of active vibration control (e.g. active magnetic shape memory alloy and damping Alloy) was also done in the study. [38]

There are different theories regarding vibrations of beams, each of which can be implemented according to situations, dimensions and displacement of the beam.

Among them, Euler–Bernoulli’s theory, Rayleigh's theory, and Timoshenko's theory are the most relevant ones. For example, the Euler Bernoulli theory can be used for the vibrations of thin beams. Control of the vibration of a beam with a sensor and a piezoelectric control system is illustrated in figure 15.

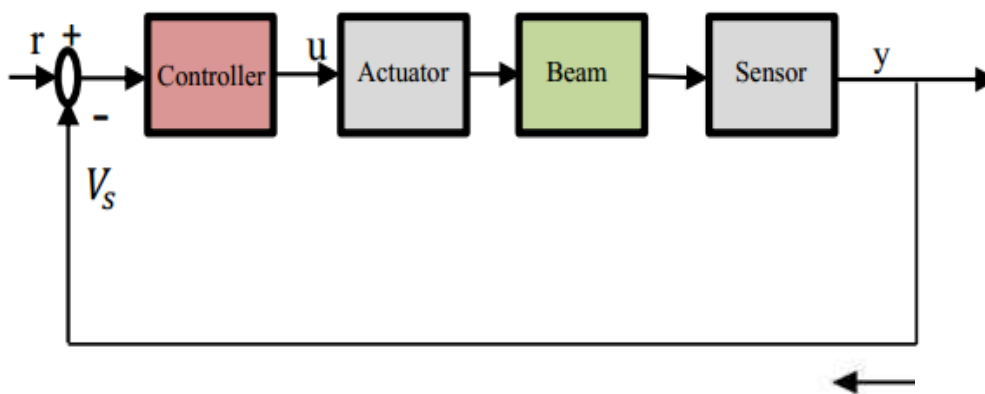


Figure 16: Piezoelectric-based vibration control

In the next section, the controlling vibrations of a beam and different methods to address that are closely examined.

2.4.1) Modelling smart structures

Developing a mathematical model that demonstrates the dynamics of a system is found challenging in any systems. Different studies have analysed the free vibration analysis of composite structures. (Marur et al.) suggests an active vibration control system based on the Linear-Quadratic-Gaussian controller (LQG) to reduce the low amplitude vibrations of a flexible cantilever beam. Parametric system identification method determines the physical characteristics of the system.[39]

(Peng et al.) analysed this issue and proposed a finite element model based on the third-order laminate method to control the active position and active vibration of composite beams with piezoelectric sensors and distributed operators. Furthermore, they studied the effects of the number and position of operators on the control system. They implemented a cantilever composite beam from graphite/epoxy along with symmetric piezoelectric ceramics for both upper and lower surfaces. Analysis of different centre-line deviation graph for cantilever beams shows that the position of sensors/actuators has a significant effect on shape control and vibration suppression in smart structures. The highest level of efficiency will be achieved when high strain areas (the fixed end of the cantilever beam) are far from the low pressure areas (the suspended end of the cantilever beam). In addition, an increase in the number of sensors/actuators will increase efficiency and reduce the voltage required to suppress vibrations [40].

(Liu et al.) created a finite element model based on the classical theory of laminated plates in order to control the shape and to suppress the active vibrations of composite plates using piezoelectric sensors and actuators. The formulation is obtained through the Hamilton principle. Using a simple velocity control algorithm, actuators and sensors are coupled to the piezo so that the controlling effects of active feedback on plates are based on higher order shear deformation theory [41,42]

(valoor et al.) created a finite element model to simulate the response beam vibration. They implemented a diagonal recurrent neural network to control the vibrations of the beam through the installed piezoelectric operator on the surface. Hung and sun [43] modelled vibration control in composite cantilever beam through higher order piezoelectric operator using Reissner–Mindlin plate theory[43]

Using the finite element method, (Moita et al.) analysed the capability of active controlling in composite structures covered by piezoelectric layers. A finite element model is developed based on third-order shear deformation theory to control thin laminated structures with piezoelectric and actuator layers. They concluded that the negative velocity feedback algorithm used in this model affects the active control of damping in vibration. [44]

(Gu and Xinke.) carried out a numerical analysis on active vibration control on a cantilever piezoelectric beam. Hamilton and Euler–Bernoulli’s theories were used to obtain the governing motion equations of beam vibrations [45]. In another study, through combining a classical theory of layer plates with a matrix model, (Yumsh and Runjun.) created a finite element model for composite plates with the installed piezoelectric actuator on the surface and surface cracks [46].

2.4.2) Controlling piezoelectric based vibrations

As explained, piezoelectric materials like pzt can be used effectively in the development of smart structures. Up to now, there have been a lot of studies on smart structures with piezoelectric actuation. Some of these strategies are applied in the industry, especially in aerospace engineering, instrumentation engineering, and mechatronics. However; these strategies cannot be implemented widely due to the low efficiency of piezoelectric ceramics and polymers. Some of the piezoelectric materials possess pyroelectric and electrocaloric features that made them capable of converting thermal energy into electricity and vice versa. Converting thermal energy into mechanical energy through the process of thermal expansion and vice versa as well as piezo – caloric effects of piezothermoelectric materials have been investigated by (Irschik.) [47]. Although it has been observed that these effects boost the efficiency of control actuation considerably, the interaction of mechanical, magnetic, and thermal fields complicated the issue.

A finite element formulation to control and suppress vibrations of smart structures along with piezoelectric plate element was validated by (Chen et al.) using negative velocity feedback control and numeric examples [48]. Furthermore, an analytical formulation was developed for composite beams with piezoelectric actuation along with positive velocity displacement feedback (PVDF) and a sensor based on first-order shear deformation theory. Also, an analytical approximate solution was obtained for a smart two-layer beam under external harmonic vibration load. (Sun and chiung.) used negative feedback control principle to control the amplitude of vibrations [49].

(Kermani et al.) suggested that reducing pzt thickness improves its performance even if brownout (or voltage decrease) happens. They also concluded that placing pzt in the beams would do the nodes controller processes smoother [50]. Using S/A of the piezoelectric groove as a substitution was recommended by (Bilargeon and Wol.), in which a vertical polarization magnetic field creates shear deformation of materials [51].

(Hu and vokovich.) analysed the resistant shape control of flexible aluminum plate using attached piezoelectric operators and pressure sensors [52]. They created a mathematic model with the aim of being resistant, and then they examined it practically. The adaptive shape control by the use of modal piezoelectric sensor/actuators to suppress the vibrations of a cantilever beam was presented by (lin and nien.) [53]. The dynamic behaviour of smart systems was discussed using linear equations of modal S/A.

The optimal placement of pzt patches was achieved using the Genetic Algorithm technique by (Moita.) [54]. In a research paper by (Donoso and Sigmund.) [55], authors have examined the optimization of piezoelectric actuators thickness and width. They concluded that instead of designing a changeable thickness, it is preferred to design a changeable width of the variable. A dynamical model was developed to control the vibration in the SiO₂ microcantilever beam with a pzt operator installed on the surface (Zhang et al.) [56]. In another study, the shape of the modes and the natural frequency changes were addressed using ANSYS software. An experimental study was conducted on the active control of cantilever beam vibrations with a piezoelectric actuators, and a simulation was also performed using ANSYS software (Kiral et al.) [57].

2.4.3) Memory alloy based controlling of vibrations

An active control shape, in order to deform a flexible structural component like a submarine surface or aerospace control surface or wing, needs an actuator that can cause force or momentum. As mentioned before, various actuators like piezoelectric materials, shape memory alloys, and thermal gradients were implemented to control shape, among which, shape memory alloys attracted a lot of attention as an actuator to control the shape of structures. This is because the Shape Memory Actuator has a specific formability improvement that can generate considerable forces during contraction; because it experiences an unprecedented change in phase as a result of the change in the temperature.

(Baz et al.) have theoretically and empirically studied the possibility of using Shape Memory

Actuators (SMA) in controlling the bending vibration of a flexible cantilevered beam. The beam dynamics is modelled using the finite element method and integrated with the thermal and dynamic characteristics of SMA to create a mathematical model of the compound beam-actuator launching system. An active computer controlled model is also designed based on this model. They assessed the performance of the control system in different operating conditions when the beam was exposed to displacement. They also used a flexible cantilever beam, as shown in the figure17.[58]

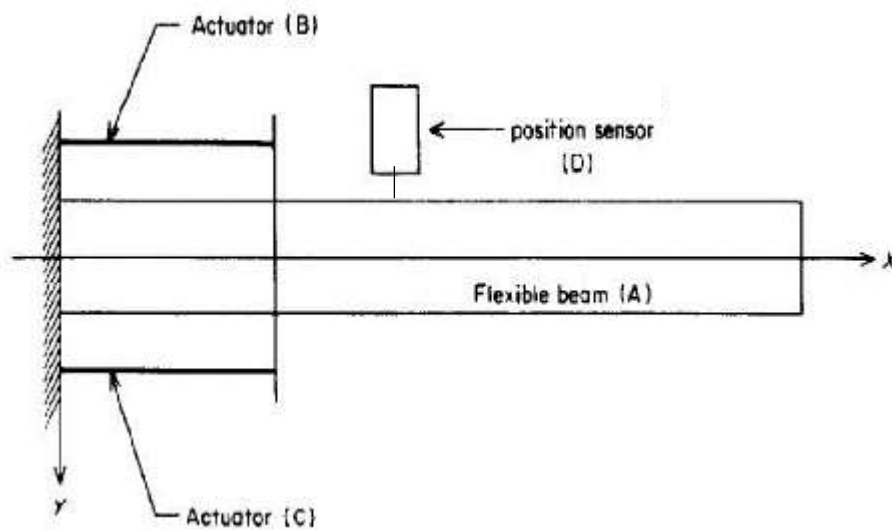


Figure 17: The beam used in [58] for shape control

The beam is made of polymethyl methacrylate with 2.5 cm width and 0.075 cm thickness and 25 cm height with two Nitinol wired actuators (with 50 mm of length and 0.4 mm of diameter) installed at the end of the fixed beam to reach the shape control. These actuators were set to maintain the shape of the beam with no deviation or the maximum deviation of 0.0625 cm. They were operating in 2.3-Hertz frequency. This research concluded that implementing two Nitinol actuators would lead to a considerable decrease in vibration. They also showed that an increase in the input power of the actuators could be effective in structural vibrations damping; however, the stability of the control system decreased. [58]

2.4.4) Beam controlling systems

Active controlling of vibrations in beam-like structures with piezoelectric sensors and actuating layers attached to the lower and upper surface of the beam have been studied by (song et al.) [59]. A finite element model of the beam was generated based on Euler–Bernoulli’s theory. Four types of classic control strategies, namely direct proportional feedback, negative velocity

feedback gain, and Lyapunov feedback, and an optimal control strategy were used to study the effectiveness of control. Also, the control performance was assessed in different loading methods such as impulse, staged, harmonic, and random loading. They concluded that velocity feedback is more effective in comparison with displacement feedback as the latter's changes lead to changing in damping of the system, while the former's changes would cause changes in natural frequencies of the system. In another study, (Vazquez and Rodriguez.) [60] presented analysis and comparison of classical control strategies like Constant Amplitude Velocity Feedback, Constant Gain Velocity Feedback, LQG and LQR controllers, as well as optimal control of smart piezoelectric beams. These researchers suggested that the optimal techniques are more efficient than the classical ones even if we face the problem of developing a model for the system.

The comparison of the Positive Position Feedback control system (PPF) and the Strain Rate Feedback (SRF) Control Model has been confirmed using Euler beam theory and experimental tests. The SRF controller and PPF control were used to prevent the vibration of a flexible steel cantilever beam connected to the piezoelectric actuator (Fi et al.) [61]. Subsequently, using the SRF control, suppression of dominant mode vibrations was achieved and the best result was obtained. A simple negative-velocity control algorithm was used to control the dynamic response of the epoxy/graphite compound beam under axial load pressure through a closed loop. The effect of the feedback control gain was evaluated on the response of the beam (Chen et al.) [62]. (Chouy and Han.) set up a Constant Amplitude Control system (CAC) to obtain vibration control in a flexible rotating structure (used in airborne equipment, helicopter blades, etc.) [63]

LQG controller was designed to control the vibrations of smart piezoelectric structures using system identification technique. (Koomagay et al.) [64] created a dynamic model of SMA actuator using a neuro-fuzzy inference system proposed in MATLAB software. Using fuzzy-neural logic, the systemic identification of the dynamic system was performed by observing the change of state (displacement and velocity) variables to a known input (input voltage to the current amplifier for the SMA actuator). Then, using the dynamic model, the required input voltage to seek for the desirable path was computed in an open loop method. The real input voltage that would be supplied into this amplifier would be the sum of this open-loop input voltage and an input voltage calculated by a PID controller. This controlling plan, which is based on neuro-fuzzy logic, is a general plan and can be applied for a range of SMA actuators.

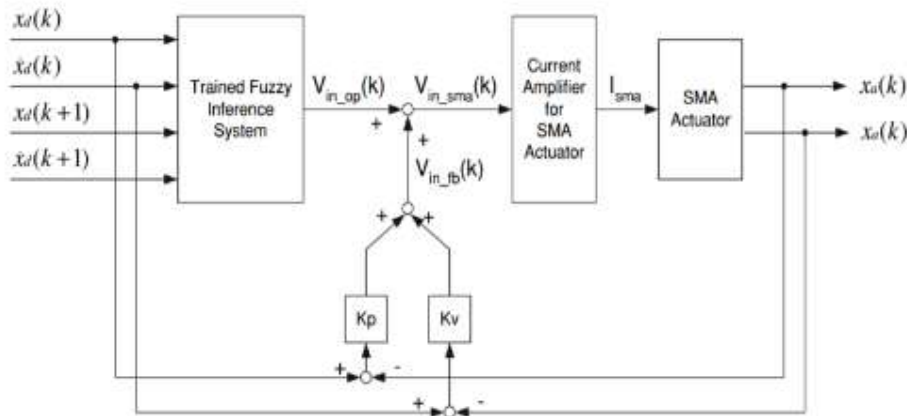


Figure 18: Control system schema based on neuro-fuzzy feedback controller [64]

The control of the vibration of the pre-twisted thin-walled beam of composite with rotating composite with Macro Fiber Composite actuators and PVDF sensors was investigated by (Choi and Han.)[65]. The results of this study show that an active damping effect can be obtained through a negative-velocity feedback control algorithm with PVDF sensors and a MFC (Macro Fiber Composite) actuator. The active damping effect is linearly related to the feedback control gain; so vibrations can be diminished faster than when the higher feedback control gain is applied to the actuator voltage range.

(Zhi-Cheng et al.) [66] used piezoelectric patches as sensors and actuators to control the vibration of the smart flexible clamped plates. First, the modal equations and piezoelectric control equations were obtained in the cantilever sheet. Then, an optimal positioning method for the site of the piezoelectric actuator and sensors was developed. Finally, an efficient control method was proposed with Positive Position Feedback (PPF) and PD control to reduce vibration. Analytical and experimental results show that the proposed control method can be feasible and the optimal displacement method is effective.

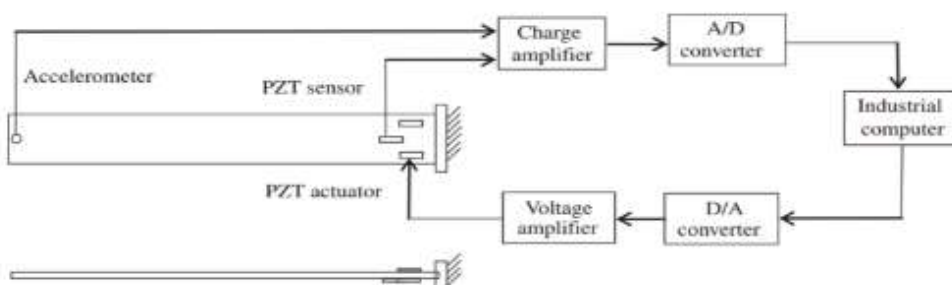


Figure 19: Schematic representation of experimental test

2.5) Forklift body and mast vibration

(Nguyen et al.)[67] analysed the vibrations of the forklift mast. Having developed a simplified model of the forklift system, they examined the mode and frequency of these systems based on the finite element method. In Fig. 20, the shape of the obtained modes of forklift system by finite element method is illustrated in two modes of full loading and semi-loading.

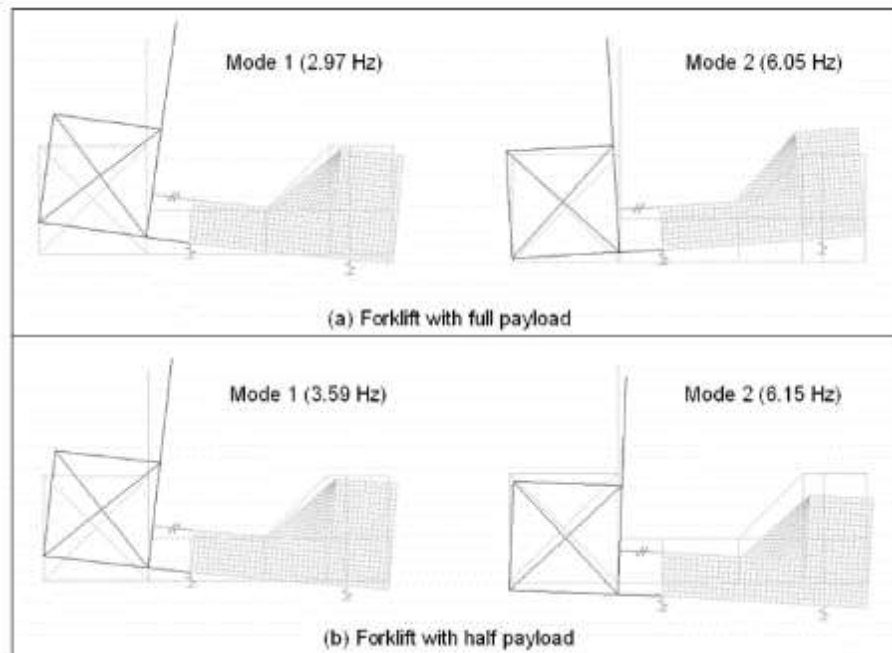


Figure 20: Forklift system model forms in two modes of full loading and semi-loading [67]

In this study, a simplified model was used to calculate the vertical forces transferred to the forklift wheels based on the following relationships.

$$F(t) = mg \left(1 + e^{-\zeta \omega_n t} (DLF - 1) \sin(\omega_n t) \right) \quad \text{Equation 4}$$

Where DLF is equal to:

$$DLF = \sqrt{1 + \left(\frac{\omega_n V}{g} \right)^2}$$

Figure 21 demonstrates a schematic of the simplified model of the forklift, as well as the loaded force change diagram in terms of time.

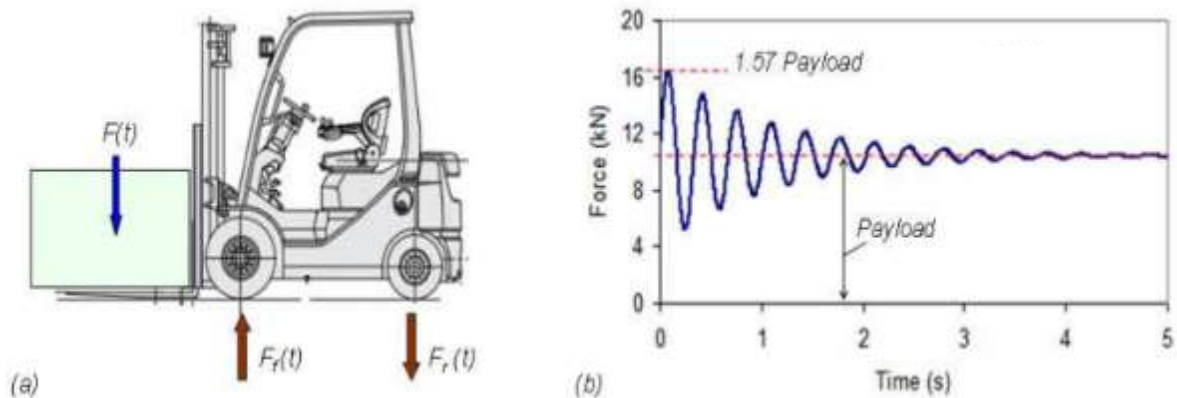


Figure 21: simplified model and loaded force changes diagram in terms of time [67]

By writing the equations of equilibrium for a simplified model, we can calculate each of the input forces. The diagrams below show the changes in the force brought to the front and rear of the forklift system. As shown in Fig. 22, the force on the forklift front axle has been greater than that in its rear axle.

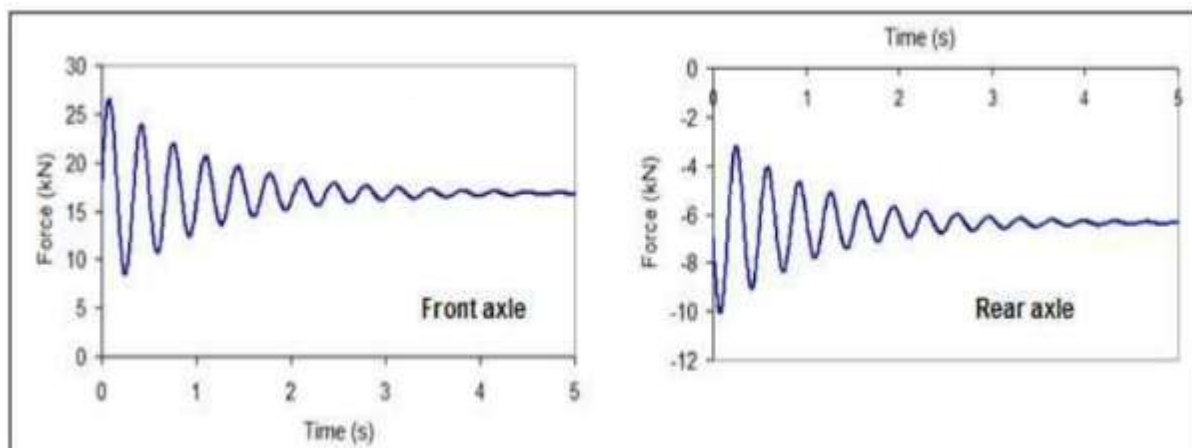


Figure 22: Changes in the forces brought into the front and rear of the forklift system [67]

(Baroudi et al.)[68] have studied vibrations and control of a flexible arm. In this research, after extraction of dynamic equations for the rotation of this component based on Lagrangian theory (based on the model in Fig. 23) and considering an actuator, the effect of two methods of state feedback control and linear-quadratic regulator (LQR) on its vibrations were investigated.

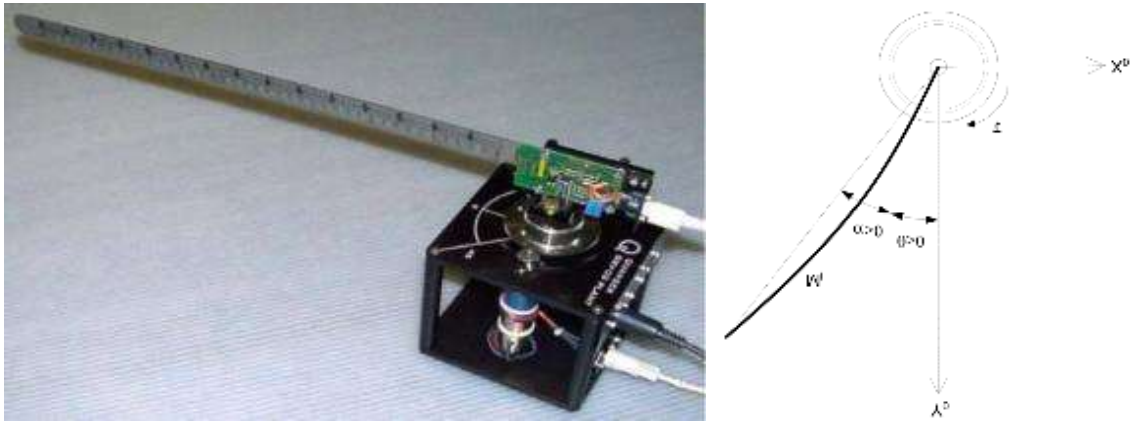


Figure 23: The realistic model of the flexible link and its schematic of rotary motor [68]

The servo motor will apply variable torques based on input voltage variations. The vibration control entered into this component was investigated, based on the block diagram shown in figure 24, which illustrates the methods of state feedback control and LQR.

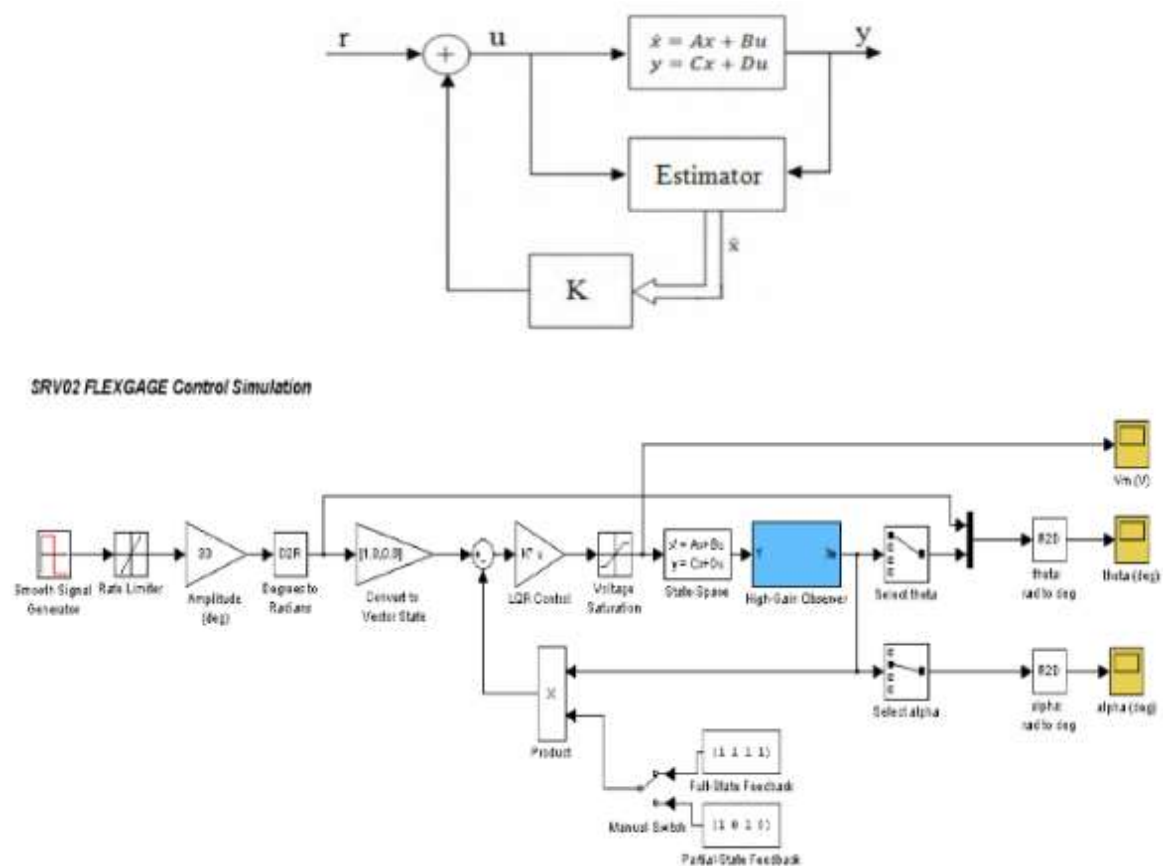


Figure 24: Block diagram of state feedback control and LQR[68]

In order to implement and test two methods of control, various simulations have been performed. In figure 25, the left diagram shows the output of the system based on the state

feedback controller and on the right it shows that of the LQR controller and a reference angle of $\theta(t)$. As shown in the figure, the system responses show less vibration based on the LQR controller and show better performance than state feedback controllers.

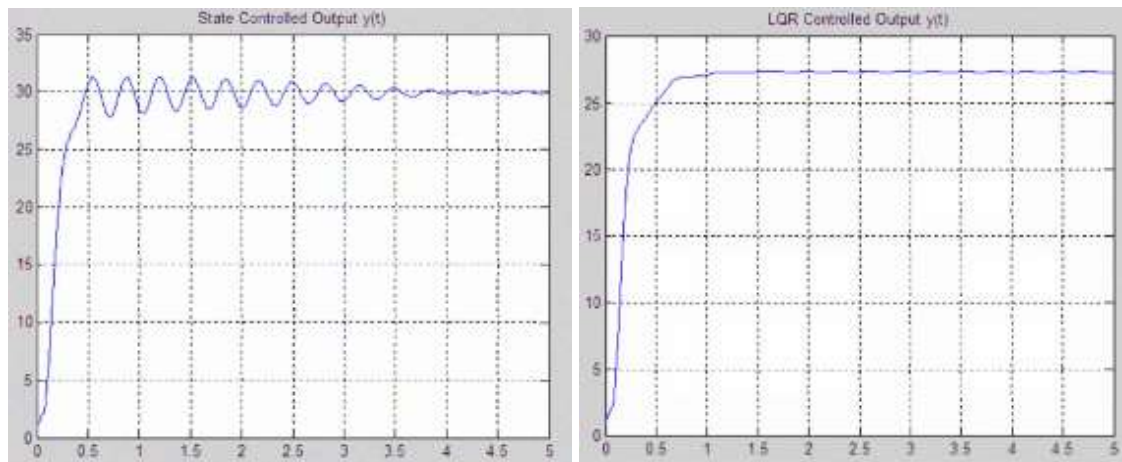


Figure 25: System responses based on LQR and state feedback controllers [68]

In another study, (Zimmert et al.) [69] analysed the vibrations of the forklift mast system. An active damper was used as the main servo in this research. Then, in order to track the optimal movement path and to reduce the vibrations of the forklift mast, the design of two feedback and feedforward controllers was considered. Figure 26 shows the schematic of the forklift system and the location of the strain gauge sensor.

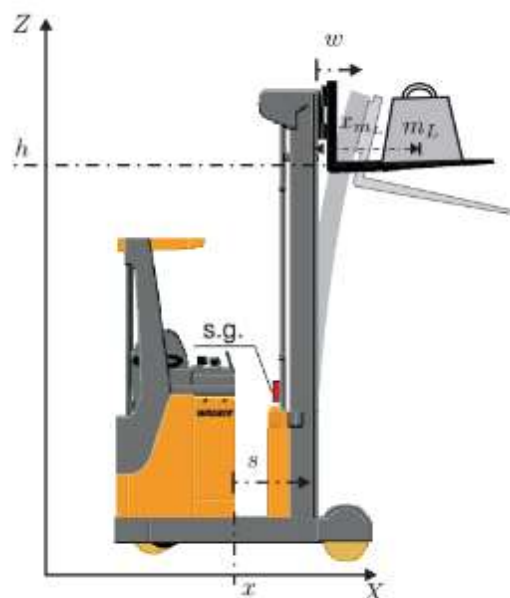


Figure 26: Schematic of the forklift system and location of the strain gauge sensor [69]

Also in Fig. 27, the block diagram of the feedback and feedforward controllers used in this study is shown.

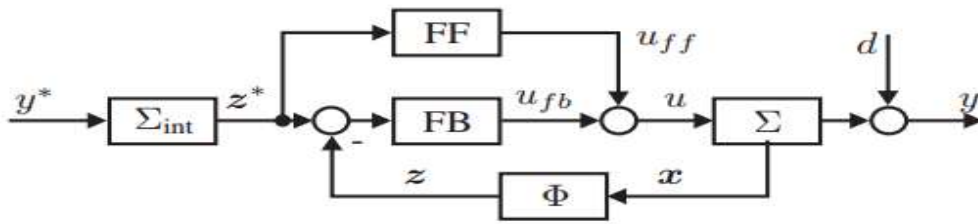


Figure 27: Block diagram of the feedback and feedforward controllers [69]

With the design of the controllers previously discussed, the performance of the system is examined based on the results of the movement of the forklift mast unit and the tracking of the desired route by it. In Fig. 27, the deformation diagram of the forklift mast unit is shown in braking mode (left side figure) and normal mode (right side figure) based on the output of the strain gauge sensor. The forklift mast unit performs preferably in the presence of the active damper control system.

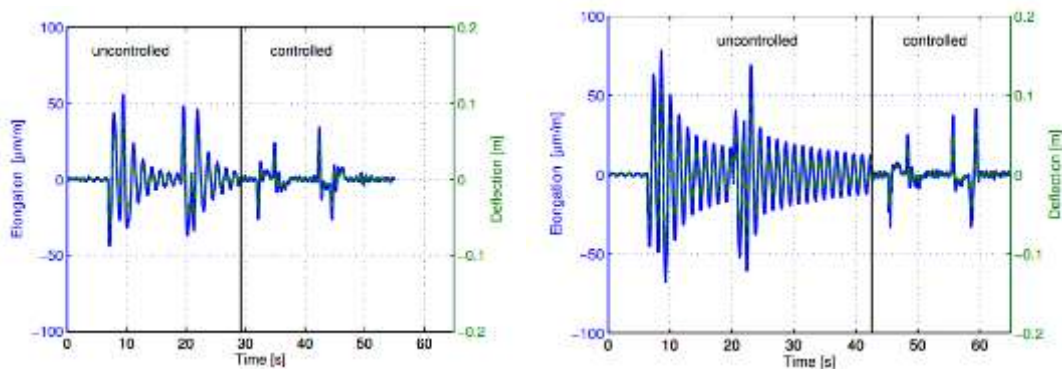


Figure 28: Deflection diagram of the forklift mast unit without braking (left side figure) and with braking (right side figure) [69]

Also, in the same research, the results of tracking the longitudinal speed of the forklift system are discussed. In Figure 29, the performance of the control system is shown by tracking the output of the forklift longitudinal speed and the input of the control system.

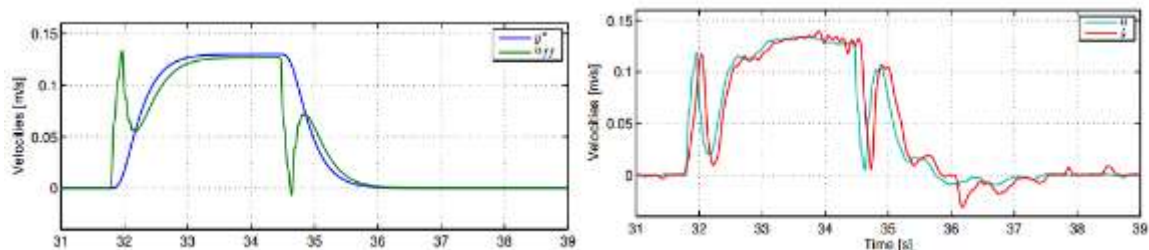


Figure 29: Control system performance based on the output of forklift's longitudinal speed and input of control system [69]

In another study by (Zhang et al.), to optimize the dynamical performance of the forklift mast unit, its efficiency has been investigated [70]. In this study, seven principles have been used for the optimization process including The Principle of Highest Modal Frequency, The Lowest Gravity Structure, Frequency Uniform Distribution, The Principle of Equal-stiffness, The Principle of Avoiding Natural frequency and excitation, Frequency Superposition, The Principle of Main Force Direction and Main Stiffness Superposition and The Principle of the Centre of Mass near the Constraint. Also, to determine the optimization process settings, the two factors of Flexibility and Distribution of Damping were used to investigate this relationship.

In Fig. 30, some of the simulation results of the process for forklift mast unit optimization is presented.

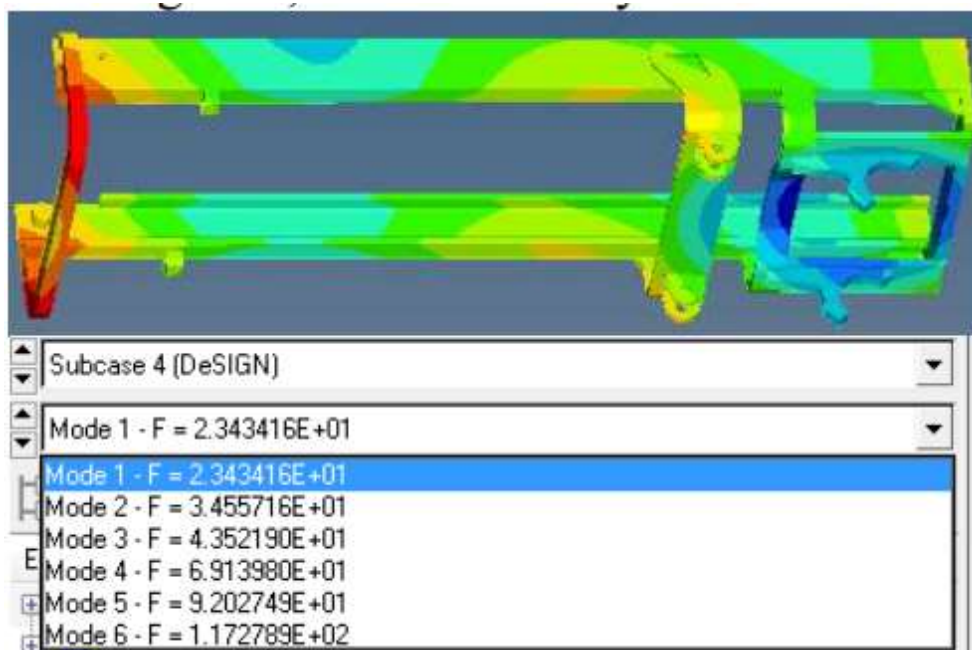


Figure 30: Simulation results of the process for the forklift mast unit optimization. [70]

To further examine the vibration reduction methods in the forklift mast section, an invention was investigated (EP 2 038 202 B1.) [71]. In this report, researchers examined the model of a forklift system to investigate the shape of the vibrational modes of the forklift mast unit. In this method the critical characteristics of mast structure is measured and computed and some of these details are fed into the computing system in advance. Then the lowest natural frequency of the mast and the phase of vibration is computed from the collected data, and the order for movement is obtained from the driver or master system. The movement guidance to the speed

controller is generated from above mentioned characteristics of the vibration. The order for movement is divided into two parts (impulses I), and the actuator is controlled with speed controller for moving the truck or load onto the truck according to the order for movement. Fig. 30 shows a schematic representation of three lowest natural frequencies that can be generated in the mast structure. Mass (load) is described as a square 11 at the top of the mast 12. Also the mass of mast 12 has to be included in the calculations of the natural frequencies of the structure. Another characteristic that is influencing on the natural frequencies is the stiffness of mast structure (spring rate K) and damping constant (c) (partly built in the structure and also including air drag). The most important frequency is the lowest natural frequency (left figure). [71]

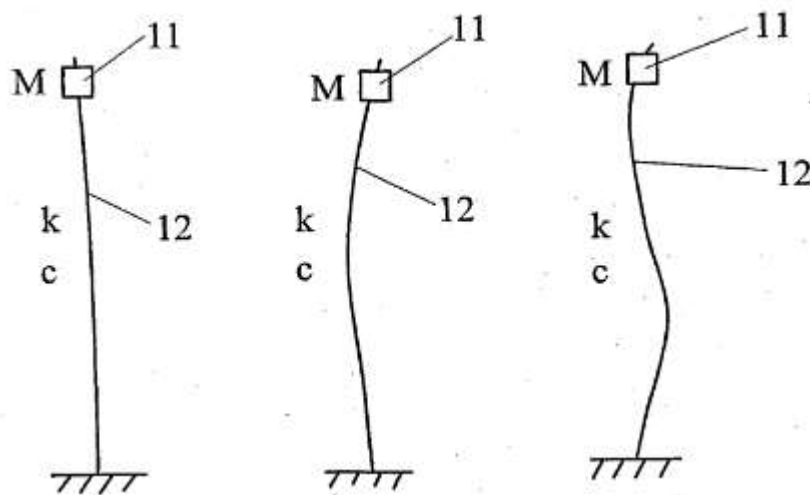


Figure 31: Three lowest natural frequencies that can be generated in the mast structure.[71]

Also, this report presented two prior strategies for reducing the structure vibration of mast based on active controller, as shown in Fig. 31.

Based on the diagram given in Fig. 31, first the lowest natural frequency and phase of the system is considered based on the dynamics of the system. Then the order of movement is obtained from driver or master system, the critical characteristics are fed into the computing system, the movement guidance to the speed controller is generated from above mentioned characteristics of the vibration, and finally the actuator is controlled with speed controller for moving the mast according to the order for movement.

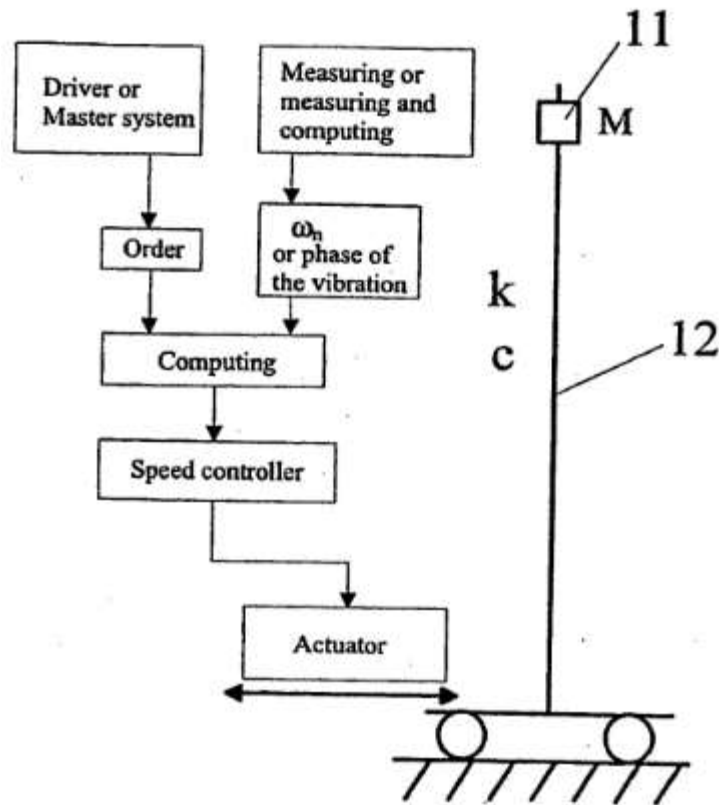


Figure 32: Mast vibration reduction method based on the research in [71]

Also other inventions have been investigated (EP0427001A1, DE4019075A1 and GB2379434). In these inventions, researchers presented passive damping systems with separate dampers assembled between the truck mast and the truck body. These systems are quite similar, only difference being the position of the damper system. In GB2379434A researchers presented a mass-damper system for controlling the vibration of structure. Figure 32 is related to EP0427001A1, DE4019075A1, which are described in two passive damping control. In figure 32a the mast structure 12 is isolated and the vibrations are damped with a damper 13. Load 11 is situated at the top of the mast 12. In figure 32b is presented schematically a dynamic mass damper system. The balancing mass (m) and the damper 12 are situated to the top of the mast. This solution to reduce vibration is fixed to certain mass (M) and to certain height of mast 12. In both figures M is a mass, c is a damping factor and K is a spring factor. [72,73]

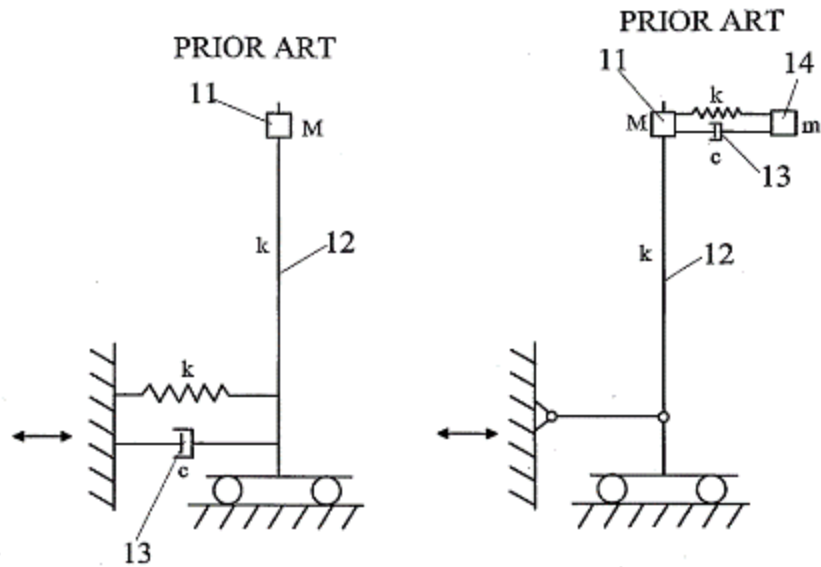


Figure 33: Passive control of mast vibration a (left) and b [72,73]

Further invention (DE3617026) has been conducted on the mast of forklift vibration, which proposed a brake system disposed below the pivot bearing, to dampen the vibration of the mast between fixed forklift parts where mast is mounted onto the base.[74]

Also another invention (US4082199A) proposes a stabilizer that is provided for the mast of a lift truck for resisting torsional forces applied to the elevating system as the lift truck changes altitude. The stabilizer includes a pair of "A" frames with the apexes of the frames pivotally secured together. The spaced legs of the frames are connected, in the case of the one "A" frame, to the respective uprights of the mast and, in the case of the other "A" frame, to the vehicle chassis. The connections between the "A" frames, the mast and the vehicle chassis are such that the forward and backward tilt of the mast is not restricted; instead twisting forces between the mast and the chassis are restrained. [75]

2.6) Comparative analysis of the previous studies

Based on the literature presented in this chapter, the research on the vibrations of the forklift system can be summarised as follows:

Body and the seat: Research in this field is based on the measurement of the frequency and the vibrating modes that use numerical methods as well as experimental tests. The numerical methods described in this section include the finite element method (Nguyen et al.) and the Newton-Euler methods based on the rigid mass dynamics (Ventura et al.). Also, some researchers compared two different types of seats based on air and mechanical suspension system to reduce vibration entered into the driver's body (Blood et al.).

Forklift mast section:

Research in this area was also based on mast specifications (Zhang et al.) and the design of different controllers to reduce the vibrations of this unit. (Zimmert et al.) designed feedback and feedforward controllers based on the state feedback technique for an active damper that detects the longitudinal speed of the system and reduces the vibration of the Forklift mast. (Baroudi's) presented two LQR and state feedback controllers for a torsional active damper, designed to reduce the range of vibrations of an operator's arm. The system outputs provided a better performance of the LQR controller. Also, in the report related to the invention, the design of a speed controller is based on the frequency and phase of the Forklift mast sector, and the design system can also prevent the fluctuations of the system by changing its condition.

On the other hand, due to the vibrations of smart beams and the similarity of cantilever beams with the structure of the forklift mast system, beam vibration theories can be used for modelling the vibration behaviour. However, it is important to note that, despite advances in electronic and mechanical engineering technologies and the availability of different electronic components, the application of vibration control techniques for these structures is hindered due to the following reasons:

1. These systems are quite sophisticated, costly and in many cases must compete with semi-active and passive systems.
2. It is difficult to adjust electronic components, sensors and actuators.
3. These systems are limited to a specific frequency band called bandwidth and can depreciate vibrations and disturbances within this limit; but in most cases, they enhance vibrations out of this limit.

Therefore, according to what is mentioned above and especially the cost of smart large-scale beams, the vibration control of the load-bearing structure is not economically feasible. Therefore, although it is possible to use intelligent beam methods to control the vibrations of these structures, these methods are not used for the purpose of this study. To this end, in order to control the costs of the manufacturing process and to increase the efficiency of the system, a semi-active control system is used to reduce the vibration of the mast. Therefore, the additional costs of intelligent and active systems are avoided and additional and complex systems can be removed from the forklift system.

Whilst taking into account the advantages and disadvantages of the various control systems as stated in this chapter, reducing the vibration of the Forklift mast based on the semi-active control methods sounds appealing. Accordingly, in this research, by controlling and guiding the damper forces in a forklift system, the effect of this system on reducing the vibration of the forklift mast sector is addressed.

Dynamic modelling of the forklift mast based on the movement variable of the forklift system and the fluctuation angle of the mast is carried out in order to extract the movement equations, whilst considering the damper force input and the state variables associated with the position and longitudinal speed of the forklift system, as well as the angular position of the forklift mast, and its rate.

In the current study, a robust controller is developed based on robust control theories to improve the fluctuation performance of the forklift mast unit. In order to apply the force proposed by the previous step of the control method, a PID controller is designed to control the flow of the inlet and outlet valves in cylinder system. Then, by setting the parameters of the control method, its performance is studied based on different conditions. It is believed that this research can lead to the improvement of the dynamic behaviour of the forklift mast system. Moreover, due to the adoption of semi-active control systems, it does not cost extra to the manufacturers and consumers.

In order to achieve the above-mentioned goal, in the first step, numerical modelling of the forklift system based on the vibration of the forklift mast part is carried out. For this purpose, the vibrational relations of the system based on energy rules are extracted, and then the numerical dynamic problem solving step using the MATLAB / SIMULINK software is conducted. The experimental results are examined and the performance of the control system is discussed. For this purpose, a 3D modelling of the forklift mast system is initially considered. Then a sample of the 3D model is made using existing materials. The fluctuations of the mast sector in different situations with different controllers are measured using different sensors aided with MATLAB and LabVIEW software tools .

The materials related to the extraction of vibrational relations and numerical modelling of the forklift system, as well as the design and implementation of the control system will be described in chapter 4.

Chapter 3 Numerical analysis

Highlights:

- ❖ System movement Equations
- ❖ The D'Alembert's principle
- ❖ Modelling of forklift system
- ❖ System control equations
- ❖ Dampers equations

This chapter consists of all numerical equations related to the forklift's mast and beam, along with explanations of the different control systems and validation of the model. Also the analytical techniques used throughout this research to reduce vibration of forklift's mast are described.

3.1) The system movement equations

Since vibration can be considered as a conversion between kinetic energy and potential energy, a vibrating system must have the means to store and release both types of energy. Kinetic energy storage and release are usually done with the help of mass and potential energy, as well as, springs, or change in position of the centre of mass relative to the direction of acceleration of the centre of gravity. Therefore, the main components of vibrations are not the presence of inertia and elastic elements such as mass and spring. In order to study the vibrations of a dynamic system, the degrees of freedom for the system must be determined in advance. The degrees of freedom in a vibration system equals the minimum number of coordinates required to fully determine the movement of all components of the system at any given time.

In order to extract the amplitude of the system fluctuations as well as the natural frequencies, based on theoretical methods, the system's equations of movement are needed. On the other hand, there are several methods for extracting the movement equations, including the Newton method and the energy method. In the Newton method, based on the free diagram of the system components and the removal of constraint forces, the equations of the system motions are extracted, which is difficult to implement for complex systems with high degrees of freedom. On the other hand, in the energy method, the kinetic energy and system potential and their changes are calculated. This method is explained in the following section, as it is used for deriving the vibrational equations of the forklift mast system in this study.

3.1.1) Energy method

An energy method, as an alternative to the Newton one, can be used to study the vibration of dynamic systems. It should be noted that the Newton method is based on the Newton's second law, whilst the energy method is based on the energy consistency law. To understand the energy method, the equilibrium of a dynamic system needs to be explained. The virtual work principle, which is in fact a statement of the equilibrium definition for a dynamical system, is also examined. This principle is the basis of the energy method for analysing a dynamic system. In the following, we first outline the virtual work principle for the static state of a dynamic system, and then it is generalised to the dynamic state.

The virtual movements of a dynamic system are defined as infinitely small and intentional variations in the system's coordinates. These changes are extremely small, so the physical friction of the system is maintained. Also, the discretion of these changes shows that they are

not real movements and do not change over time. If the \mathbf{R} system's displacement is in terms of n then the generalized coordinates q_i ($i=1,2,\dots,n$) are as follows:

$$\mathbf{r}_k = \mathbf{r}_k(q_1, q_2, \dots, q_n) \quad \text{Equation 5}$$

In this case, virtual displacements are displayed by δq_i ($i=1,2,\dots,n$). The sign δ is used to discriminate between differential symbols of d or ∂ . These virtual displacements are small changes to the actual situation of the system, but should be compatible with the system constraints. For example, an equilibrium pendulum can be considered. For virtual adaptations to be compatible with the constraints, one can only consider the small angle variations, and the pendulum cannot be bent or moved up and down.

3.1.2) Virtual work principle

For a system with n degrees of freedom in static equilibrium, all forces that affect the degrees of freedom of k in the system (\mathbf{R}_k) can be divided into two categories according to the following equation: One associated with the external forces (\mathbf{F}_k) and the other with the forces of the constraint (\mathbf{f}_k):

$$\mathbf{R}_k = \mathbf{F}_k + \mathbf{f}_k \quad \text{Equation 6}$$

The real (and not virtual) displacement of the k^{th} component of the system in terms of generalized coordinates is:

$$\mathbf{r}_k = \mathbf{r}_k(q_1, q_2, \dots, q_n, t) \quad \text{Equation 7}$$

And the work done by all forces during the virtual moves of $\delta \mathbf{r}_k$ ($k=1,2,\dots,n$) will be as follows:

$$\delta W = \sum_{k=1}^n \mathbf{R}_k \cdot \delta \mathbf{r}_k \quad \text{Equation 8}$$

On the other hand, in a conservative system, constrain forces do not do any work during virtual transitions. Therefore, the principle of virtual work points out that the system is in equilibrium if and only if the total works done by external forces during displacement equals zero:

$$\delta W = \sum_{k=1}^n \mathbf{F}_k \cdot \delta \mathbf{r}_k = 0 \quad \text{Equation 9}$$

The virtual work can also be expressed in terms of generalized coordinates. Accordingly, the movement \mathbf{r}_k can be obtained as follows:

$$\delta \mathbf{r}_k = \sum_{i=1}^n \frac{\partial \mathbf{r}_k}{\partial q_i} \delta q_i \quad \text{Equation 10}$$

In this formula, the time variable t does not exist because the virtual movement does not change over time. Therefore, virtual work is achieved in accordance with the following equation:

$$\delta W = \sum_{k=1}^n \mathbf{F}_k \cdot \delta \mathbf{r}_k = \sum_{k=1}^n \sum_{i=1}^n \mathbf{F}_k \cdot \frac{\partial \mathbf{r}_k}{\partial q_i} \delta q_i \quad \text{Equation 11}$$

By adding plus marks the following equation can be obtained:

$$\delta W = \sum_{k=1}^n \mathbf{F}_k \cdot \delta \mathbf{r}_k = \sum_{i=1}^n \sum_{k=1}^n \mathbf{F}_k \cdot \frac{\partial \mathbf{r}_k}{\partial q_i} \delta q_i \quad \text{Equation 12}$$

The generalized force is also defined as follows:

$$\mathbf{Q}_i = \sum_{k=1}^n \mathbf{F}_k \cdot \frac{\partial \mathbf{r}_k}{\partial q_i} \quad (i=1,2,\dots,n) \quad \text{Equation 13}$$

Finally, the principle of virtual work is described with the aid of the analytic relationship as shown below:

$$\delta W = \sum_{i=1}^n \mathbf{Q}_i \delta q_i = 0 \quad (i=1,2,\dots,n) \quad \text{Equation 14}$$

This relationship means that for a static equilibrium system, the virtual work done by all generalised forces during virtual displacement is zero. Since virtual displacements (δq_i) associated with the q_i component are optional, it can be concluded that:

$$Q_i = 0 \quad (i=1,2,\dots,n)$$

Equation 15

In other words, in a system that is statically balanced, all the generalized forces associated with the selected virtual displacements are equal to zero.

3.2) Modelling of a forklift system

As outlined in the introduction chapter, forklift systems consist of several sections, each of which plays a certain role. In this section, the simplified dynamic model of the forklift system is discussed. For this purpose, the relationship between the location and velocity of the mass centres of different parts of the forklift system are examined based on a reference framework. This is used to calculate the kinetic and potential energies based on the vibrations of the forklift mast system. Then, the Lagrangian relations will be extracted based on the vibrations and displacement of the forklift mast system using the input of the control forces of the cylinders, as well as the vibrational equations of the system. In Figure 34, a forklift system produced by the Yale Corporation is shown.



Figure 34: A forklift system produced by the Yale Corp.

A simplified model of the system is presented to investigate the positions and velocities of the mass centres. For this purpose, a schematic model of the forklift system during load movement is developed, as shown in figure 34.

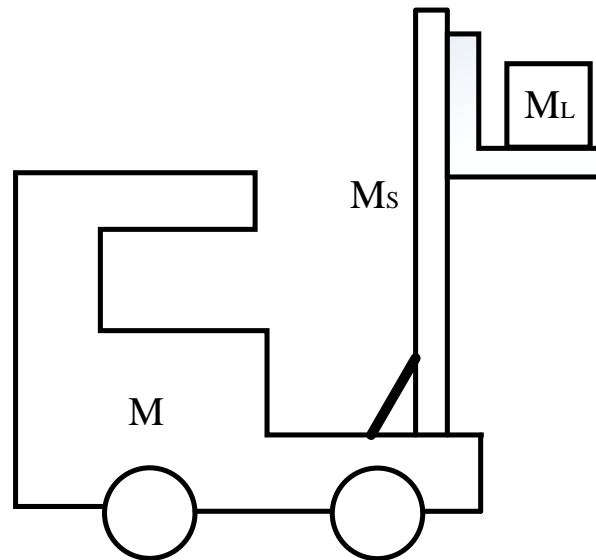


Figure 35: A schematic model of the forklift system during load movement

In order to utilize the forklift system model more efficiently to derive the vibrational equations, the simplification of the model in Fig. 35 is investigated. Because of the importance of the vibrations of the mast and the low importance of the other components, other parts are simplified and a simple two-axle cart is considered. In Fig. 36, the simplified schematic model of the forklift system presented is shown.

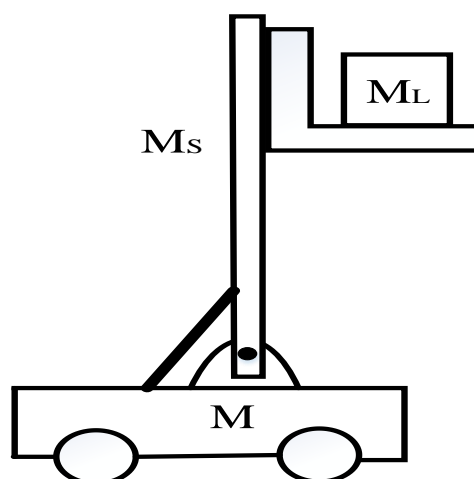


Figure 36: Simplified schematic model of the forklift mast

Furthermore, the schematic model presented in Figure 36 is used to derive the equations of the system movements. In this way, with the movement of the cart, the vibration of the mast sector

can be increased. Thus kinetic and potential energies of the system are calculated based on these vibrations. In Fig. 37, the simplified model of the movement of the forklift mast part is shown. In the next section, the dynamic relations of the forklift mast sector will be extracted based on the above-mentioned model.

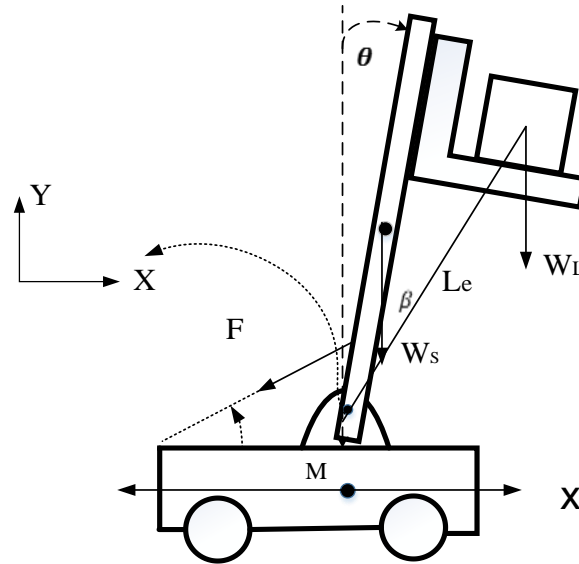


Figure 37: Simplified model of the movement of the forklift mast

3.2.1) The kinetic energy of the system

The kinetic energy of the entire forklift system can be calculated based on the linear and rotational movements derived from the vibration of the forklift mast unit according to the model presented in Fig. 36, as follows:

$$E_K = \frac{1}{2}M\dot{x}^2 + \frac{1}{2}M_s v_s^2 + \frac{1}{2}M_L v_L^2 + \frac{1}{2}j\dot{\theta}^2 \quad \text{Equation 16}$$

Where M is the mass of the forklift without its mast mass, M_s is the mast's mass, and M_L is the mass of load sitting on the mast. Also V_s and V_L are the velocity of the mass centres of the forklift mast and load, respectively, which can be found by the kinetic relationships of the vectors in terms of the two variables X and θ . Also, x denotes the longitudinal velocity of the forklift system, while j denotes the polar inertia of the total load and the mast around the joint attached to the floor of the forklift system.

According to the figure 37 and the positioning relationship at the mass centres of the load and forklift mast, the velocities v_s and v_l are calculated as follows:

$$S = (X_S, Y_S) = (x + l_s \sin \theta, l_s \cos \theta) \quad \text{Equation 17}$$

$$L = (X_L, Y_L) = \left(x + \frac{l_2}{2} + l_e \sin(\theta + \beta), l_e \cos(\theta + \beta) \right) \quad \text{Equation 18}$$

Where β denotes the angle between the contour of the joint and the centre of mass (l_e) with the vertical axis. The length l_2 is also the length of the bearing, on which the load is placed, and l_1 is the vertical distance between the joint and the bearing. By achieving derivatives of the displacements calculated above, the velocity of the mass centre for the mast unit is calculated, as follows:

$$v_{x_s} = \dot{x} + l_s \dot{\theta} \cos \theta \quad \text{Equation 19}$$

$$v_{y_s} = -l_s \dot{\theta} \sin \theta$$

Based on the following equation, the velocity of the mass centre for the mast unit is obtained as follows:

$$v_s^2 = v_{x_s}^2 + v_{y_s}^2 = \dot{x}^2 + l_s^2 \dot{\theta}^2 + 2\dot{x}l_s \dot{\theta} \cos \theta \quad \text{Equation 20}$$

Also, by repeating the above steps, the velocity of the mass centre of the load in the directions of the axes x and y are calculated as follows:

$$v_{x_L} = \dot{x} + l_e \dot{\theta} \cos(\theta + \beta) \quad \text{Equation 21}$$

$$v_{y_L} = -l_e \dot{\theta} \sin(\theta + \beta)$$

The quantity of the velocity of the centre of the load is obtained via:

$$v_L^2 = v_{x_L}^2 + v_{y_L}^2 = \dot{x}^2 + l_e^2 \dot{\theta}^2 + 2\dot{x}l_e \dot{\theta} \cos(\theta + \beta) \quad \text{Equation 22}$$

By replacing the relations (18 and 20) in (15), the kinetic energy of the system is obtained as follows:

$$E_K = \frac{1}{2}M_s(\dot{x}^2 + l_s^2\dot{\theta}^2 + 2\dot{x}l_s\dot{\theta}\cos\theta) + \frac{1}{2}M_L(\dot{x}^2 + l_e^2\dot{\theta}^2 + 2\dot{x}l_e\dot{\theta}\cos(\theta + \beta)) + \frac{1}{2}M\dot{x}^2 + \frac{1}{2}j\dot{\theta}^2 \quad \text{Equation 23}$$

3.2.2) System potential energy:

The potential energy of a forklift system includes gravity potential energy, which can be determined by the vibrational motion of the forklift mast unit and the vertical displacement of the mass centres of these two units as follows:

$$E_q = M_sgl_s\cos\theta + M_Lgl_e\cos(\theta + \beta) \quad \text{Equation 24}$$

3.3) Equations of the system movements

The kinetic and potential energies extracted in the previous section are used to derive the equations of the system movements. Thus, in the first step, the calculation of the Lagrangian function is carried out based on the subtraction of kinetic energy from the potential energy of the system as follows:

$$L = \frac{1}{2}M_s(\dot{x}^2 + l_s^2\dot{\theta}^2 + 2\dot{x}l_s\dot{\theta}\cos\theta) + \frac{1}{2}M_L(\dot{x}^2 + l_e^2\dot{\theta}^2 + 2\dot{x}l_e\dot{\theta}\cos(\theta + \beta)) + \frac{1}{2}M\dot{x}^2 + \frac{1}{2}j\dot{\theta}^2 - M_sgl_s\cos\theta - M_Lgl_e\cos(\theta + \beta) \quad \text{Equation 25}$$

Then, the Lagrangian partial derivatives are calculated based on two variables $\theta(t)$ and $x(t)$. Initially, the Lagrangian partial derivatives are calculated based on the $q_1(t) = \theta(t)$ equation as follows:

$$\frac{\partial L}{\partial \dot{\theta}} = M_sl_s^2\dot{\theta} + M_sl_s\dot{x}\cos\theta + M_Ll_e^2\dot{\theta} + M_L\dot{x}l_e\dot{\theta}\cos(\theta + \beta) + j\dot{\theta} \quad \text{Equation 26}$$

The following relationship is obtained using the time derivation:

$$\begin{aligned} \frac{d}{dt} \left(\frac{\partial L}{\partial \dot{\theta}} \right) &= M_s l_s^2 \ddot{\theta} + M_s l_s \ddot{x} \cos \theta - M_s l_s \dot{x} \dot{\theta} \sin \theta + M_L l_e^2 \ddot{\theta} + M_L l_e \ddot{x} \cos(\theta + \beta) \\ &- M_L l_e \dot{x} \dot{\theta} \sin(\theta + \beta) + j \ddot{\theta} \end{aligned} \quad \text{Equation 27}$$

Then by derivation of the Lagrangian function to the θ variable, the following equation is obtained:

$$\frac{\partial L}{\partial \theta} = -M_s l_s \dot{x} \dot{\theta} \sin \theta + M_s g l_s \sin \theta - M_L l_e \dot{x} \dot{\theta} \sin(\theta + \beta) + M_L g l_e \sin(\theta + \beta) \quad \text{Equation 28}$$

By repeating the above steps, the Lagrangian partial derivatives based on the $q_2(t) = x(t)$ variable is calculated as follows:

$$\frac{\partial L}{\partial \dot{x}} = (M + M_s + M_L) \dot{x} + M_s l_s \dot{\theta} \cos \theta + M_L l_e \dot{\theta} \cos(\theta + \beta) \quad \text{Equation 29}$$

The following relationship is extracted using the time derivation:

$$\begin{aligned} \frac{d}{dt} \left(\frac{\partial L}{\partial \dot{x}} \right) &= (M + M_s + M_L) \ddot{x} + M_s l_s \ddot{\theta} \cos \theta - M_s l_s \dot{\theta}^2 \sin \theta + M_L l_e \ddot{\theta} \cos(\theta + \beta) \\ &- M_L l_e \dot{\theta}^2 \sin(\theta + \beta) \end{aligned} \quad \text{Equation 30}$$

Then by derivation of the Lagrangian function to the x variable the following equation is obtained:

$$\frac{\partial L}{\partial x} = 0 \quad \text{Equation 31}$$

In order to calculate the right-hand side of the Lagrangian equation, for both the $\theta(t)$ and $x(t)$ variables, the displacement of the cylinder connection point with the forklift mast unit body is measured. Subsequently, the cylinders force in two horizontal and vertical directions are analysed through extracting the final relation.

$$\vec{r}_c = (x + l_c \sin \theta) \hat{i} + l_c \cos \theta \hat{j} \quad \text{Equation 32}$$

Then, the partial derivatives of \vec{r}_c , to the degrees of freedom is carried out:

$$\delta r_c = \frac{\delta r_c}{\delta \theta} \delta \theta + \frac{\delta r_c}{\delta x} \delta x = (l_c \cos \theta \delta \theta + \delta x) \hat{i} - l_c \sin \theta \delta \theta \hat{j}$$

$$\vec{F} = |\vec{F}| (\cos(\theta_c) \hat{i} + \sin(\theta_c) \hat{j}) \quad \text{Equation 33}$$

Then, the right side of the Lagrangian relationship is calculated using the force of the cylinders:

$$\delta W = \sum_{i=1}^n F_{q_i} \delta q_i \quad \text{Equation 34}$$

The following relationships are also used to calculate cylinder work force

$$\begin{aligned} \delta W &= \vec{F} \cdot \delta r_c = |\vec{F}| (\cos(\theta_c) \hat{i} + \sin(\theta_c) \hat{j}) \cdot ((l_c \cos \theta \delta \theta + \delta x) \hat{i} - l_c \sin \theta \delta \theta \hat{j}) \delta W \\ &= (|\vec{F}| l_c \cos \theta \cos(\theta_c) - |\vec{F}| l_c \sin \theta \sin(\theta_c)) \delta \theta + (|\vec{F}| \cos(\theta_c)) \delta x \end{aligned}$$

$$\text{Equation 35}$$

On this basis, F_{q_1} and F_{q_2} are obtained via simplifying the above equations:

$$F_{q_1} = |\vec{F}| l_c \cos(\theta + \theta_c)$$

$$F_{q_2} = |\vec{F}| \cos(\theta_c) \quad \text{Equation 36}$$

By placing the equation (34) in the Lagrangian formula, the equations of the system movement are derived from the two variables θ (t) and x (t):

$$\begin{aligned} M_s l_s^2 \ddot{\theta} + M_s l_s \dot{x} \cos \theta - M_s l_s \dot{\theta} \sin \theta + M_L l_e^2 \ddot{\theta} + M_L l_e \dot{x} \cos(\theta + \beta) \\ - M_L l_e \dot{\theta} \sin(\theta + \beta) + j \ddot{\theta} + M_s l_s \dot{x} \sin \theta - M_s g l_s \sin \theta + M_L l_e \dot{x} \sin(\theta + \beta) \\ - M_L g l_e \sin(\theta + \beta) = |\vec{F}| l_c \cos(\theta + \theta_c) \\ (M + M_s + M_L) \ddot{x} + M_s l_s \ddot{\theta} \cos \theta - M_s l_s \dot{\theta}^2 \sin \theta + M_L l_e \ddot{\theta} \cos(\theta + \beta) \\ - M_L l_e \dot{\theta}^2 \sin(\theta + \beta) = |\vec{F}| \cos(\theta_c) \end{aligned}$$

$$\text{Equation 37}$$

By simplifying the above relationships, a simplified version of the system movement equation is obtained:

$$\left\{ \begin{array}{l} (M_s l_s^2 + M_L l_e^2) \ddot{\theta} + (M_s l_s \cos \theta + M_L l_e \cos(\theta + \beta)) \ddot{x} - (M_s g l_s \sin \theta \\ \quad + M_L g l_e \sin(\theta + \beta)) = F(t) l_c \cos(\theta + \theta_c) \\ (M_s l_s \cos \theta + M_L l_e \cos(\theta + \beta)) \ddot{\theta} + (M + M_s + M_L) \ddot{x} - \\ \quad (M_s l_s \dot{\theta}^2 \sin \theta + M_L l_e \sin(\theta + \beta)) \dot{\theta}^2 = F(t) \cos(\theta_c) \end{array} \right. \quad \text{Equation 38}$$

In order to simplify the relations further and to design the controller, the system equations are formulated in the following format:

$$\begin{aligned} \alpha_1 \ddot{\theta} + \beta_1 \ddot{x} + f_1 &= g_1 \\ \beta_1 \ddot{\theta} + \alpha_2 \ddot{x} + f_2 &= g_2 \end{aligned} \quad \text{Equation 39}$$

According to the elimination rules of the Algebra, independent equations for $\ddot{\theta}$ and \ddot{x} are obtained. This can be done via multiplying the first equation by $(-\alpha_2)$ and multiplying the second equation by β_1 :

$$\begin{aligned} -\alpha_2 \alpha_1 \ddot{\theta} - \alpha_2 \beta_1 \ddot{x} - \alpha_2 f_1 &= -\alpha_2 g_1 \\ \beta_1^2 \ddot{\theta} + \beta_1 \alpha_2 \ddot{x} + \beta_1 f_2 &= \beta_1 g_2 \end{aligned} \quad \text{Equation 40}$$

Then these two equations has been add up to extract equations for each $\ddot{\theta}$ and \ddot{x} :

$$\begin{aligned} \ddot{\theta} &= \frac{(\alpha_2 f_1 - \alpha_2 g_1 + \beta_1 g_2 - \beta_1 f_2)}{\beta_1^2 - \alpha_2 \alpha_1} \\ \ddot{x} &= \frac{(\beta_1 g_2 - \beta_1 f_2)(\beta_1^2 - \alpha_2 \alpha_1) - \beta_1^2 (\alpha_2 f_1 - \alpha_2 g_1 + \beta_1 g_2 - \beta_1 f_2)}{(\beta_1^2 - \alpha_2 \alpha_1) \beta_1 \alpha_2} \end{aligned} \quad \text{Equation 41}$$

The block diagram of relation (38), simulated by the Simulink / MATLAB software is shown in figure 38.

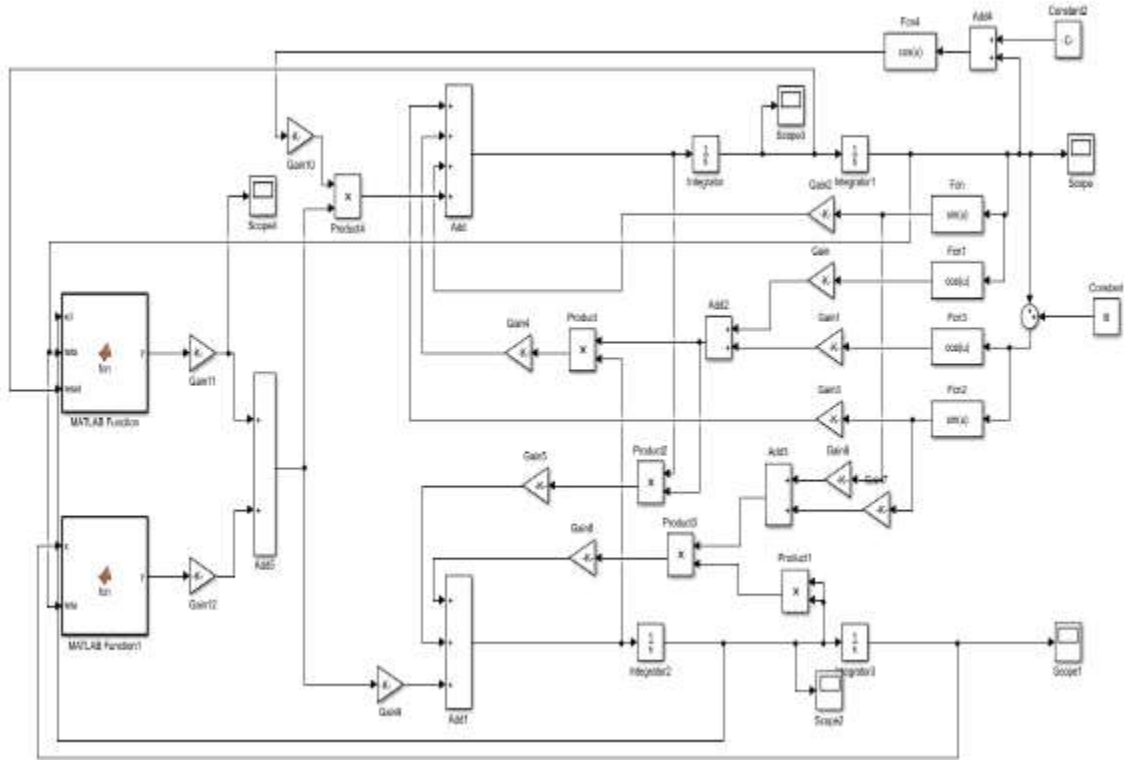


Figure 38: Block diagram of a two-degree freedom vibrational model from the movement of the forklift mast system in the Simulink / MATLAB software .

3.4) A linear model around the operating point

Assuming that the changes in the angle θ around the operating point $\theta_0 = 0$ are small, one can derive the linear motion equations of the system. Therefore:

$$\cos\theta \approx 1$$

$$\sin\theta \approx 0$$

Accordingly, the equations of the system movement around the work point can be simplified as follows:

$$\begin{cases} (M_s l_s^2 + M_L l_e^2) \ddot{\theta} + (M_s l_s + M_L l_e (1 - \sin(\beta))) \ddot{x} \\ - M_s g l_s \theta + M_L g l_e (\theta \cos\beta + \sin\beta) = l_c (1 - \sin(\beta)) F(t) \\ (M_s l_s + M_L l_e (1 - \sin(\beta))) \ddot{\theta} + (M + M_s + M_L) \ddot{x} = F(t) \cos(\theta_c) \end{cases} \quad \text{Equation 42}$$

The inertial torque J can be calculated according to the following equation:

$$J = \frac{M_L l_e^2}{12} + \frac{M_s l_s^2}{3} \quad \text{Equation 43}$$

As can be seen from the above equation, the system can be described using a 2nd degree differential equation. Similarly, the system state vector can be considered as:

$$x = [\theta \ \dot{\theta} \ x \ \dot{x}]^T$$

$$\cos\theta \simeq 1$$

$$\sin\theta \simeq 0$$

3.5) Equations of the system with one degree of freedom

With Regards to the equations (38) and (39), in the case of modelling of the forklift system with mast part and two degrees of freedom, in both nonlinear and linear modes, the variable θ depends on the displacement variable and its derivatives. On the other hand, considering the fact that the aim of the current research is to reduce the vibrations of the forklift mast unit, the degree of freedom related to the longitudinal movement of the forklift system can be ignored. The same issue can be seen in the design and implementation of controllers. So if controller design is aimed for a system with two degrees of freedom, variable measurement sensors are required. This solution will bring both cost-inefficiency and an adverse effect on the control model in terms of speed and precision.

In the following, the vibrational equations of the forklift mast system is studied based on the elimination of the variable x from its motion equations. The schematic model shown in figure 39 is used to extract dynamic relationships and to implement the controller.

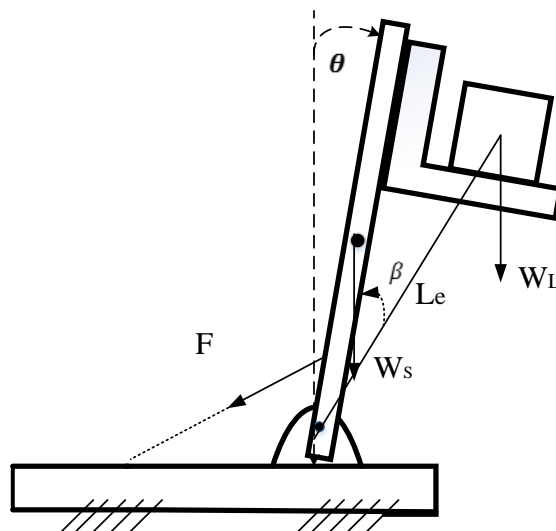


Figure 39: simplified schematic model with one degree of freedom to extract the dynamic equations of the system

To derive system equations based on the variable θ and its derivatives, the Lagrangian relation is simplified based on the elimination of the variable x . As a result, the following Lagrangian relationship is obtained:

$$L = \frac{1}{2}M_s l_s^2 \dot{\theta}^2 + \frac{1}{2}M_L l_e^2 \dot{\theta}^2 + \frac{1}{2}j_s \dot{\theta}^2 - M_s g l_s \cos\theta - M_L g l_e \cos(\theta + \beta) \quad \text{Equation 44}$$

Its derivatives are also extracted as follows:

$$\frac{\partial L}{\partial \theta} = M_s g l_s \sin\theta + M_L g l_e \sin(\theta + \beta)$$

$$\frac{\partial L}{\partial \dot{\theta}} = M_s l_s^2 \dot{\theta} + M_L l_e^2 \dot{\theta} + j_s \dot{\theta}$$

$$\frac{d}{dt} \left(\frac{\partial L}{\partial \dot{\theta}} \right) = M_s l_s^2 \ddot{\theta} + M_L l_e^2 \ddot{\theta} + j_s \ddot{\theta} \quad \text{Equation 45}$$

Also, the work of the external forces obtained in the previous section are simplified:

$$\delta W = \vec{F} \cdot \delta r_c = -|\vec{F}|(\cos(\theta_c) \hat{i}$$

$$+ \sin(\theta_c) \hat{j}) \cdot ((l_c \cos\theta \delta\theta) \hat{i} - l_c \sin\theta \delta\theta \hat{j})$$

$$\delta W = -(|\vec{F}| l_c \cos\theta \cos(\theta_c) - |\vec{F}| l_c \sin\theta \sin(\theta_c)) \delta\theta \quad \text{Equation 46}$$

The equivalent force relations and the derivatives can be inserted into the Lagrangian equation:

$$M_s l_s^2 \ddot{\theta} + M_L l_e^2 \ddot{\theta} + j_s \ddot{\theta} - M_s g l_s \sin\theta - M_L g l_e \sin(\theta + \beta)$$

$$= -|\vec{F}| l_c \cos\theta \cos(\theta_c) + |\vec{F}| l_c \sin\theta \sin(\theta_c) \quad \text{Equation 47}$$

Then, in order to continuously stimulate the forklift mast system, a horizontal force is introduced at a given distance, with the vector defined as follows.

$$\vec{F}_e = |\vec{F}_e| \hat{i} \quad \text{Equation 48}$$

Considering its work, its effect on the equations of motion of the system can be applied as follows:

$$\begin{aligned}
 & M_s l_s^2 \ddot{\theta} + M_L l_e^2 \ddot{\theta} + j_s \ddot{\theta} - M_s g l_s \sin \theta - M_L g l_e \sin(\theta + \beta) \\
 & = -|\vec{F}| l_c \cos \theta \cos(\theta_c) + |\vec{F}| l_c \sin \theta \sin(\theta_c) + |\vec{F}_e| l_c \cos \theta
 \end{aligned}
 \tag{Equation 49}$$

The input control variable $u = |\vec{F}|$ is replaced, and then the above-mentioned relation can be simplified:

$$\ddot{\theta} = \left(\frac{1}{M_s l_s^2 + M_L l_e^2 + j_s} \right) \begin{bmatrix} M_s g l_s \sin \theta + M_L g l_e \sin(\theta + \beta) + |\vec{F}_e| l_c \cos \theta \\ -l_c \cos(\theta + \theta_c) u \end{bmatrix}
 \tag{Equation 50}$$

3.5) Space state equations of the system

The system form of the space state can be obtained by defining the following variables state.

$$x_1 = \theta$$

$$x_2 = \dot{\theta}$$

On this basis, the system equations can be rewritten as follows:

$$\dot{x}_1 = x_2$$

$$\dot{x}_2 = f + bu
 \tag{Equation 51}$$

By extracting f and u from the dynamics of the system, the following equations are obtained.

$$\begin{aligned}
 f & = \left(\frac{M_s g l_s \sin \theta + M_L g l_e \sin(\theta + \beta) + |\vec{F}_e| l_c \cos \theta}{(M_s l_s^2 + M_L l_e^2 + j_s)} \right) \\
 b & = \frac{l_c \cos(\theta + \theta_c)}{(M_s l_s^2 + M_L l_e^2 + j_s)}
 \end{aligned}
 \tag{Equation 52}$$

3.6) System control

In this section, the vibration control of the system based on the dynamics equations extracted in the previous stage is dealt with. Thus, in the first step, two LQR and sliding mode controllers are presented as cylinder controllers. For this purpose, they are presented with a method for their implementation, as well as an examination of the control input applied to the system cylinders. Then a PID controller is provided to control the inlet and outlet valves of the cylinders. For this purpose, at first the governing relationship between the electro-hydraulic

control valves based on the input electric flow and the output fluid is extracted. Then a PID controller is designed to control the cylinder force based on the amount of inlet and outlet fluid. The desired cylinder power is also obtained in the design stage of the high-level system control based on two LQR modes and a sliding mode. With feedback from this level of power, the input and output values will be calculated. By simulating the vibrating model of the forklift mast system using the controllers, the adjustment for the values of these controllers is achieved.

3.6.1) LQR controller

This method of control for linear systems can be accomplished in different ways. At best, the subject of this design can be defined in the form of dynamic optimization and optimized controlling, which can be solved using the LQR approach. The LQR controller used in this study consists of two feed-forward and feed-backward compensators, which respectively provide the desired response and the error between the optimal and actual response of the system to reduce the vibrations of the forklift mast system. In order to design the controller, the tracking error can be defined as:

$$e_l = x_l - x_r \quad \text{Equation 53}$$

With the derivation of the above relation and placing it in the right expression in the system's state-space dynamic ($\dot{x}_l = A_l x_l + B_l u_l$), the differential equation governing the tracking error can be expressed as:

$$\begin{aligned} \dot{e}_l &= \dot{x}_l - \dot{x}_r = A_l x_l - A_l x_r + B_l u_l - \dot{x}_r + A_l x_r \\ &= A_l (x_l - x_r) + B_l u_l - \dot{x}_r + A_l x_r \\ &= A_l e_l + B_l u_l - \dot{x}_r + A_l x_r \end{aligned} \quad \text{Equation 54}$$

Now the control input can be defined as two parts of the feed-forward and feed-backward as follows:

$$u_l = u_{ff} + u_{fb} \quad \text{Equation 55}$$

In the above relationship, u_{ff} is the input of feed-forward and u_{fb} is the feed-backward input.

Placing (51) in (50) results in the following equation:

$$\dot{e}_l = A_l e_l + B_l u_{fb} + B_l u_{ff} - \dot{x}_r + A_l x_r \quad \text{Equation 56}$$

Accordingly, the input control of feed-forward is defined as follows:

$$u_{ff} = B_l^{-1}(\dot{x}_r - A_l x_r) \quad \text{Equation 57}$$

It should be noted that the matrix B_l is not a square one and B_l^{-1} is its pseudo inverse one that is used to calculate the feed-forward's input. Now, by combining (56) and (57), the equation of error mode is expressed in the conventional form as follows:

$$\dot{e}_l = A_l e_l + B_l u_{fb} \quad \text{Equation 58}$$

The u_{fb} feedback control is determined using the optimal control rule. The optimal feed-backward control input can be obtained when minimizing the following functional index:

$$J = \int_0^{\infty} (e_l^T Q_l e_l + u_{fb}^T R_l u_{fb}) dt \quad \text{Equation 59}$$

In the above equation, Q_l is a positive-definite (or semi-definite) symmetric matrix, and R_l is a positive-definite symmetric matrix. By adjusting the Q_l matrix entries, the priority of adjusting each control variables can be changed in order to achieve the proper dynamic response of the joint machine. Also, by setting the R_l entries, restrictions on the control operators can be considered. Finally, the control input is defined as follows:

$$u_{fb} = -K_l e_l$$

$$K_l = R_l^{-1} B_l^{-1} P_l \quad \text{Equation 60}$$

P_l is the response to the following Riccati equation:

$$A_l^T P_l + P_l A_l - P_l B_l R_l^{-1} B_l^T P_l + Q_l = 0 \quad \text{Equation 61}$$

The block diagram of the LQR controller based on the feedback on the state variables of θ is shown in Figure 40 where θ is considered on the basis of zero reference values.

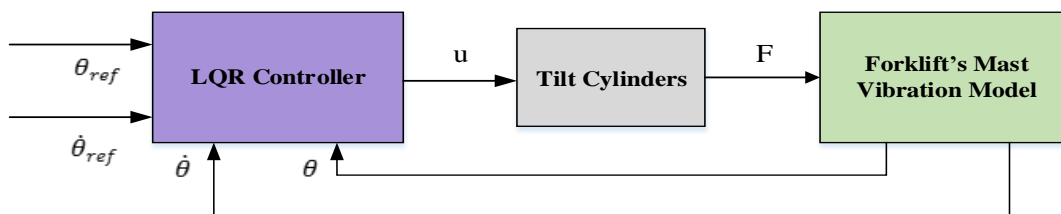


Figure 40: Block diagram of the LQR controller based on the vibration model of the forklift mast unit

3.6.2) Sliding mode controller

Sliding mode control is a nonlinear control system containing remarkable properties of accuracy, robustness, and easy tuning. SMC is intended to drive the system states onto a specific surface in the state space.

Inaccuracy in modelling can have serious adverse effects on nonlinear systems. Therefore, any practical plan should explicitly address this. The structure of a resistant controller consists of a nominal part, similar to feedback, that aims to counteract the modelled uncertainties.

A simple method for resistant controlling is what is known as a sliding mode control method. The basis of this method is the concept that, instead of general systems of n-order, the first-order systems (whether non-linear or indefinite) are controlled; therefore the simplicity allows n-order problems to be replaced with their equivalent first-order problems. Then it can be shown that for transformed problems, the "complete" function can be achieved in principle with the desired inaccuracy of the parameter. But such a performance is achieved at a great price for controlling activities. This is typically in contradiction with other sources of modelling uncertainty. An example is the presence of neglected dynamics, which may stimulate a lot of control activities. This leads us to the best of the control rules, with a reasonable control activity, by obtaining a compromise between the tracking function and the parameter uncertainty.

Sliding controller designs are a legitimate way to keep the stability and performance consistency in facing the inaccuracies of modelling. In addition, by allowing the compromise between modelling and performance to be simply quantified, the whole design process can be illuminated. The next sections provide different ways to design a robust sliding mode controller.

3.6.2.1) The first SMC method

The dynamic equation of the system is considered as follows:

$$\dot{x} = f_0[x] + \delta_1(x) + G(x)[u + \delta_2(x, u)] \quad \text{Equation 62}$$

where $x \in R$ is the state and $u \in R^P$ is the control input. On the other hand, assuming that f_0 and G are known, and δ_1 and δ_2 are uncertainty terms, then δ_2 and δ_1 are defined as compatible and incompatible uncertainties, respectively. Considering the change in the following variables:

$$\begin{bmatrix} \eta \\ \xi \end{bmatrix} = T(x)$$

The system equations can be calculated as follows:

$$\dot{\eta} = f(\eta, \xi) + \delta_{\eta}(\eta, \xi)$$

$$\dot{\xi} = f_a(\eta, \xi) + G_a(\eta, \xi)[u + \delta_{\xi}(\eta, \xi, u)] \quad \text{Equation 63}$$

Where ξ is the control input. , we want to find the feedback control of the stabilizer state $\xi = \phi(\eta)$ with the conditions of $\phi(0) = 0$ so that it forms the origin of the asymptotic stable system.

$$\dot{\eta} = f(\eta, \phi(\eta)) + \delta_{\eta}(\eta, \phi(\eta))$$

Subsequently, by defining the variable $z = \xi - \phi(\eta)$ and checking the condition $z = 0$, we can conclude that $\xi = \phi(\eta)$ and the variable η asymptotically approaches to the centre. In this approach, the control u is designed in such a way that z approaches to zero at a finite time, and then maintains the conditions for $z = 0$ in all future moments, thus $z = 0$ would be in the form of a positive stable closed-loop system. To achieve this goal, the equation z is presented as follows:

$$\dot{z} = \dot{\xi} - \dot{\phi}(\eta) = f_a(\eta, \xi) + G_a(\eta, \xi)[u + \delta_{\xi}(\eta, \xi)] - \frac{\partial \phi}{\partial \eta} [f(\eta, \xi) + \delta_{\eta}(\eta, \xi)] \quad \text{Equation 64}$$

And u signal is also considered as follows:

$$u = u_{eq} + G_a^{-1}(\eta, \xi)v = G_a^{-1}(\eta, \xi) \left[-f_a(\eta, \xi) + \frac{\partial \phi}{\partial \eta} f(\eta, \xi) \right] - G_a^{-1}(\eta, \xi) \frac{\beta(G_a^{-1}(\eta, \xi))}{1 - k} \text{sgn}(z) \quad \text{Equation 65}$$

u_{eq} is chosen so that the definite terms in the right side of the equation (61) are eliminated, that is:

$$u_{eq} = G_a^{-1}(\eta, \xi) \left[-f_a(\eta, \xi) + \frac{\partial \phi}{\partial \eta} f(\eta, \xi) \right] \quad \text{Equation 66}$$

u_{eq} Controlling element is called equivalent control. In the absence of uncertainty, and by choosing $u = u_{eq}$, then $z = 0$, which guarantees the survival of the condition $z = 0$ at all times.

$$\dot{z} = v + G_a(\eta, \xi)\delta_\xi(\eta, \xi, u_{eq} + G_a^{-1}(\eta, \xi)v) - \frac{\partial\phi}{\partial\eta}\delta_\eta(\eta, \xi)$$

$$\Delta(\eta, \xi, v) = G_a((\eta, \xi)\delta_\xi(\eta, \xi, u_{eq} + G_a^{-1}(\eta, \xi)v) - \frac{\partial\phi}{\partial\eta}\delta_\eta(\eta, \xi)) \quad \text{Equation 67}$$

Assuming that Δ holds in the following inequality:

$$\|\Delta(\eta, \xi, v)\|_\infty \leq \rho(\eta, \xi) + k\|v\|_\infty, \forall[\eta, \xi, v] \quad \text{Equation 68}$$

Where $\rho(\eta, \xi) \geq 0$ and it is a continuous function. Also $K \in [0, 1]$, and both of them are known. Using $V = \frac{1}{2}z^2$ as the candidate of the Lyapunov function, it can be re-written as:

$$\dot{V} = z\dot{z} = zv + z\Delta(\eta, \xi, v) \leq zv + |z|[\rho(\eta, \xi) + k\|v\|_\infty] \quad \text{Equation 69}$$

Where v can be considered as:

$$v = -\frac{\beta(\eta, \xi)}{1-K} \text{sgn}(z)$$

$$\beta(\eta, \xi) \geq \rho(\eta, \xi) + b, \forall(\eta, \xi) \in D \quad \text{Equation 70}$$

where b is positive and $\text{sgn}()$ is also the non-linearity of the sign; therefore:

$$\begin{aligned} \dot{V} &\leq zv + |z|[\rho(\eta, \xi) + k\|v\|_\infty] \\ &\leq -\frac{\beta(\eta, \xi)}{1-K}|z| + \rho(\eta, \xi)|z| + \frac{k\beta(\eta, \xi)}{1-K}|z| \\ &= -\beta(\eta, \xi)|z| + \rho(\eta, \xi)|z| \leq -b|z| \end{aligned} \quad \text{Equation 71}$$

One of the zig-zag elimination methods is the use of continuous approximation for a discontinuous sliding mode controller. Using this approximation, one can also avoid theoretical problems caused by discontinuous controllers. To this end, the nonlinear sign can be

approximated with a saturated gradient linear sign. Therefore, the slippery mode control components are described as follows:

$$\begin{aligned}
 v &= -\frac{\beta(\eta, \xi)}{1-K} \text{sgn}(z) \\
 &= -\frac{\beta(\eta, \xi)}{1-K} \text{sgn}\left(\frac{z}{\varepsilon}\right)
 \end{aligned}
 \tag{Equation 72}$$

Where the saturation function is considered with the following approximation.

$$\text{sat}(y) = \begin{cases} y & \text{if } |y| \leq 1 \\ \text{sgn}(y) & \text{if } |y| \geq 1 \end{cases}
 \tag{Equation 73}$$

3.6.2.2) The second SMC method

Assuming that the dynamic equation is a single-input dynamic system, it is defined as follows:

$$x^{(n)} = f(x) + b(x)u
 \tag{Equation 74}$$

Where the scalar u is the control input and $x = [x \ \dot{x} \ \dots \ x^{(n-1)}]^T$ is the state vector. The control problem is to find the state of x such that a variable state at a given time follows $x = [x_d \ \dot{x}_d \ \dots \ x_d^{(n-1)}]^T$ with the presence of error in $f(x)$ and $b(x)$. The tracking error in the variable x is defined as $X = X - X_d$, which is simplified as follows:

$$\tilde{X} = x - x_d = [\tilde{x}, \dot{\tilde{x}}, \dots, \tilde{x}^{(n-1)}]^T = [x - x_d, \dot{x} - \dot{x}_d, \dots, x^{(n-1)} - x_d^{(n-1)}]^T
 \tag{Equation 75}$$

Where \tilde{X} is the tracking error vector. Furthermore, the scalar equation $s(x, t) = 0$ is defined while considering a variable surface with the time $S(t)$ in the state space $R^{(n)}$:

$$s(\dot{x}, t) = \left(\frac{d}{dt} + \lambda\right)^{n-1} \tilde{x}
 \tag{Equation 76}$$

Where λ is a strongly positive constant. Given the dynamics of the system based on the equation (51) as well as the point that the dynamics of f (possibly nonlinear or variable with time) would

not exactly be definite, but estimated as \hat{f} , it is assumed that the estimation error of f is a definite function of $F = F(X, \dot{X})$:

$$|\hat{f} - f| \leq F \quad \text{Equation 77}$$

So that the control gain b (possibly variable with time or state dependent) is indefinite, but with certain limits (this itself is possibly variable with time or state dependent).

$$0 \leq b_{min} \leq b \leq b_{max}$$

Since the control input in the dynamics appears as a result of multiplication, it is natural that the estimation of \hat{b} and gain of b are considered as the geometric mean of the above limits.

$$\hat{b} = (b_{min} b_{max})^{1/2} \quad \text{Equation 78}$$

These limits can be written as follows:

$$\beta^{-1} = \sqrt{\frac{b_{min}}{b_{max}}} \leq b^{-1} \hat{b} = \frac{\sqrt{b_{min} b_{max}}}{b} \leq \sqrt{\frac{b_{max}}{b_{min}}} = \beta \quad \text{Equation 79}$$

Because the control law is designed in a way that it is resistant to the multiplied uncertainty, β is considered as the marginal gain of design. From now on, the control rule is defined as follows:

$$u = \hat{b}^{-1} [u_{eq} - K sgn(s)] \quad \text{Equation 80}$$

Which stipulates the sliding condition. By expanding above equation A and calculating the time derivation, the following equation is obtained:

$$\begin{aligned} \dot{s} &= f + bu - \ddot{x}_d + \lambda \dot{\tilde{x}} \\ &= f - b\hat{b}^{-1}\hat{f} + b\hat{b}^{-1}\ddot{x}_d - \ddot{x}_d - b\hat{b}^{-1}\lambda(\ddot{x} - \ddot{x}_d) + \lambda(\dot{x} - \dot{x}_d) - b\hat{b}^{-1}Ksgn(s) \end{aligned} \quad \text{Equation 81}$$

given that K must meet the following condition

$$\begin{aligned}
 K &\geq (b\hat{b}^{-1})^{-1} [|f - b\hat{b}^{-1}\hat{f} + b\hat{b}^{-1}\ddot{x}_d - \ddot{x}_d - b\hat{b}^{-1}\lambda(\dot{x} - \dot{x}_d) + \lambda(\dot{x} - \dot{x}_d)| + \eta] \\
 &= |b^{-1}\hat{b}f - \hat{f} + (1 - b^{-1}\hat{b})\ddot{x}_d - (1 - b^{-1}\hat{b})\lambda(\dot{x} - \dot{x}_d) + \eta b^{-1}\hat{b}| \\
 &= |b^{-1}\hat{b}(f - \hat{f}) + (1 - b^{-1}\hat{b})[-\hat{f} + \ddot{x}_d - \lambda(\dot{x} - \dot{x}_d)]| + \eta b^{-1}\hat{b}
 \end{aligned} \tag{Equation 82}$$

And so the control discontinuity has been increased to take into account the uncertainty in control gain of b. Meanwhile, to select the control signal the following condition should be met:

$$\frac{1}{2} \frac{d}{dt} s^2 = \dot{s}s \leq -\eta|s| \tag{Equation 83}$$

This relationship also leads to the stability of the Lyapunov function.

3.6.2.3) SMC implementation

In this section, with the definition of the controller's goal, based on the reduction of the forklift mast unit vibrations, the sliding mode controller design is discussed. First a sliding surface is defined by considering the dynamic equations of the system as well as the control objective of the problem:

$$S(x_1, x_2) = x_2 + \lambda x_1 \tag{Equation 84}$$

By using derivation from this level of the sliding surface, the following equation is obtained:

$$\dot{S} = \dot{x}_2 + \lambda \dot{x}_1 \tag{Equation 85}$$

By placing the dynamics of the system in the above equation, the relationship between the time variations of the sliding surface based on the problem-state variables can be re-written as follows:

$$\begin{aligned}
 \dot{S} &= f + bu + \lambda x_2 = \left(\frac{M_s g l_s \sin(x_1) + M_L g l_e \sin(x_1 + \beta) + |\vec{F}_e| l_c \cos(x_1)}{(M_s l_s^2 + M_L l_e^2 + j_s)} \right) \\
 &\quad - \left(\frac{l_c \cos(x_1 + \theta_c)}{(M_s l_s^2 + M_L l_e^2 + j_s)} \right) u + \lambda x_2
 \end{aligned} \tag{Equation 86}$$

On the other hand, taking into account the definite uncertainties of f and b , the input control can be re-written as follows:

$$u = \hat{b}^{-1} [u_{eq} - K \text{sgn}(s)] \quad \text{Equation 87}$$

where:

$$u_{eq} = \hat{f} + \lambda x_2$$

$$= \left(\frac{M_s g l_s \sin(x_1) + M_L g l_e \sin(x_1 + \beta) + |\vec{F}_e| l_c \cos(x_1)}{(M_s l_s^2 + M_L l_e^2 + j_s)} \right) + \lambda x_2 \quad \text{Equation 88}$$

Therefore, the input of the controller is:

$$u = \left(\frac{(M_s l_s^2 + M_L l_e^2 + j_s)}{l_c \cos(x_1 + \theta_c)} \right) \left[\left(\frac{M_s g l_s \sin(x_1) + M_L g l_e \sin(x_1 + \beta) + |\vec{F}_e| l_c \cos(x_1)}{(M_s l_s^2 + M_L l_e^2 + j_s)} \right) + \lambda x_2 - K \text{sgn}(x_2 + \lambda x_1) \right] \quad \text{Equation 89}$$

where λ is a characteristic of the damping coefficient on the sliding surface, which is considered to be positive. Also, K indicates the speed of movement towards the sliding surface. By simulating the dynamics of the system and defining the input control of u in the Simulink/MATLab software, the results of the designed controller tests can be examined and the appropriate coefficients of λ and K based on the appropriate responses can be obtained. It should be noted that in the above relations, $|\vec{F}_e|$ is a limited disturbance that will be investigated in different situations. The block diagram of the system with a sliding mode controller is illustrated in figure 41.

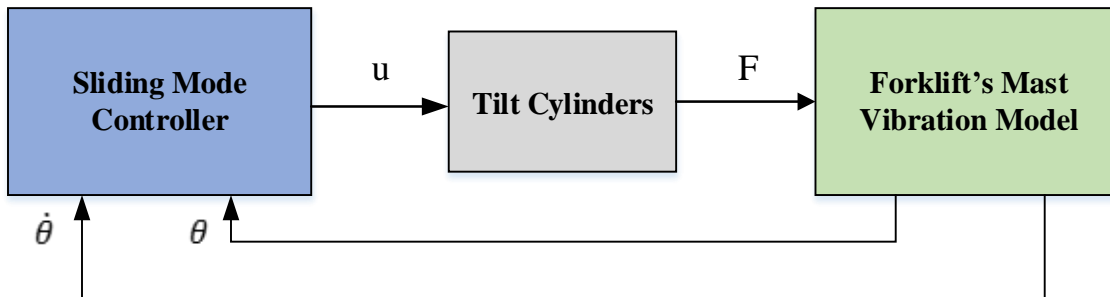


Figure 41: Sliding mode controller diagram block based on a vibration model of forklift mast

3.6.3) PID controller

PID controllers are one of the most widely used controllers in the industry, owing to their design simplicity, proper sustainability and quick response in systems. This controller is of several types based on their implementation and function.

The basic rules and equations around PID and their tuning system have been explained in detail in the first chapter. This controller consists of three parts: proportional (to increase the system response speed), integrator (to reduce the error of the permanent state) and a derivative (to reduce the fluctuations of the system response). PID is used to control the input and output valves of the two cylinders. So, after implementing the cylinders control of the system, using two methods LQR and SMC, the desired force of the cylinders is calculated during vibration of the forklift mast unit. Then, based on a closed loop method in real time, the inlet and outlet valves to the cylinders are controlled by a PID controller to reach the desired cylinder power.

3.6.3.1) Electro-Hydraulic Control Valve

Electro-Hydraulic Control Valve is a hydraulic valve that measures the oil flow in response to an electric inlet signal in order to control the position, pressure, and even power in a various range of vehicles and types of equipment. Electro-Hydraulic Control Valves are closed-circuit control devices that can be designed in one, two, or three ways. In these kinds of valves, a servo engine controls the discharge amount. A servo valve is an electric valve that is under permanent control and itself controls the position, discharge, velocity, and pressure of the operators according to the received feedback. The inlet signal that enters the servo valve controls the position and state of the outlet valve opening in both digital and analogue modes. Servo valves accomplish their job with a low level of potential difference or electric level. The signal that controls the inlet affects the coil and moves the spool in the servo valve to discharge a certain amount of fluid. In fact, this valve is under constant control and self-controls pressure, position, discharge, or velocity of the desired machine according to the feedback that it receives. The technology of these types of valves will be more advantageous with greater speed and accuracy.

3.6.3.2) Dampers (cylinders)

Dual channel cylinders which are responsible for vertical displacement of loads are used in this study as dampers. Accordingly, in order to control the vibrations of the forklift mast system,

the control of these two cylinders, which are located on both sides of the mast body, is addressed. To reach this end, the governing relations of reaction force in these cylinders are discussed in this section. In the following, a block diagram based on the relationship of inlet and outlet Electro-Hydraulic Control Valves in the cylinders would be illustrated. A schematic model of a dual-channel cylinder and its simplified model are shown in figure 42.

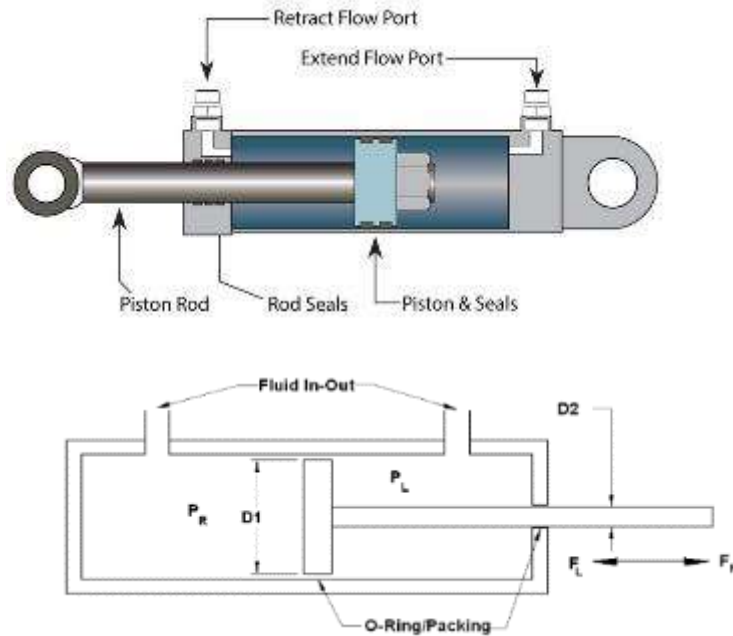


Figure 42: Schematic model of a dual-channel cylinder and its simplified model

In the following, relations related to the forward and backward forces of the current system are presented. Given the figure 43 and geometric characteristics of cylinders and pistons (based on a certain number of each cylinder), the magnitude of the force can be calculated as follows.

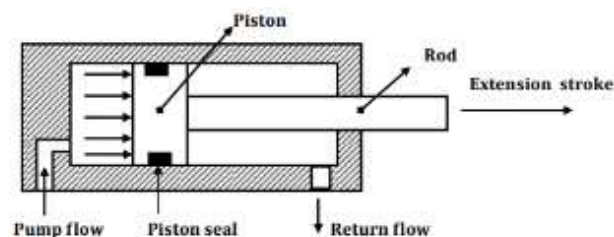


Figure 43: Schematic model of a two-channel cylinder in extension stroke (forward motion)

$$F_R = \left(\frac{\pi D I^2}{4} \right) P_R$$

Equation 90

Also, the generated force in return stroke of the piston as a result of applied pressure is obtained as follows:

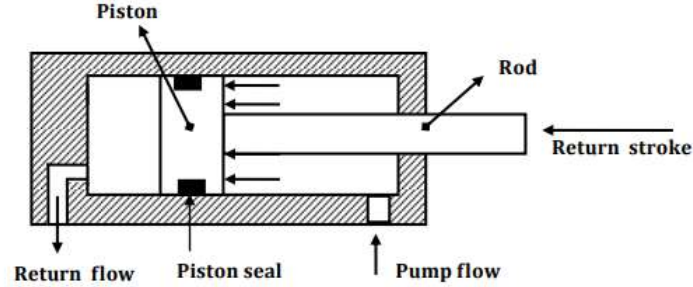


Figure 44: Schematic model of a two-channel cylinder in pressure mode (backward motion)

$$F_L = \frac{\Pi (D1^2 - D2^2) P_L}{4} \quad \text{Equation 91}$$

In the following, the dynamic equations related to servo valves movement are addressed based on the inlet flow. To reach this end, a second order transform function is presented.

Then, by using a block diagram, the procedure to implement the PID controller on the flow of the valves is presented.

$$\frac{d^2 x_v}{dt^2} + 2\zeta_v \omega_v \frac{dx_v}{dt} + \omega_v^2 x_v = \omega_v^2 k_v i_v \quad \text{Equation 92}$$

where x_v , i_v , k_v , ω_v , and ζ_v represent servo valve spool position, the inlet flow of valve from the control unit, the efficiency rate of the valve, natural frequency and damping rate of servo valve, respectively.

$$i_v = \begin{cases} i - I_1 & \text{if } i > I_1 \\ 0 & \text{if } |i| \leq I_1 \\ i + I_1 & \text{if } i < -I_1 \end{cases} \quad \text{Equation 93}$$

Where I_1 refers to the dead zone. Whilst considering the relationship between the flows of servo valves under different assumptions, the flow relations of fluid in both the positive and negative spool displacement states can be obtained as follows.

$$q_f = C_d W x_v \operatorname{sgn}(P_s - P_f) \sqrt{\frac{2}{\rho} |P_s - P_f|}$$

$$q_n = C_d W x_v \operatorname{sgn}(P_n) \sqrt{\frac{2}{\rho} |P_n|}$$

Equation 94

Also, for the spool negative displacement, the following equation can be obtained:

$$q_f = C_d W x_v \operatorname{sgn}(P_f) \sqrt{\frac{2}{\rho} |P_f|}$$

$$q_n = C_d W x_v \operatorname{sgn}(P_s - P_n) \sqrt{\frac{2}{\rho} |P_s - P_n|}$$

Equation 95

Where P_s , ρ , C_d , and W represent supply pressure, the mass density of oil, discharge coefficient of opening, and width of the opening, respectively. In addition, f and n stand for the lateral and total parts of the loop. On the other hand, the force equation for the rod attached to the cylinder can be obtained as follows:

$$F_{R,L} = \begin{cases} (x - x_E) K_p v & \text{if } x > x_E, v > 0 \\ (x - x_R) K_p v & \text{if } x < x_R, v < 0 \\ 0 & \text{otherwise} \end{cases}$$

Equation 96

Where v is the velocity of the rod, K_p penetration coefficient and x is the piston position.

Also x_E and x_R are obtained using the following relationships:

$$x_E = s - x_0$$

$$x_R = -x_0$$

Equation 97

where s represents piston stroke and x_0 is the initial distance of the piston from the input port.

Furthermore, the following relation for v can be used:

$$v = \frac{dx}{dt}$$

Equation 98

In order to alter the force of damper into the desired amount, which has been extracted from LQR and SMC controllers, a PID controller based on the inlet and outlet cylinder valves is used. Accordingly, a PID controller is designed on the basis of defining the tracking error function of the desired force as follows:

$$e(t) = F_d(t) - F_c(t)$$

Equation 99

Also, having in mind the dynamical relations of the servo valve, the inlet of these valves is based on the voltage controlled by the PID controller as follows:

$$v = K_p e(t) + K_i \int e(t) dt + K_D \frac{de(t)}{dt}$$

Equation 100

A schematic illustration of the cylinder position and the connections of the inlet and outlet valves are presented in figure 45.

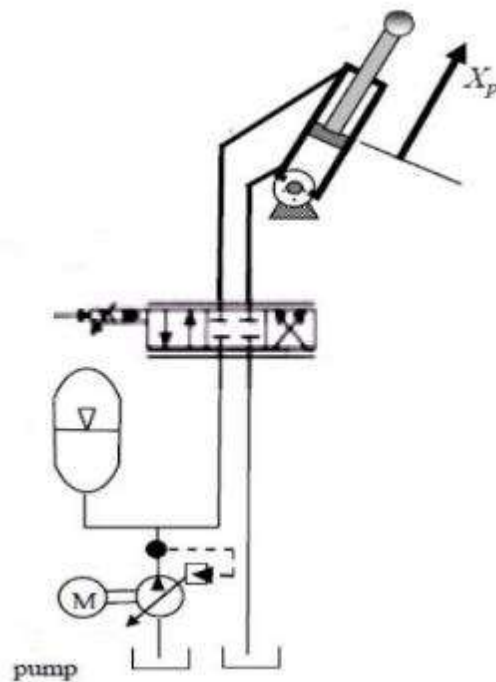


Figure 45: A schematic illustration of the cylinder position and the connections of the inlet and outlet valves

In addition, a block diagram related to a dual-channel hydraulic operator as developed in SIMULINK/MATLAB software, which is based on the existence of the controlling valves and a power source, is exhibited in figure 46.

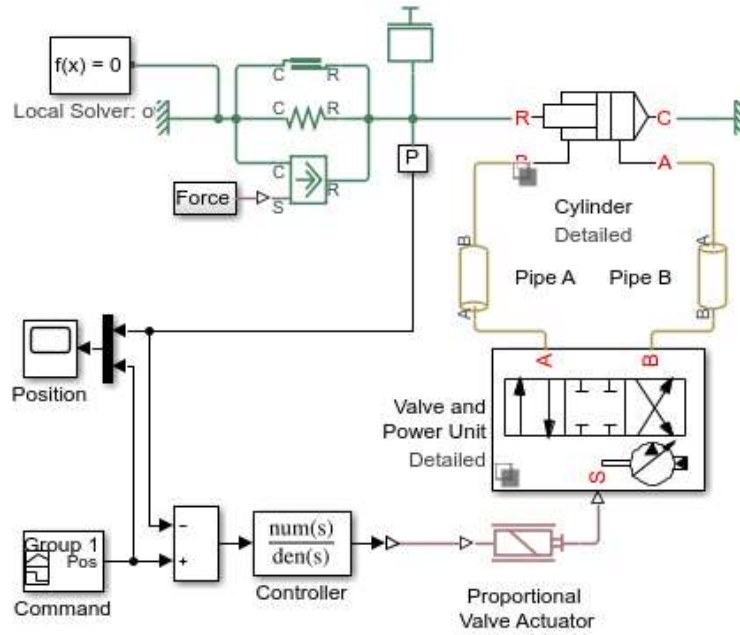


Figure 46: Block diagram related to a dual-channel hydraulic valves operator

A schematic illustration of the block diagram for the final control method of the system is presented in figure 47, which is based on the presence of LQR and SMC cylinder controllers and PID as valves controller

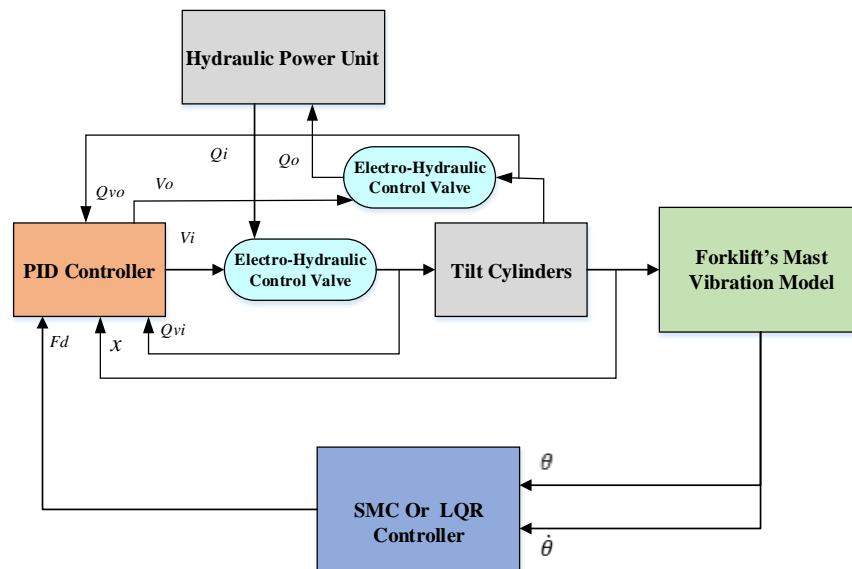


Figure 47: Block diagram for the final control method of the system

3.7)Chapter Conclusion :

The use of numerical methods has led to a tremendous transformation in the development of basic science and engineering theories. Generally, the use of these methods has contributed to major progress in the design and production of structures, in terms of reducing costs and time. In this chapter, in order to study the dynamics of the forklift system, the movement equations of the simplified model are obtained based on the energy methods. The forklift system is simplified and the degrees of freedom of the system are determined, after which kinetic and potential energy equations extracted for the system. Then, considering the forklift mast section's behaviour, the simplification of the motion equations of this section is carried out based on the definition of the output of the vibration angle and the controlling input of the cylinder forces.

By defining the control objectives based on the reduction of vibration in the forklift mast system, as well as specifying the control rules, control this system based on two methods of sliding modes and LQR. Then, by drawing a block diagram of the control methods, the implementation of control systems are presented based on the vibrating equations of the forklift mast system. Finally, the design and implementation of a PID controller is based on the desired outputs of the previous stage for the cylinder valves of the forklift system. The overall implementation of the forklift mast controlling system is proposed to reduce its vibration.

Chapter 4 Experimental setup

Highlights:

- ❖ Sourcing equipment and material
- ❖ Equipment's specifications
- ❖ Labview setup
- ❖ Calibration test
- ❖ Implementing control systems

This chapter is entirely dedicated to explaining the design of forklift, mast and using semi-active control system on a forklift by using hydraulic pump and accelerometer. In order for that, several experimental tests are conducted, which is presented in this chapter. The testing procedures and their standards are comprehensively explained. Their results and effectiveness for using a semi-active controller will be discussed in the next chapter.

4.1) Forklift Body

Hyster Yale forklifts are built from two different types of materials; the chassis (main body) and the mast components. The chassis profiles of the forklift are made from S355 steel, which is a high strength low alloy steel; whilst the mast profiles are cast from HC90 (High Carbon Steel), which has tensile strength of 620 MPa and yield strength of 483MPa, compared to tensile and yield strength of 470MPa and 390MPa for S355 steel, respectively. [76] Although the ideal materials should have been chosen as HC90 and SC355, but due to their unavailability in the project, the most viable alternative materials were found, as listed in table 2.

Table 2: Comparison of alternative Materials

Material	Young's Modulus	Proof Stress, 0.2% offset (recommended)	Other Properties
T6061 – T6 Aluminium	69 GPa	140 MPa	Low density, good corrosion resistance, use structural components
304 Stainless Steel	200 GPa	206 MPa	Excellent toughness, good forming and welding properties, high tensile strength
Cold Rolled Steel	210 GPa	140 MPa	Deep drawing, welding properties
Carbon Steel 1090	248GPa	208MPa	Excellent toughness, good forming and welding properties, high tensile strength

4.2) Tyre

Tyres are an integral part of a forklift, contributing to the efficiency, performance, and safety of the forklift. There are three types of forklift tyres available on the current market; these are pneumatic, solid, and polyurethane tyres. Pneumatic tyres are air-filled which are manufactured from strong rubber, ensuring extra durability as they are comparable to the tyres which are used on heavy-duty trucks. Pneumatic tyres are ideal for an application where wear and tear are expected. Solid rubber tyres, as their name states, are a solid piece of rubber. A significant

advantage is its overcoming ability to the failures a pneumatic tyre would suffer from punctures and popping. Finally, polyurethane tyres are more durable when used indoors in comparison to pneumatic and solid rubber tyres due to the significant traction gains.

Tyres are the contact point between the ground and the Forklift. Therefore, the vibration caused by the mast can cause the forklift to unbalance if the incorrect tyres are used. Therefore, finding the correct tyres for the scaled project was an important factor. A rubber bush or bumper was assumed to be a good alternative because they act as a vibration isolator and can provide an interface between the body of the forklift. The bumper will also prevent the ground causing any additional vibrations within the body. Therefore, four bumpers were required; Figure 48 and Table 3 illustrate the specifications of the rubber bumper used in this research. The rubber bumper has been screwed to the base of the forklift body for a stronger connection.

Table 3: Specifications of the rubber bumper

Material					
Rubber on silver zinc plated steel					
Dimensions				Energy to 1 m/s (kg.m)	Max. Axial load (Kgf)
d_1	h	d_2	l	-	-
40	32	M8	28	5	850

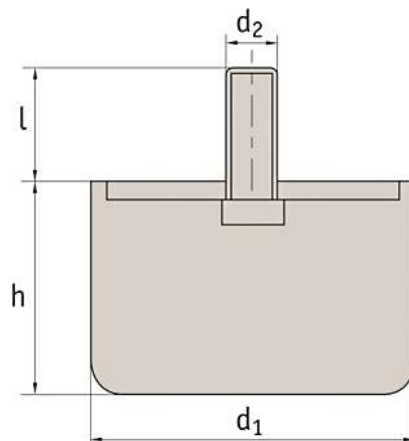


Figure 48: 2D drawing of the rubber bumper

4.3) Design

The ideal forklift design should be comprised of two masts that will be able to replicate the frequency produced by an actual forklift of 1Hz; the vibrations produced are then read and recorded using vibration analysis equipment. The dimensions of the test rig have been scaled by a factor of 1:4 from the original dimensions of a forklift.

Following few initial designs, the final design of the forklift has incorporated the best aspects of the previous conceptual designs leading to a test rig that would be able to replicate the vibrations produced when a mast is tilted forward or backward. Brief specifications of each body part are explained in the next section.

4.3.1) Base

The base of the test forklift is a square part of 485 x 500mm and 10mm thick, providing a stable base for the test rig. 16 M6 threaded holes are drilled into the base where the pivots for both the masts and hydraulic cylinders will be positioned. Furthermore, to duplicate the tyres of an actual forklift, a rubber bush is used, where bushes interface between the ground and the base without causing additional vibrations and disrupting the validity of any data collected

4.3.2) Pivot

The pivot designed for the test rig allows for the tilting action data to be acquired. There are three sets of pivots that have been used for the test rig. The first pivot on the base connects to the hydraulic valves (appendix), an 11mm pin of length 75mm (appendix) slots through the top section securing the pivot in place. Connecting the hydraulics (appendix) to the mast is a 27mm pin length 75mm (appendix). The third pivot (appendix) is then used to connect the mast to the base again with another 11 mm pin to secure the connection.

4.3.3) Mast

Final design for the mast with the length of 2m has been optimised. The mast contains ten M6 threaded holes for the attachment of the forks. In addition, 2 M4 holes are positioned 40mm from the base of the forklift and 40mm apart; enabling the pivot to be attached to the mast allowing the tilting movement. In order for the hydraulics to be directly attached and move the masts, a further two M6 threaded holes are placed 304mm from the bottom of the mast and 30mm apart.

4.3.4) Forks

The design of the forks split into two, with the angled sectioned being welded to the horizontal section. A new feature is the added triangular plates in the corners of the forks increasing the stability of the forks and providing extra support when additional weight is placed upon the forks. The plates have to be welded on, as this would be the only right way for them to have a direct effect upon the rigidity of the forks.

4.3.5) Tilt Cylinder

Tilt cylinders are double-acting hydraulic cylinders that are mounted to the forklift body and the mast, which could apply force in either direction. Usually two tilt cylinders are used on the truck. The tilt cylinders pivot the mast to assist in engaging a load. The speed of the cylinders depend on the exerted force by the hydraulic fluid, which is routed through the electro-hydraulic control valve. This will allow the mast to move forward and backward. The technical drawing of the tilt cylinders has been provided in the Appendix3.

Table 4: The specific parameters and the supporting dimensions

Cylinder Assembly Part No	8604726
Tube Weldment Part No	520041613
Rod Part No	519517618
Stroke	98.0
Effective Stroke	65.0
Dimension A	301.0
Dimension C	58
Angle D°	90°
Angle E°	90°

4.3.6) Electro-Hydraulic Control Valve

HAWE SK 7650 HST model electro-hydraulic control valve was used to control the fluid flow. These lifting and lowering valves were established, especially for the actuation of hoists. They contain a combination of various valve types (flow control valves, throttles, directional control valves) suited for the control of the main lift and other purposes. The internal control design of the main valve is very flexible and can be personalised to meet precisely the necessities of any drive concept (continuous delivery or speed-controlled pump) as well as the intended

application.

The pressurised fluid from the HPU will be gasped through the port into the control valve. The returning unpressurized fluid will return to the HPU through the second port. Solenoids, which are attached to the electro-hydro control valve, acts as a switch to allow fluid flow through the electro function valve to the cylinders. If the solenoid receives the voltage to open valves type A, it allows the pressurised fluid from the HPU to pass through to valves type A going to the cylinder in order to tilt the cylinder. At the same time, the valves type B will allow the returning fluid from the cylinder.



Figure 49: Electro-Hydraulic Control Valve

4.3.7) Flexible hose, pipe fittings and seal materials

For this particular application, flexible hoses were chosen as the fluid transmitting mean, as the mechanical parts are continually moving and flexibility was one of the concerns. A key factor of temperature range and the maximum pressure was used to determine the specific flexible hoses. The specifications of the hoses are provided in Table 5.

Table 5: The specifications of the hoses

Part Number	301SN-4
Hose Internal Diameter	¼ inch or 6.3 mm
Hose External Diameter	15 mm
Maximum Dynamic Pressure	40 MPa
Minimum Burst Pressure	160 MPa

4.3.5) Overall design

The final design as presented in figure 50 has the overall dimensions of 755 (L) x 480 (W) x 2000mm (H), which can fit within the designated testing area within the laboratory. To ensure that both masts tilt as one, three bars were manufactured and placed accordingly along the back of the mast. The bars were secured on the back due to the forks being free to be placed along the entire mast. It is essential that the bars can be placed even when the forks are within the same region. A feature of the final design that is dissimilar from that of an actual forklift is the positioning of the hydraulics as opposed to the tilt cylinders being at a certain height; they were incorporated as part of the base. Ultimately this extended the angle which the masts could be displaced; however this design was deemed to be acceptable in comparison to building an extra body upon the base to rest the hydraulics on, which would increase the manufacturing time.



Figure 50: Optimised Design of the forklift test rig

4.4) Hydraulic Power Unit

As previously discussed, the hydraulic motor, gear pump, and the hydraulic tanks have been replaced by a Hydraulic Power Unit (HPU). HPU is a self-contained power package consisting of a pump and motor mounted to a reservoir which has been sized to achieve a specific range of flow and pressure. The HPU will provide pressurised flow to cylinders. Unlike standard pumps, these power units use multi-stage pressurisation networks to move fluids (figure 51).



Figure 51: Hydraulic Power Unit

4.4.1) Hydraulic system circuit and operation

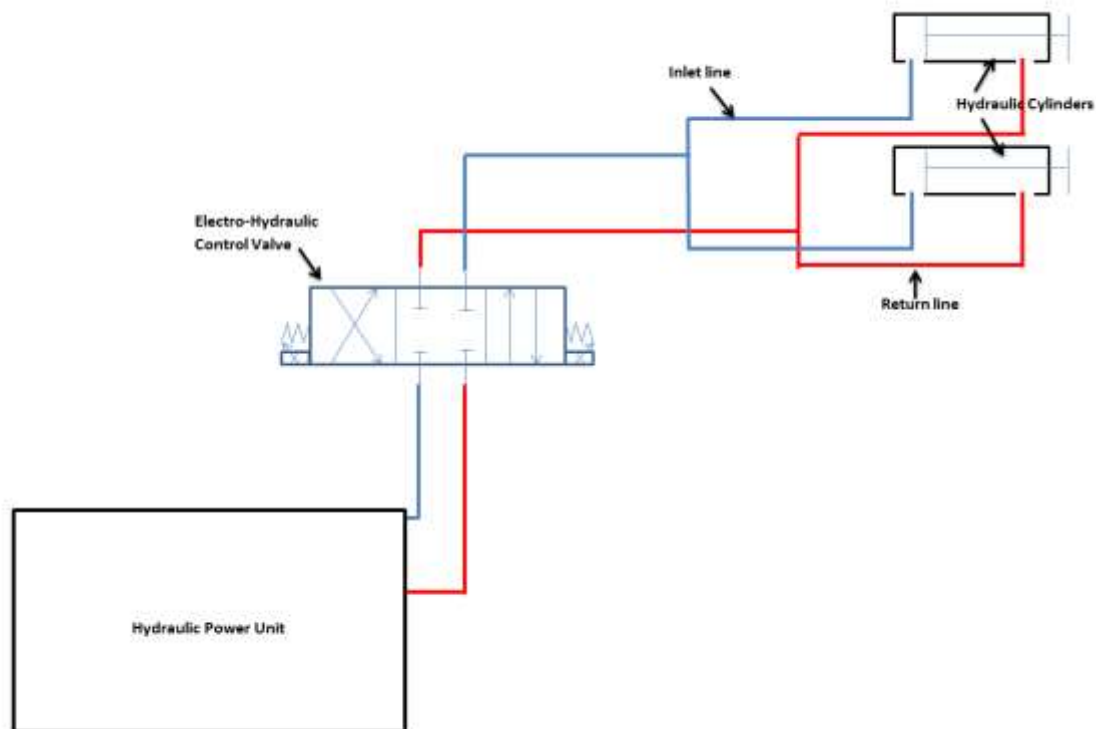


Figure 52: Hydraulic system circuit for scale down forklift

Figure 52 shows the hydraulic circuit of the constructed hydraulic system. As shown in the diagram, the inlet hoses will carry the pressurised hydraulic fluid from the HPU (when energised) to the electro-hydraulic control valve, which will be activated through the solenoids by the LabVIEW control system. From the control valve, the fluid will travel towards the double-acting tilt cylinders, which in turn will move the forklift's mast forward. In the meantime, due to the pressure exerted on the cylinder rod, it will move the existing hydraulic fluid (low pressure) through the return line to the control valve back to the HPU. When this operation is opposed in order for the mast to go backward, the spools inside the control valve will alter their operations.

4.5) Control system equipment

4.5.1) CompactRIO with Chassis

An NI equipment (figure 53) for real-time programming was utilised via LabVIEW. Real time controller, CompactRIO NI-9024, attached to a 8-module slot chassis NI-9114 has the ability to insert 8 input or outputs; though only two were used for this project.



Figure 53: NI-9024 cRIO with NI-9114 chassis

4.5.2) NI 9234 - 4-Channel, ± 5 V

This module was used as an analogue input for the accelerometer. The NI 9234 provides a four-channel C series dynamic signal acquisition module, of which two were used, one for lateral and the other for longitudinal signal inputs. They were used for making high-accuracy vibrational frequency measurements from integrated electronic piezoelectric (IEPE) and non-IEPE sensors with the NI CompactRIO chassis systems. The great feature of this module is the ability to deliver 102 dB of dynamic range and the availability to incorporate software-selectable AC/DC coupling; which allows for any AC signals to be read by the module. Moreover, the IEPE signal conditioning for accelerometers were used. The two out of four

input channels can simultaneously digitize signals at rates up to 51.2 kHz per channel with built-in antialiasing filters that will automatically adjust to the sampling rate.

4.5.3) NI 9472 - 8-Channel, $\pm 24V$

This module was used as a digital output to control the flow through solenoid valves. The NI 9472 supplies an eight-channel C Series sourcing digital output module, of which like the aforementioned NI 9234 utilised only two channels, one for tilting the mast forward, and the other for the opposing directional tilt. The output control was generated from a controller and output programmed application, constructed in Labview. Also, this module enables the method of PWM to operate correctly due to its digital waveform.

4.5.4) Accelerometer

An accelerometer is required to measure the output vibrations and angular displacement of cylinders. A DA-Series accelerometer was selected as the most suitable accelerometer for this investigation. In addition, the small dimensions of the accelerometer meant that it was possible to connect the accelerometer to the mast rig. The piezoelectric material inside the accelerometers is making electrical charges from mechanical forces by transforming mechanical deformation to electricity produced by the vibration of the mast. Force is proportional to the accelerometer caused by the mast vibration. The voltage gained from the accelerometers needs to be converted to the acceleration by the calibration factor, which is provided in appendix.

4.5.5) LabVIEW

Labview was used for this research as it was designed as a highly productive development environment for engineers to design rapidly and to deploy measurement and control systems within its graphical programming and adaptability to its unprecedented hardware integration. Labview is suitable for creating block diagrams and generating code into a modular way through its easy-to-use palette system using the simple visual interface.

4.5.5.1) LabVIEW MathScript

MathScript is the engine that accepts general .m file from syntax and translates that into the G language of Labview. To construct the mathematical code, a line of script was formulated within the MATLAB® software. The alternative programming method is by wiring together graphical icons on a diagram, which then compiles it directly to the machine code for the computer processors to execute it. This approach aligns with the way most scientists and

engineers do.

4.5.5.2) Low pass filter

Low-pass filter is designed and used to filter unwanted noise and to let low-frequency signals to pass while filtering the high-frequency signals. The low-pass filter used in this test has one input and two outputs, and also it has the capability to amplify the signal by ten times. This is a first order low pass filter with a low cut-off frequency set to 100 Hz. Figure 54 shows the circuit of the low pass filter.

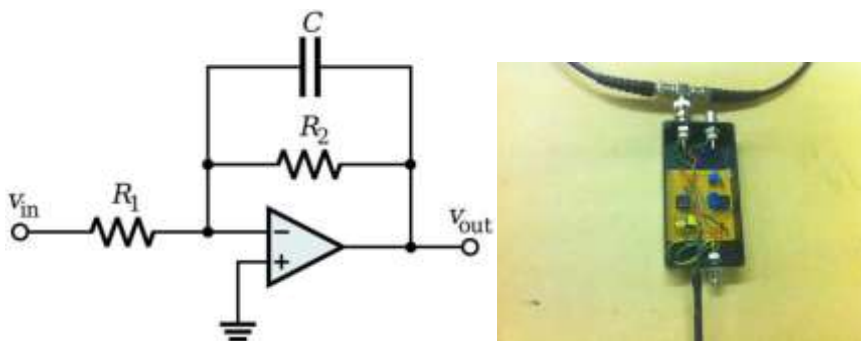


Figure 54: A low pass filter and its circuit



Figure 55: Filter used to cancel the noise

4.6) Rig Setup

Figure 56 illustrates the set-up employed to start the tests and get the measurements from the accelerometer. In summary, our primary focus was on the vibration caused by the tilting of the mast. The HPU was used in order to apply force on the tilt cylinders to angle the mast as programmed in Labview. The four-function electronic valve was controlled by our own control system (Labview), which will additionally enable us to test the vibration formed at different heights with different weights.

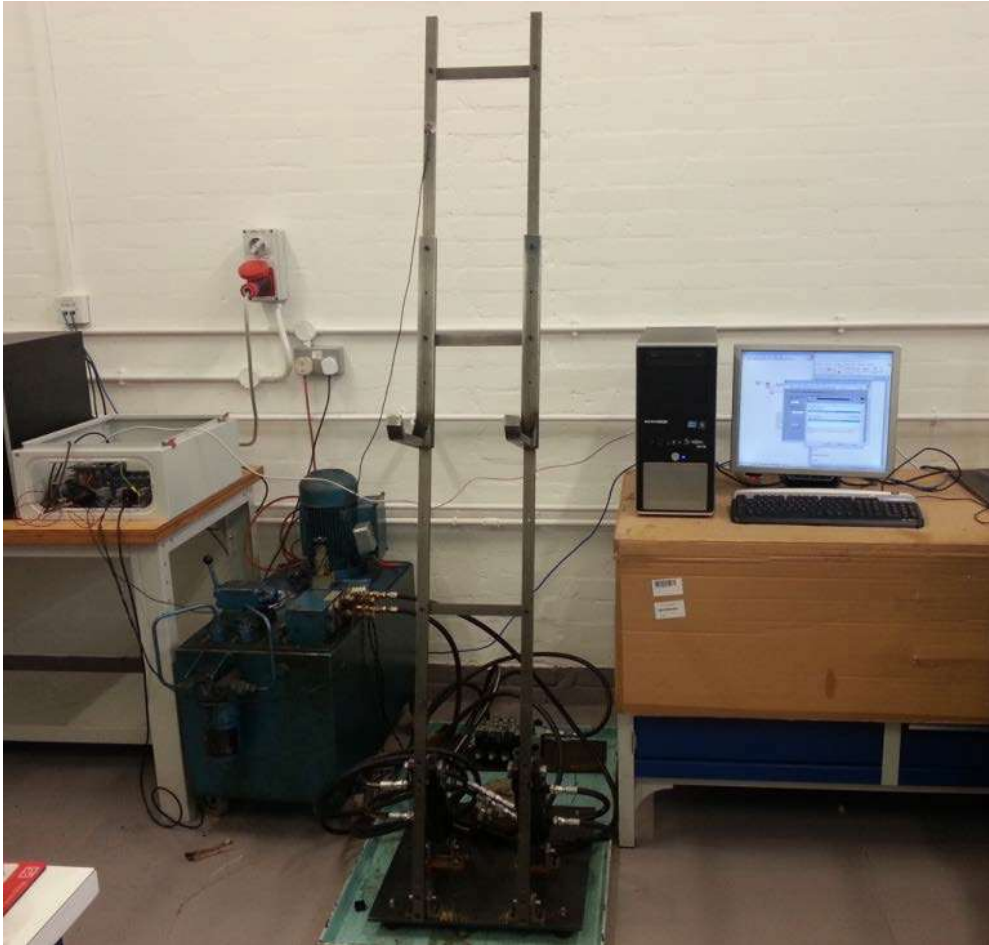


Figure 56: Equipment set-up for tests

4.6.1) Preliminary experiment – pluck test

A pluck test was conducted to validate the accelerometer readings, following the same procedure as the one conducted by Yale. This verified the accelerometer and the procedures that will follow. The test was carried out while the mast is not loaded with any weight. The pluck test was allowed while validating the accuracy of the Labview software.

4.6.2) Calibration test

The calibration test results as illustrated in Figure 57 displayed an alignment between the 1Hz frequencies generated by the shaker and the data range observed on the accelerometer. It was essential that these values were aligned to perform the remainder of the tests to the precise level necessary to deem results suitable.

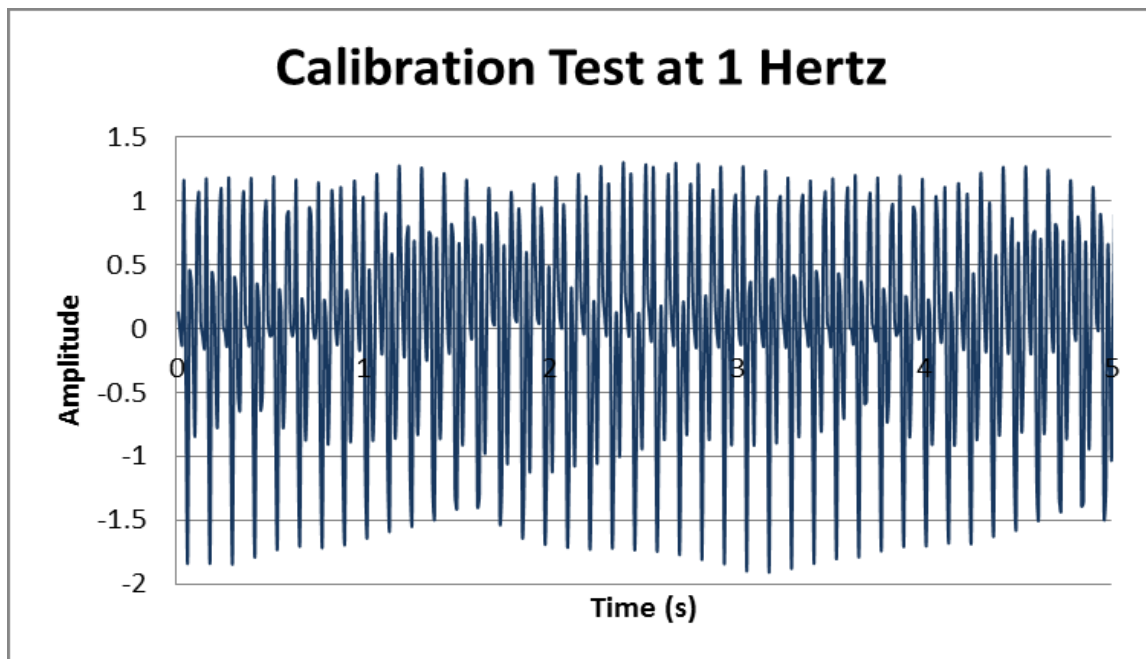


Figure 57: Calibration Test Amplitude vs. Time Results

4.7) Control system tests on Rig

In order to achieve better results and not to make confliction between input and output of modules, the test was conducted in 2 separate Labview file. One mutual PID controller to individually control the solenoid valves on the basis of desired output and another one that controls the cylinder by implementing LQR or SMC. The brief design of PID, LQR and SMC are explained in the next sections. The next chapter will include all the results in details.

4.7.1) PID controller

Proportional Integral Derivative (PID) controllers are a form of simplistic, generic three-term controller, commonly implemented in industrial applications for regulations of numerous process variables, inclusive of pressure, temperature, flow and speed. The typical process of a PID is to read an input sensor signal, to convert the attained measurement (signal) into

engineering units (distance, mm) and to subtract the measurement from a selected SetPoint (SP) to regulate and control the determined error.

This is a simple method of governing an object, influencing the error between the SP and Process Value (PV), defined as the acquired feedback follows output. The algorithm for PID is a combination of its three termed parameters; namely Proportional Action (Gain), Integral Action (Reset), and the Derivative Action (Rate, KD)

The mathematical algorithm of a PID controller's behaviour was discussed in the previous chapter. Figure 58 shows a block diagram representative of the given formulated equation and described workings of a PID controller.

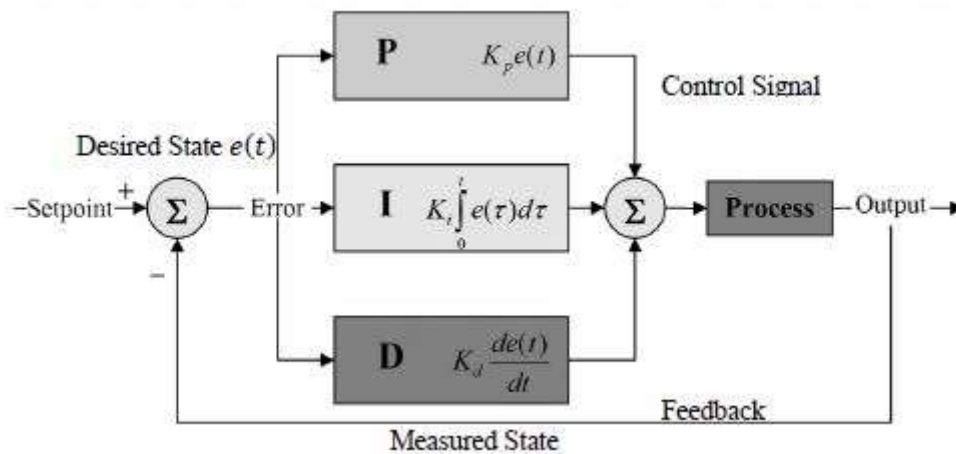


Figure 58: PID block Diagram

4.7.1.1) Gain and auto-tuning of PID controllers

The appointment of parameters for each term is defined as tuning. There are two focal methods of setting PID gains; the Ziegler Nichols and trial and error method [77].

Auto-tuning is a commanding procedure for tuning PID gain applied only when processes act conditionally or vary with time. If the process changes are predictable, the control system can be altered through the use of a gain schedule. Alternatively, an adaptive controller could be used to adjust the PID gain, to manage erratic variations. While adaptive controllers provide a general range of dissimilar situations, gain scheduling is operated to construct a table that contains numerous parameter sets for diverse conditions. Retracting distinct corresponding parameters can be implemented to modify the PID gains when process requirements change. The aforementioned adaptive control has two separate techniques for PID; the direct and the

indirect methods. The direct method for adaptive techniques alters parameters according to the data available by the output of the control signal; whereas the indirect method revises parameters through estimating parameters that are recursive as shown in Figure 59. Nonetheless, it is unfeasible to complete all control systems through an auto-tuning command. To provide previous information for even further processing, it is necessary that the process is stable. The procedure for auto-tuning a PID gain is as follows:

1. Process Disturbance Production
2. Resultant Response Evaluation
3. Analytical Calculation of Gain Parameters

Auto-tuning can be carried out in two separate key methods in accordance with the tuning procedures; namely the Rule-based and Model-based methods.

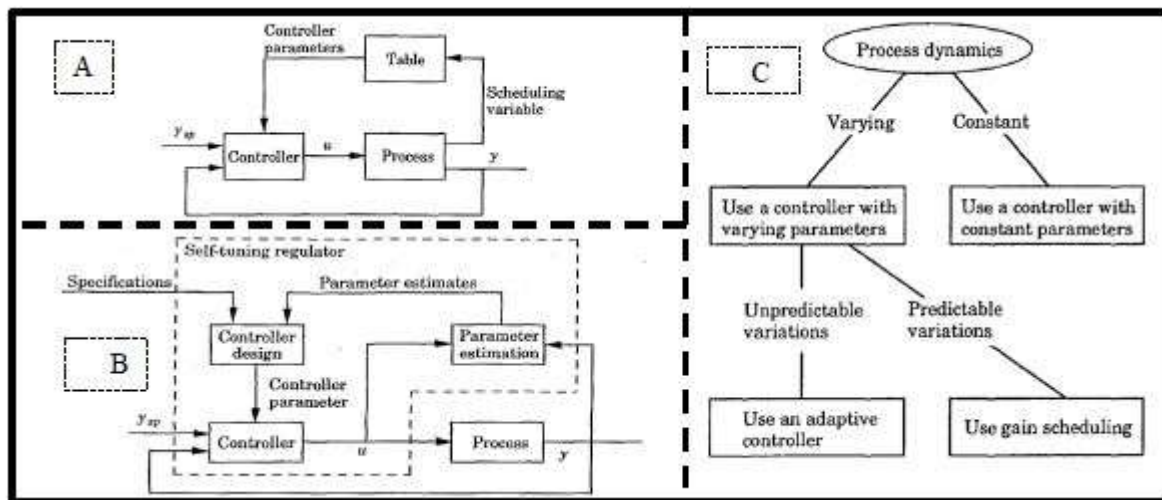


Figure 59 : (A) Gain Schedule (B) Indirect Method (C) Process Dynamics [78]

The Rule-based method does not require a source of parameters and signification or reference as it simulates manual tuning through developed experience. This method could be exercised as a compromise between stability and speed of the system. The relationships between an increase and decrease in parameters and their improvements or decline are exhibited in Table 6.1, while the overall effects of increasing each action parameter (K_P , and K_D) are illustrated in table 6.2.

Table 6: Effect of Action Parameters on a System's Dynamics

Response	Speed	Stability
K_P	Increases = Improves	Reduces = Decline
T_I	Reduces = Decline	Increases = Improves
T_D	Increases = Improves	Increases = Improves

Response	Overshoot	Rise Time	Steady State Error	Settling Time
K_P	Increase	Decrease	Decrease	No Definite Trend
K_I	Increase	Decrease	Eliminate	Increase
K_D	Decrease	No Definite Trend	No Definite Trend	Decrease

On the other hand, the model-based approach determines PID gain through acquiring specific response information from the specified model, consequently requiring a primarily stable process. This method is comprised of three separate distinct methods; namely the parameter estimate, frequency response and transient response methods.

The parameter estimation method could be applicable for real systems as it consists of determining PID gains by constructing a low-order discrete-time model, from conducting recursive parameter estimation. PID gain is calculated from the reprocessing of the model. Parameter estimation requires a pre-tuning phase and substantial prior information like alternate methods to construct the model. However the method needs no excitation signal.

The technique of moments is used to analyse PID gain within Frequency Response methods, inclusive of the relay method. A relay oscillation is sent as an input alongside calculating PID gains with Ziegler-Nichols frequency-response method. From this the method procures period and amplitude of output from a stable oscillation. The extent of output used to assess the stability of a system during tuning is defined as the Relay Amplitude, which must not be higher than the control systems actual output.

The transient response method possesses open and closed loop tuning, both of which have beneficial and detrimental tuning properties. Open loop tuning is typically used for pre-tuning as it needs less prior knowledge, yet it is considerably more sensitive to disturbances than its closed-loop tuning counterpart. Whereas the advantage of a closed loop tuning method is the stability it provides to control system from its generated feedback. On the other hand, the closed loop tuning is unable to be executed alongside an unknown process, instead it needs initial pre-

tunings to provide specifications such as time constants, damping and overshoot.

Table 7: Effect of Action Parameters on a System's Dynamics Trial & Error Method and the calculation of observed parameters from the form of the process value wave are the two main manual methods of adjusting PID gain. To calculate PID gain, it is necessary to know the shape of the wave generated. If a system is able to display its wave shape, it can become stable and the PID gain can be determined through trial and error. The trial and error method rules are mainly exercised to avoid extent in auto-tuning techniques and optimization.

The Trial & Error method is based on experience, with initial information and terms established immediately.

The Trial and Error Procedure consists of two method steps as described below:

Method One

1. Start by setting all parameters to 0.
2. Increase KP (Proportional Action) to cause the trajectory to oscillate around the desired set point.
3. Increase KD (Derivative Action) to minimise overshoot.
4. Increase KI (Integral Action) to eliminate steady-state error within the system.

Method Two

1. Start by setting all parameters to 0.
2. Increase KP (Proportional Action) to cause the trajectory to oscillate around the desired set point.
3. Increase KI (Integral Action) to minimise overshoot and put trajectory closer to set point.
4. Increase KD (Derivative Action) to maximise response speed and reduce overshoot until the system destabilises.

In this PID controller test, the system was closed-loop and thus both trial-error and Ziegler-Nichols methods were used. The VI program designed to find controller gain and its parameters of this controller can be obtained based on the graph illustrated in Figure 60 and table 7.

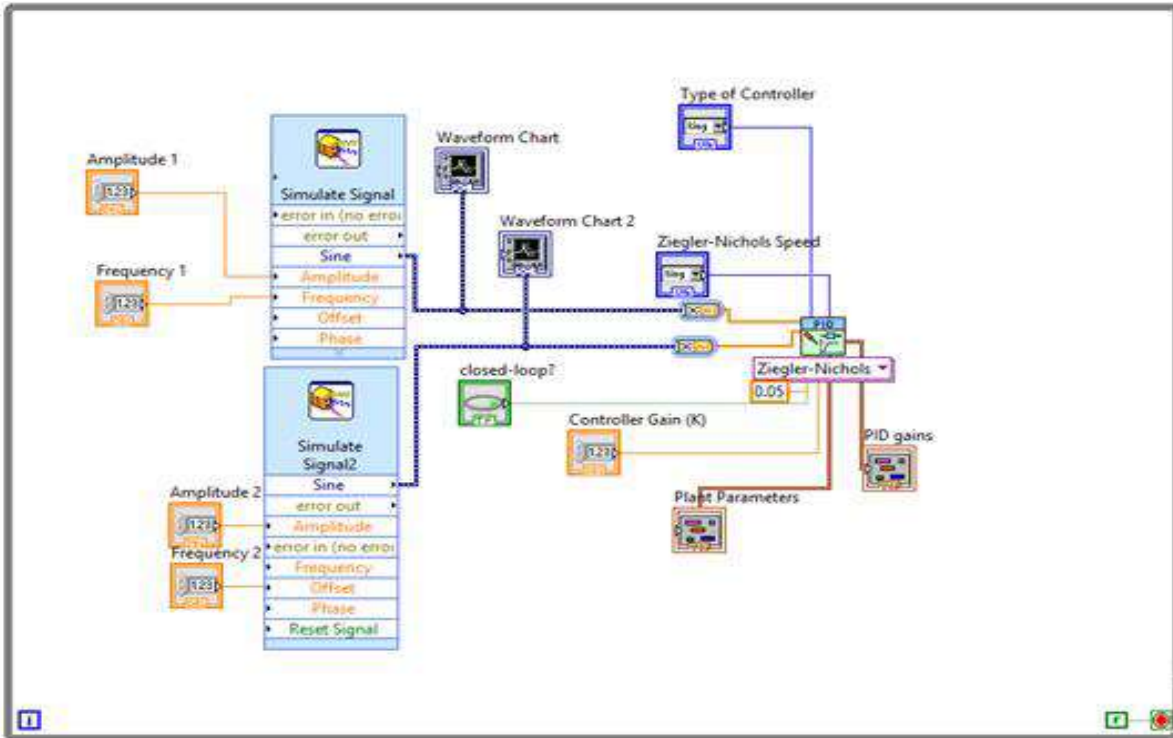


Figure 60: VI to find optimum gains via the Zeigler Nichols method

By ‘Running the program, the software automatically performs a configuration to check if any errors are present within the [.vi]. This checks the status of all individual segments of the code, ensuring that they work correctly without errors avoiding the redundant procedure of running the entire VI at once.

This configuration is based on a PWM system and ZN gain finder without the need to edit multiple outputs due to the use of one solenoid controlling both cylinders. So the codes evaluation concentrates on the analog and digital outputs separately. The complete PID controller parameters used to control valves is shown in table 7.

	P	T_I	T_D
P	$K_U/2$		
PI	$K_U/2.2$	$P_U/1.2$	
PID	$K_U/1.7$	$P_U/2$	$P_U/8$

Table 8 : Zeigler Nichols parameters

4.7.1.2) Pulse Width Modulation (PWM)

Pulse Width Modulation (PWM) is a form of signal communication, which refers to a method of transforming energy into a digital signal sequence with rapid pulses, as opposed to a continuous analogue signal with fluctuating frequency and amplitude, to simulate varied voltage in a wire [79]. Energy flow to the receiver is regulated by the controller through altering the width of the pulses. This method is applicable and regularly used for varying speeds or intensities of driven motors, solenoids, lights and heaters [79].

This is useful in implementation because of the ability to modulate the consistency of energy I/O from a source and consequently influencing a flow to respond to external conditions. Due to its intermittent pulses, Pulse Width Modulation is an efficient form of control.

Below, an example of PWM is illustrated in figure 61 with the corresponding change in pulse size dependent on the proportion of expended duty cycle. At higher frequencies, the Voltage (V) turns off and on in prompt successions, irrespective of D, to diminish the time necessary for the Current (C) to decline .

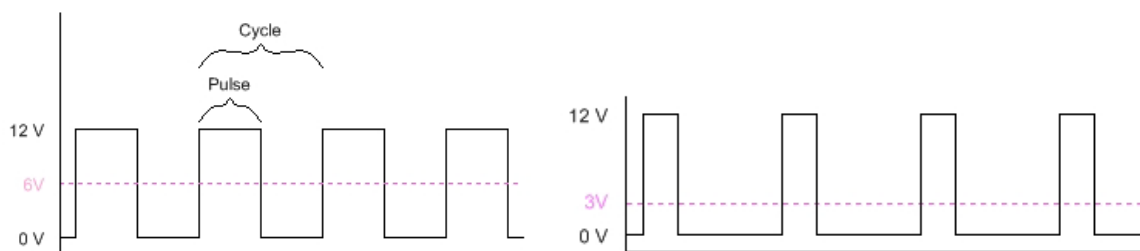


Figure 61: 50% and 25% Duty Cycle Respectively [79]

PWM can be used to regulate the intervals of flow through a solenoid, governing the restriction of flow that enters and exits the solenoid mechanically contingent on the constraints of separate mechanisms i.e. voltage or frequency. This is due to the voltage supplied through PWM equating to the duty cycle. Therefore the control can be defined relative to this.

The basic method of PWM operation is general for most PWM controllers with variations according to their use and specific implementation; a common standard method would proceed as follows [79]:

1. Set period in on-chip timer that provides modulating square wave: denoted in Figure 60 above
2. In PWM control register Set the on-time
3. Set direction of PWM output: a general principle of Input/output (I/O) pins

4. Commence Timer

5. Enable PWM Controller

Figure 62 shows the VI designed to generate PWM signal.

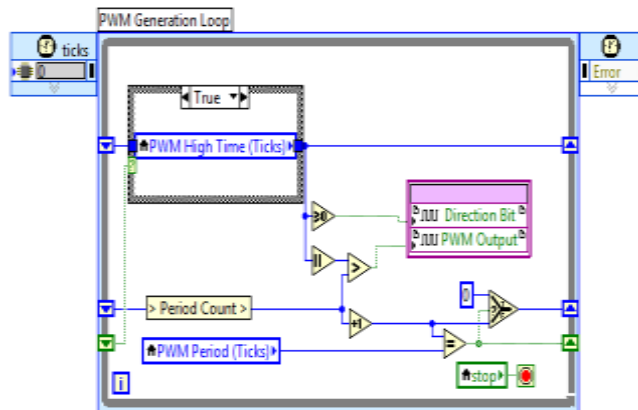


Figure 62: PWM signal generator

PWM can instead be used as an output to be coupled with a complementary controller, which is mostly used with PID controllers of digital signals. This combines both the beneficial traits of a Proportional Integral Derivative and Pulse Width Modulation to ensure full control of a system is attained.

With this combined PID control and PWM output, the set point of a determined value defines the target level an input process value is aimed at.

An example of this PID-PWM control, in which the target is to track the changes in a light output through adjusting the systems duty cycle, is displayed in Figure 63:

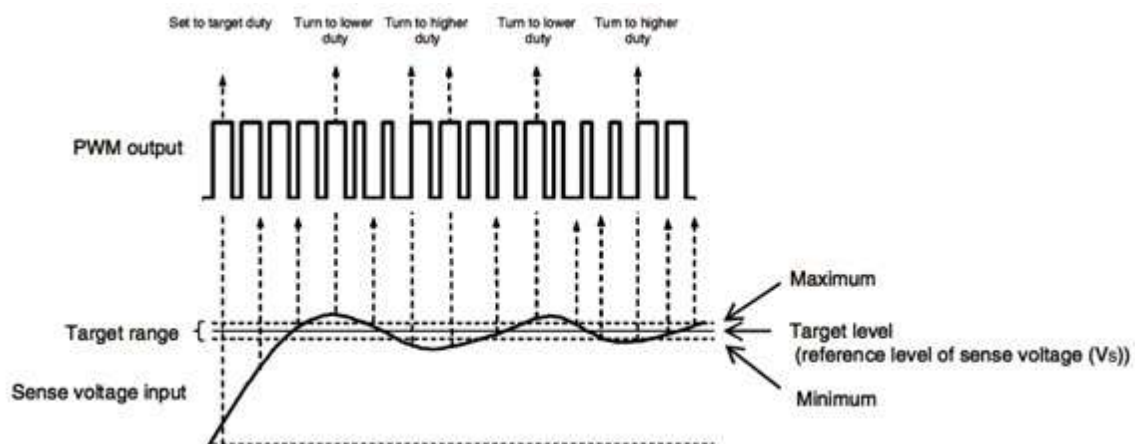


Figure 63:PID & PWM Combined Control [79]

4.7.1.3) PID controller implementation

In this section, the control system is based on PID controller using the Ziegler-Nichols tuning method that has been designed to control the solenoid valves to allow hydraulic fluid flow through the tilt after getting an order from PID controller.

A block diagram as displayed in Figures 64 and 65 outlines the exact constructed code used to assemble the subsequent VI and therefore to define the communication between the CompactRIO and LabVIEW. This block diagram is divided into three sections by a 'While loop' to separate the 'Start', main program sequence and 'Stop' of the program. This is beneficial as it only stops the running VI upon completion of its current iteration. Without the while loop structure, the program would run either continuously until the 'Abort Execution' button above the visual interface is pressed or for a set time limit as opposed to an integrated 'Stop' button. This is undesirable as the VI should incorporate all necessary actions of control without the need to execute additional commands beyond its scope. Moreover, the 'Abort Execution' button ends the active VI instantly devoid of completing the iteration in progress, effectively not releasing or resetting the iterations appropriately.

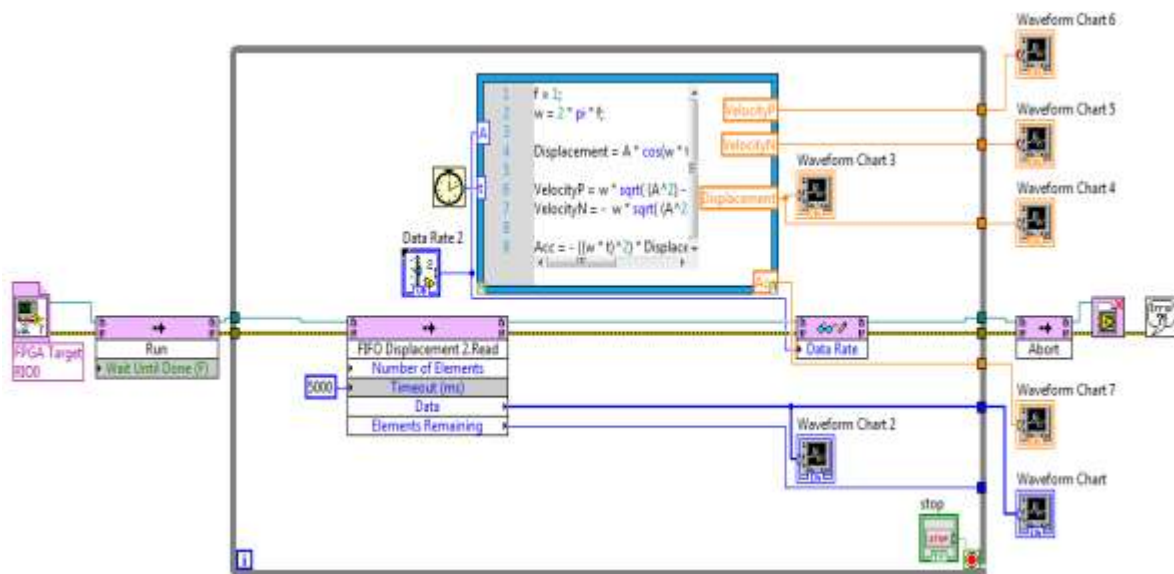


Figure 64; Input elements of PID controller

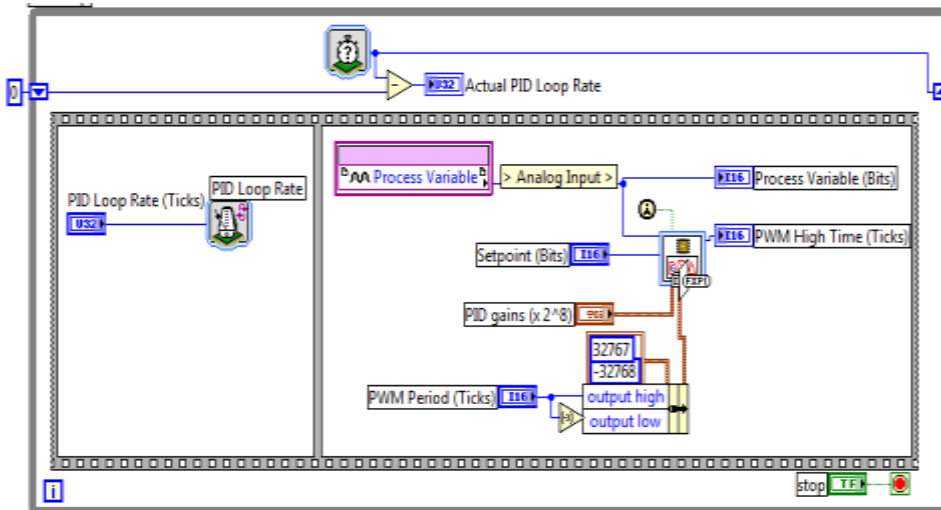


Figure 65: Output elements of PID controller

Response to the generated to the PID control PWM output; with a positive PID output, the signal sent causes the solenoid valve to push flow through the cylinders, in turn tilting the affixed masts. With a negative PID output, the cylinders should retract as the flow is withdrawn by the valves, in effect tilting the masts backward. This can be seen from Figure 66, which is done through the simple PWMPID .vi implementation.

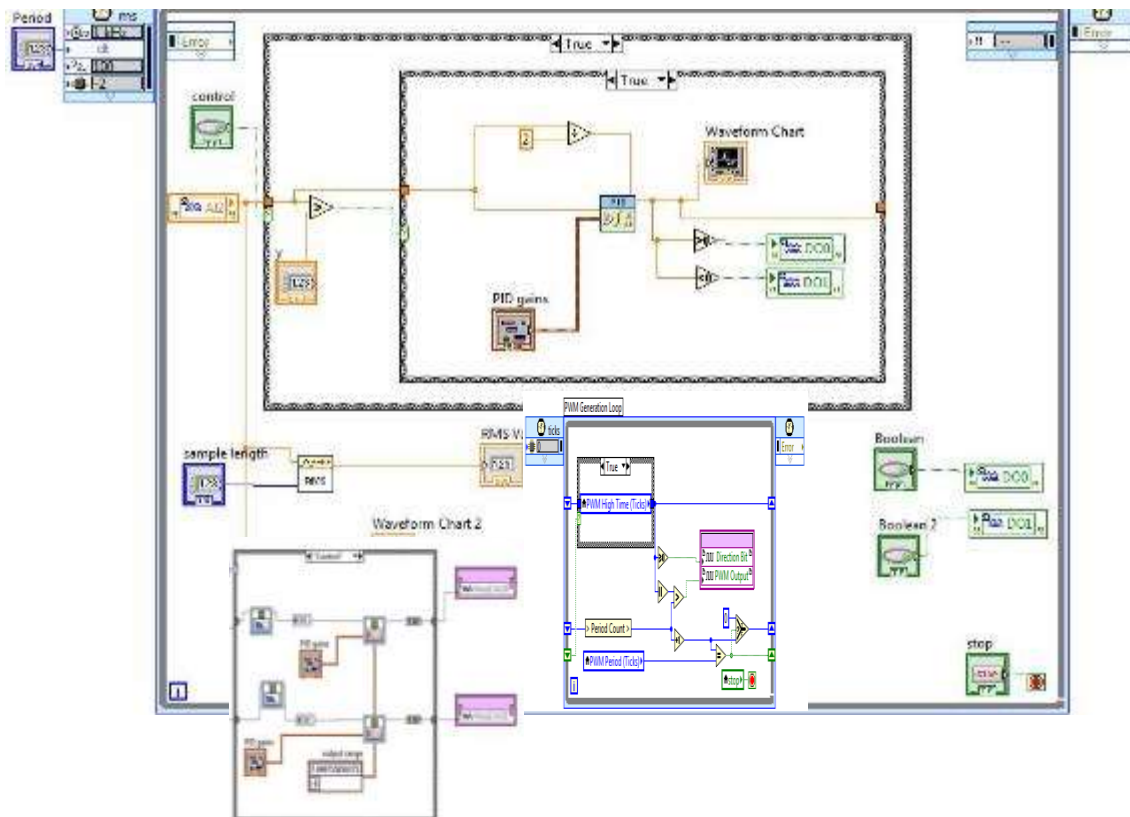


Figure 66 : Complete VI program using PID controller for valves operation

4.7.2) LQR controller

Linear Quadratic Regulator (LQR) is a state feedback controller, which is classified as an optimal control system. The system can be expressed as a state variable, where all states are assumed measurable. LQR tries to minimise the performance index J on the equation (99) below, where J is representing the energy function of the system (cylinder). By minimising J the total energy of the control loop system will be reduced; hence the system will become stable. Consider the quadratic objective function J (or cost function) as

$$J = \frac{1}{2} \int_0^T X^T (Qx + u^T Ru) dt \quad \text{Equation (99)}$$

The main design parameters Q is semidefinite and R is a positive definite matrix. Therefore, as the tuning of Q improves, the settling time will be improved as well. The structures of LQR can be seen in figure 67.

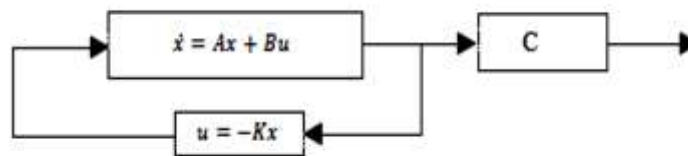


Figure 67: LQR structure

Therefore, if performance index J is minimised, then it is finite. Subsequently, it is an infinite integral of (t) , which indicates that (t) will be zero as T goes to infinity. This shows that the system is stable.

4.7.2.1) LQR implementation

The model of LQR controller as a block diagram in Labview is shown in Figure 68. In order to implement the LQR controller as described in chapter 3 and equation (99), .mathscript was used to put on the equations. In summary, after sensor received data from the cylinder and processed it through Compaq RIO this will go through LQR controller as $U(t)$. The design parameter Q and R of the LQR controller were chosen as shown below by trial and error method to achieve the best performance index. The results of this section will be discussed in the next chapter.

$$Q = \begin{bmatrix} 16650 & 0 \\ 0 & 74300 \end{bmatrix} \quad R = [32220]$$

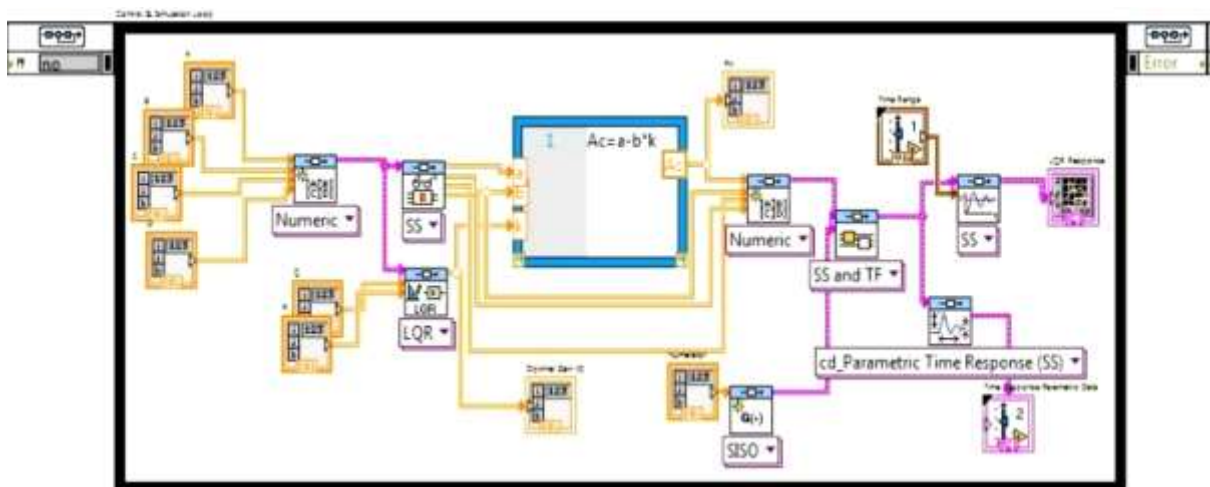
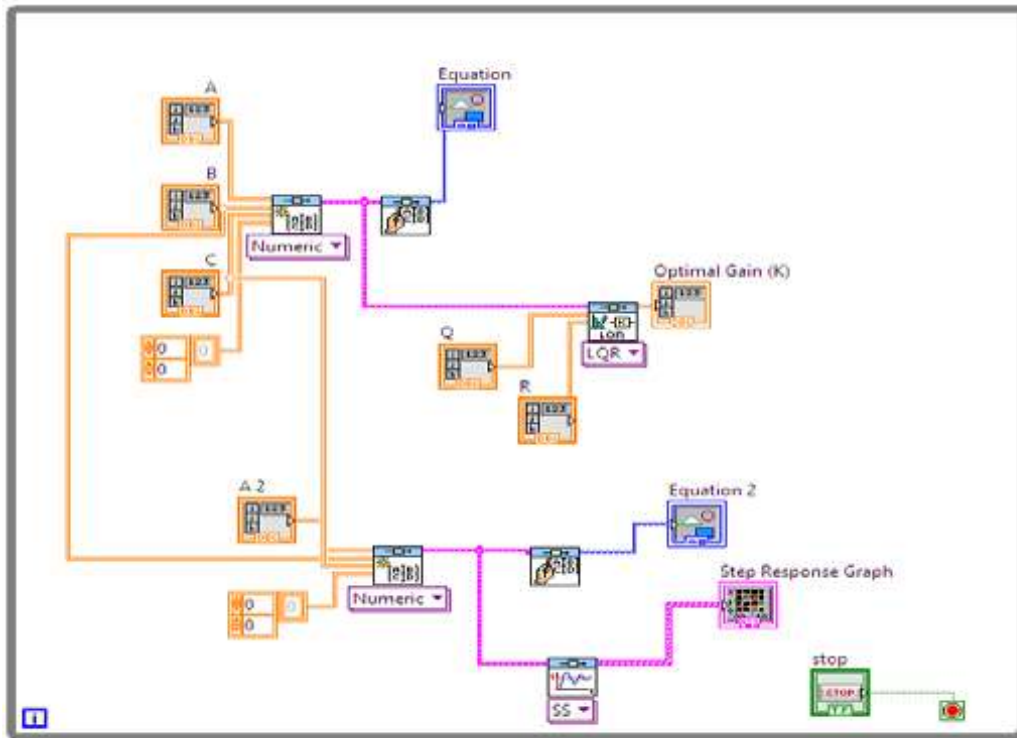


Figure 68 : LQR Labview block diagram for cylinder

4.7.3) Sliding mode controller (SMC)

Following the results taken in chapter 3, sliding mode control was chosen to control the cylinder of rig. As explained previously, SMC is based on forcing the error vector into desired dynamic and holding it in this dynamic. The main advantage of SMC is its insensitivity to changes in system parameters, external disturbances, and modelling errors. The trajectory of

these state variables is called “state trajectory”. The closer the state trajectory to origin, the lower the resulting error would be. To implement the SMC in the test rig, first the displacement control of cylinders need to be found. The control has two parts; first is the measurement of the displacement and then is the computation of the real-time control. The measurement of the displacement is taken by an electric linear sensor, which generates the output voltage as a response to the displacement of the cylinder. A Labview VI shown in figure 69 was used to convert the voltage measurement to the displacement measurement in real-time.

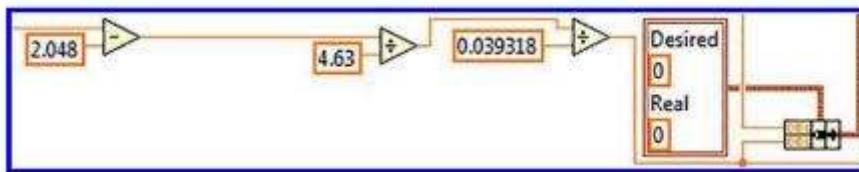


Figure 69: displacement conversion code in Labview

To elaborate on this, 2.048 is a continuously tuned figure for the real-time of the cylinder, whilst 4.63 is the driving voltage of the electric linear sensor, and 0.039318 is a constant pre-set by the manufacturer of the sensor used for the conversion to Inch. The SMC expressed in chapter 3 equations are applied in Labview, as shown in Figure 70. The parameters of the sliding mode based controller are tuned in the experiment by the trial and error method.

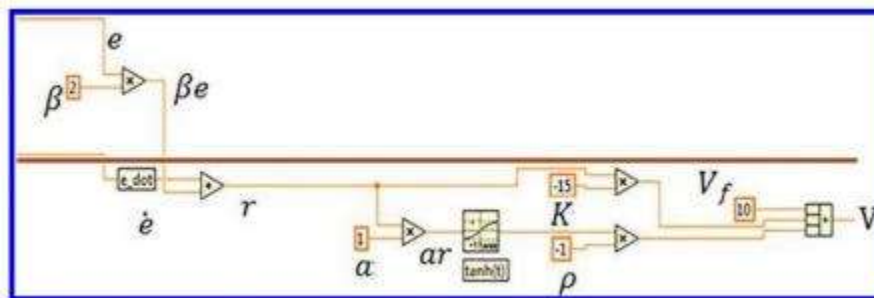


Figure 70: Implemented SMC equations in Labview via mathscript

In order to calculate the reduction of the controller, the amplitude data of the output and input signals were exported from the LabView into the Excel format. All final signals will be concluded by producing a RMS value. Full results and discussion of the tested controller will be discussed in the next chapter

4.8) Chapter Conclusion

On This chapter the design of forklift, mast and whole base of lab made forklift explained . after performing pluk test and calibration of system and in order to achieve what has been discussed in chapter 3, new lab view program perform using semi-active control system on a forklift by using hydraulic pump and accelerometerseveral experimental tests are conducted, different control system has been designed using labview to link the relation of using hydraulic pump with mast to reduce the vibration. PID,LQR and SMC has been designed to to giving required shock to cylinder while mast working to reduce the osilation of mast after final stop . try and error used in order to achieve best results of error factor for LQR and SMC.

The testing procedures and their standards are comprehensively explained. Their results and effectiveness for using a semi-active controller will be discussed in the next chapter.

Chapter 5 Results and Discussion

Highlights:

- ❖ Results of the Numerical model
- ❖ Summary of the numerical model
- ❖ Experimental Results
- ❖ Discussion and Conclusions

This chapter consists of numerical and experimental results of the different control systems and their comparison with different weights. This chapter concludes the results that have been discussed in chapter 3 and 4.

In this section, the results of the numerical and real model of the forklift's mast system will be discussed. In the first step, the dynamic results of the numerical model from the forklift's mast system that was presented in chapter 3 will be analysed. Then the results of the system without the controller (passive) is analysed based on the generated platform model and the settings presented earlier in chapter 4.

The results related to different controllers namely LQR, SMC, and PID will be discussed based on the obtained controlling rules presented in chapter 3. Through a comparative analysis of the results associated with the vibration range of acceleration variable, and the angular displacement of the forklift's mast system, the pros and cons of each controlling method under different conditions will be investigated. The gain for the controllers would be extracted based on different work conditions and performing different tests. Furthermore, the controlling inputs related to the cylinder power of controlling systems of the forklift's mast unit will be extracted based on LQR and SMC methods. Finally, the result related to the controlling inputs of Electro-Hydraulic Control Valve is considered based on the changes in voltage-time variation and the vibration in the forklift's mast unit.

5.1) Numerical model's results

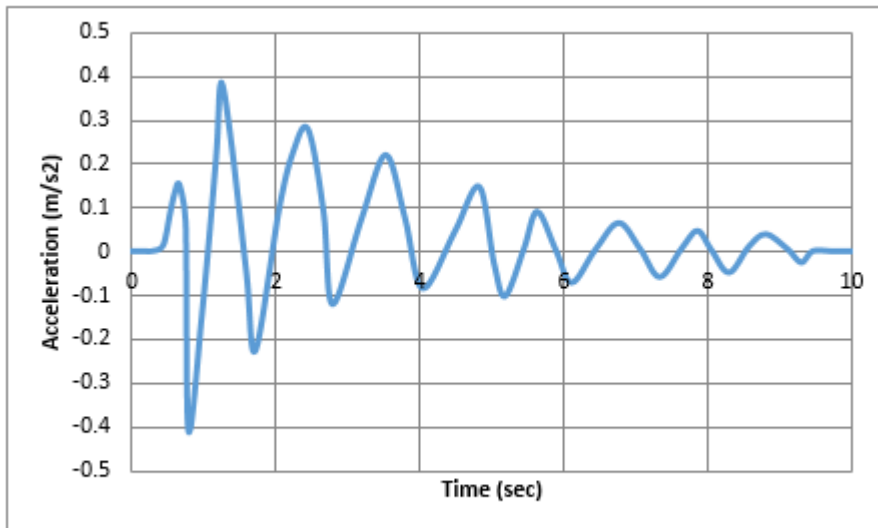
The numerical model implemented in this research was presented in Chapter 3, in which relations related to the dynamics of the movement of forklift's mast system were derived based on the obtained passive and semi-active control systems. In this section, the results of the running of the dynamic model of forklift's mast are extracted based on the explanations presented in Chapter 4, using the relationships coded in Chapter 3 (using MATLAB software). The characteristics of the forklift's mast system are shown in table 8 based on the specifications presented in the numerical model.

Table8: Geometric and Physical Characteristics of the forklift mast Section

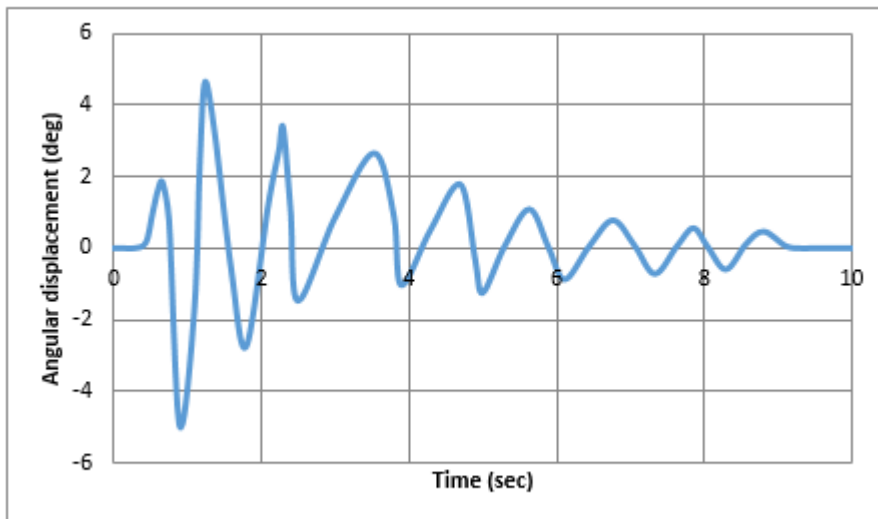
parameters	Value
L_s	2 m
L_c	0.5 m
L_e	2.06 m
M_s	12 Kg
M_L	10(20,30) Kg
J_s	16

5.1.1) Simulation

The results of the numerical model related to vibrational response of acceleration domain and angular displacement of forklift mast system (with 10 kg of weight and 2m height from the platform of a forklift) are presented based on a passive system (without controller). Then, the simulation process is replicated with the weight of the carried loads of 20kg and 30kg.



A



B

Figure 71: Vibrational response of acceleration domain and angular displacement

By analysing the system's response based on the above-mentioned simulations, it can be found that with increasing the load weight from 10kg to 30 kg the maximum vibrational response domain and angular displacement of forklift mast system reaches $0.646 \text{ (ms}^{-2}\text{)}$ and 7.39deg from $0.41 \text{ (ms}^{-2}\text{)}$ and 4.98deg , respectively.

Also RMS value for acceleration increases from $1.13 \text{ (ms}^{-2}\text{)}$ to 2.484 , whilst angular displacement goes up from 13.52 to 21.63 . This means that with a 20 kg rise in the load, the maximum acceleration and displacement increases by 57% and 48% , respectively. The results related to the controlled system based on LQR, SMC, and PID controllers are discussed separately.

5.1.2) Controllers section

This section presents the results of a semi-active forklift mast system, which is the focus of this current research. The results of the actual model of the forklift mast system are analysed separately based on the control system designed in the previous sections (upper level LQR, SMC and lower level PID control).

5.1.3) LQR controller

In this section, the numerical model results for the forklift mast with LQR controller are analysed. The simulation tests were carried out based on the equations described in chapter 3 regarding the input force of the hydraulic cylinder as well as the related block diagram. The results of the acceleration domain and angular displacement of the forklift mast unit with load weights of 10 kg and 30 kg are demonstrated in figures 72 to 74.

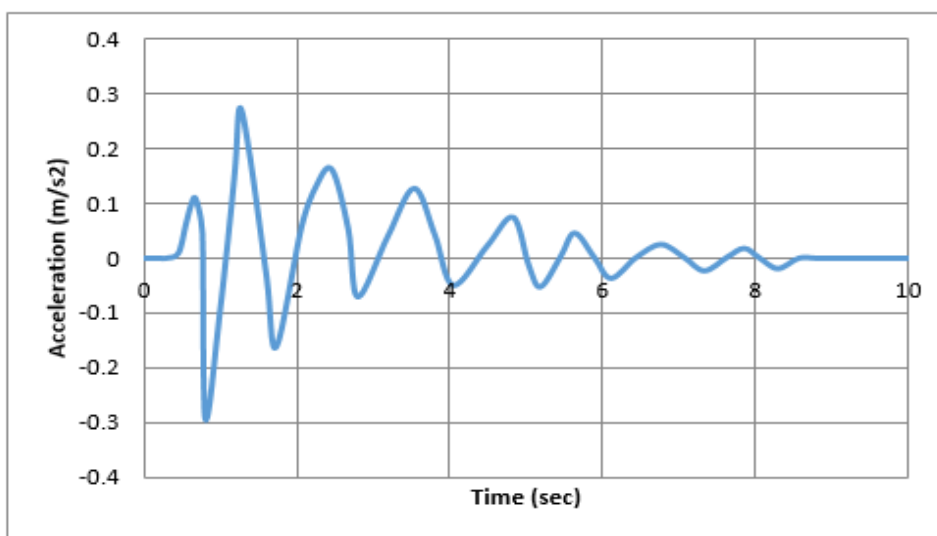


Figure 72: The acceleration domain of the forklift mast while carrying a load of 10 kg

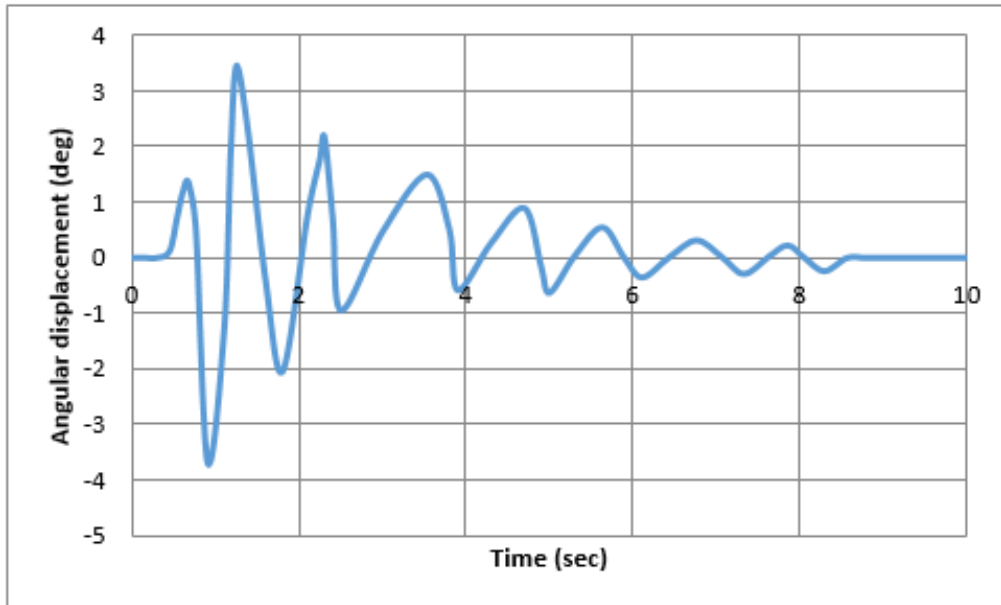


Figure 73: Angular displacement range of the mast while carrying a load of 10 kg

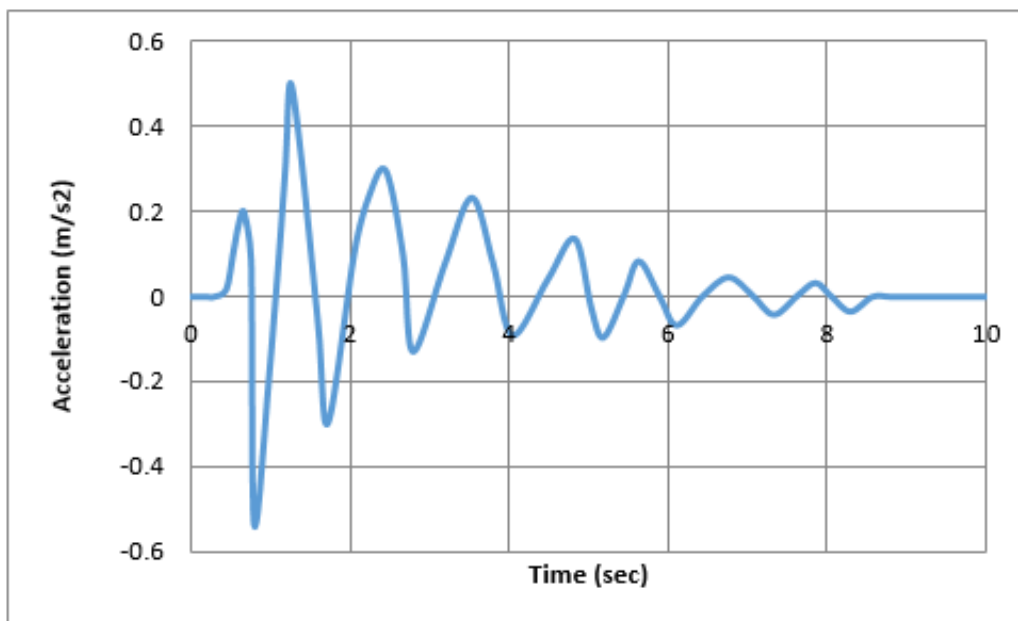


Figure 74: The acceleration domain of the mast part while carrying a load of 30 kg

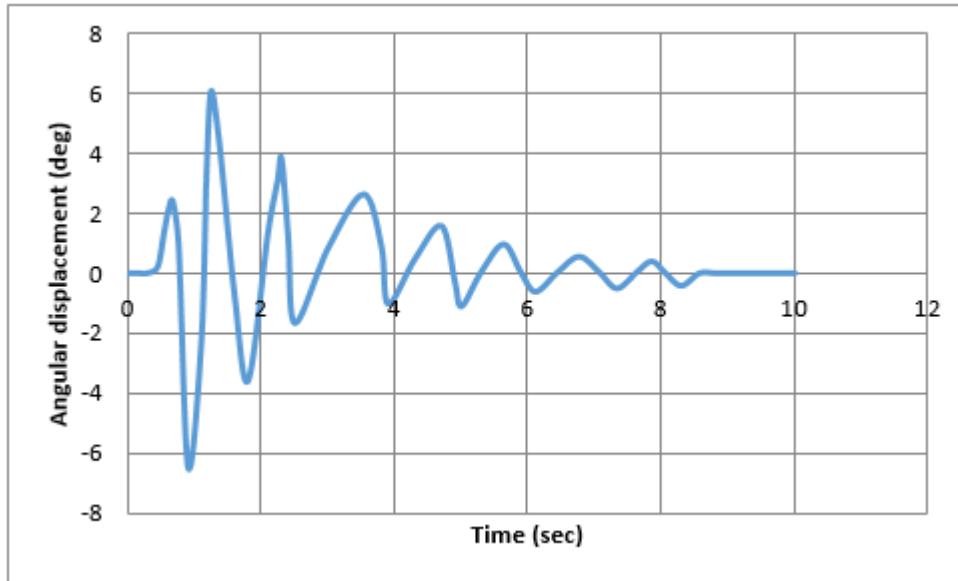


Figure 75: Angular displacement range of the mast while carrying a load of 30 kg

It should be noted that, valves section is controlled by the PID controller to control the flow rate. Also, the weight factor for the LQR controller was obtained by hit and trial method, as follows.

$$Q = \begin{bmatrix} 7000 & 0 \\ 0 & 62000 \end{bmatrix} \quad R = [25000]$$

In addition, the PID controller's gains were obtained based on the ZN method to the following values.

Proportional gain (K_p) = 38

Integral gain (K_i) = 24

Derivative gain (K_d) = 16

Furthermore, changes in the cost function for the LQR controller is presented in the figure 76, while simulating the vibrational system of forklift mast unit with 10kg of load and in 2m of height.

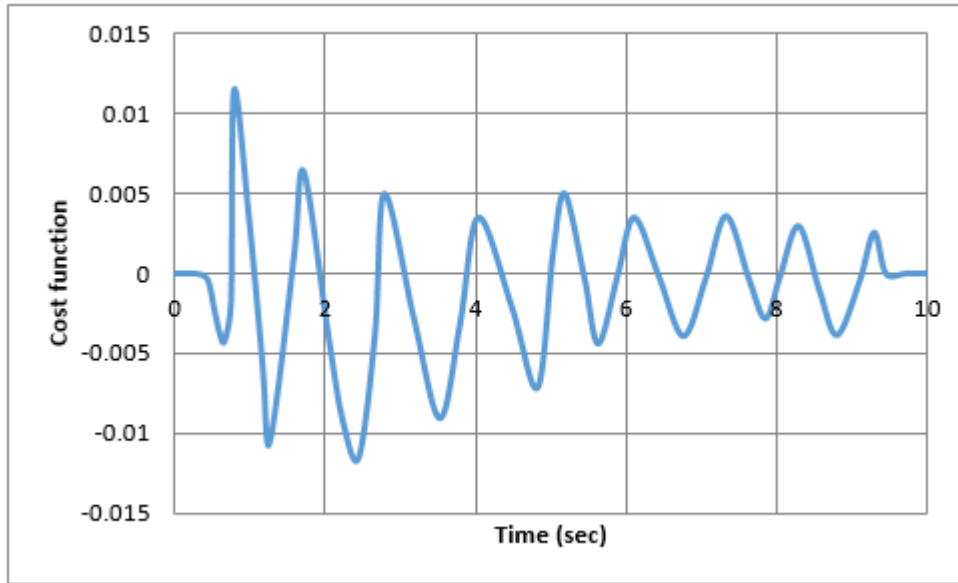


Figure 76: changes in time for LQR controller cost function while carrying a 10kg load

5.1.4) Sliding mode controller

In this section, the numerical model results for the forklift mast system with SMC controller is studied. The simulation tests were carried out based on the equations described in chapter 3 regarding the input force of the hydraulic cylinder as well as the related block diagram. Then the results related to the acceleration domain and angular displacement for the forklift mast system while carrying a load of 10 kg in the height of 2m were analysed. The results of acceleration domain and angular displacement of the forklift mast unit for 10 kg of load implementing the above-mentioned controller, LQR controller, and no controller (passive) are compared in figures 77 and 78.

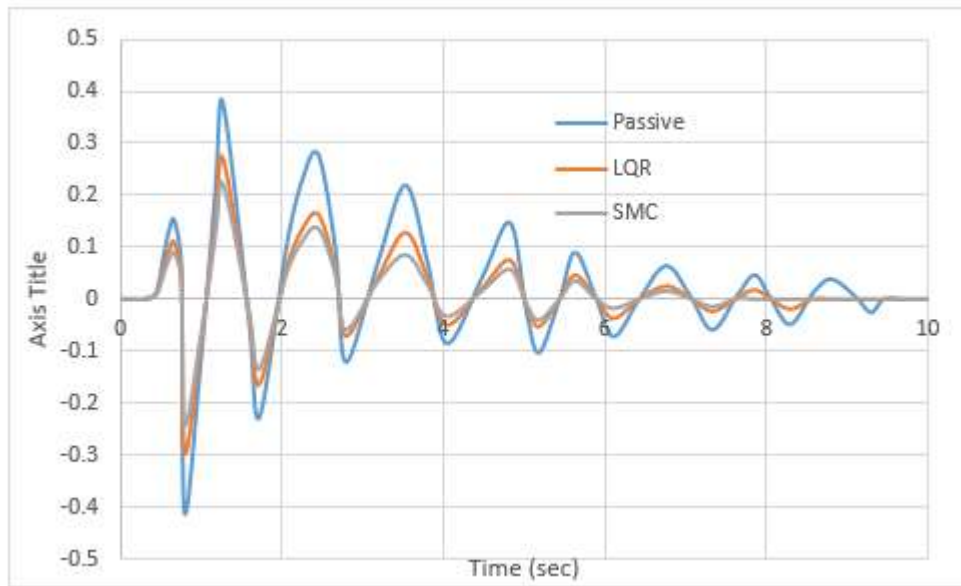


Figure 77: Comparison of the output of the acceleration domain with a load of 10kg

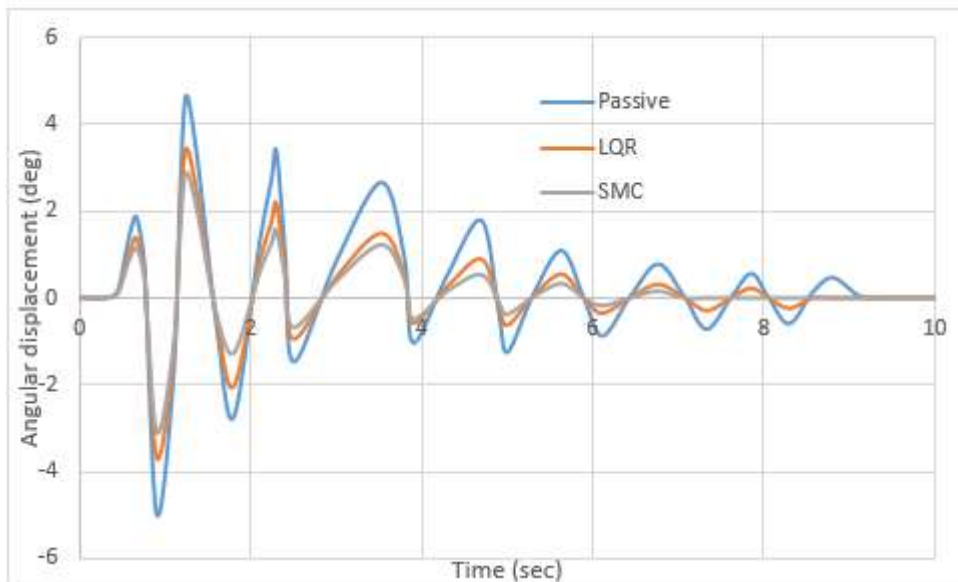


Figure 78: Comparison of Angular Displacement Range Output with load of 10kg

Similar results are demonstrated for 30 kg of load in figures 79 and 80

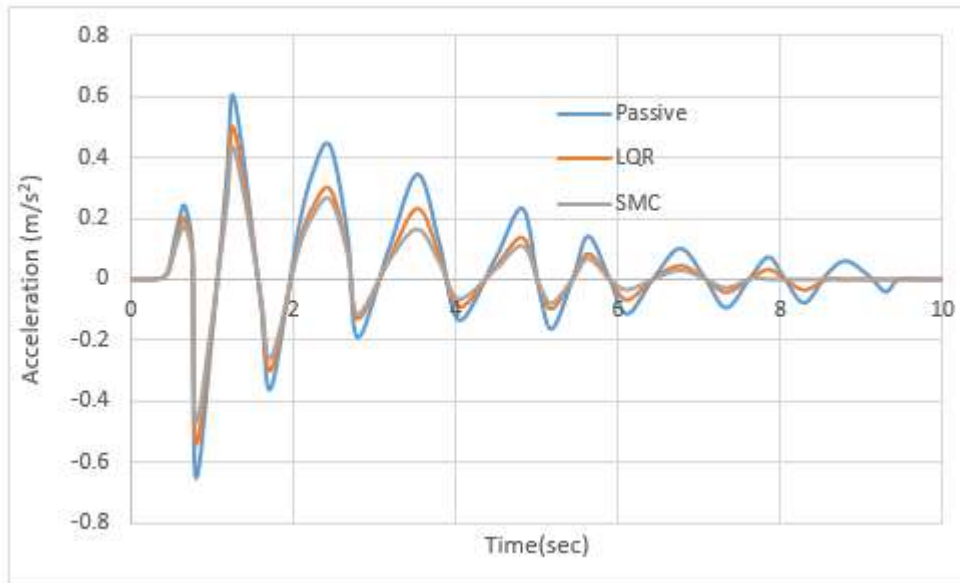


Figure 79: Comparison of the output of the acceleration domain with load of 30 kg

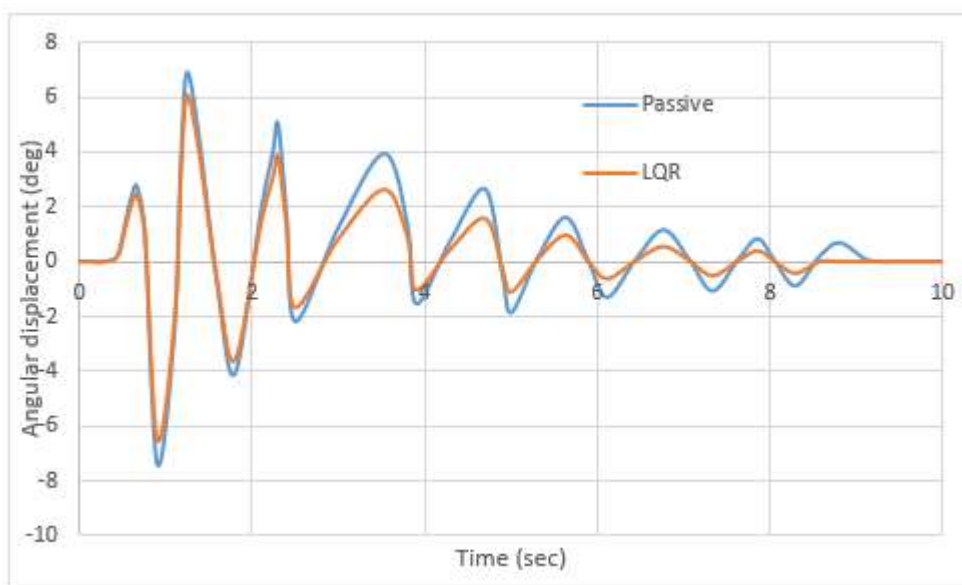


Figure 80: Comparison of Angular Displacement Range Output with load of 30kg

The weight factors for the SMC method has been set as $\lambda = 10$ and $K = 15$.

Furthermore, the PID gains were determined as follows.

Proportional gain (K_C) = 26

Integral time (T_i , min) = 18

Derivative time (T_d , min) = 12

Also, figure 81 shows the comparison of the forces of the forklift cylinders, which confirms a reduction by controlling the amount of vibrations. For this purpose, changes in the power of both control systems are presented.

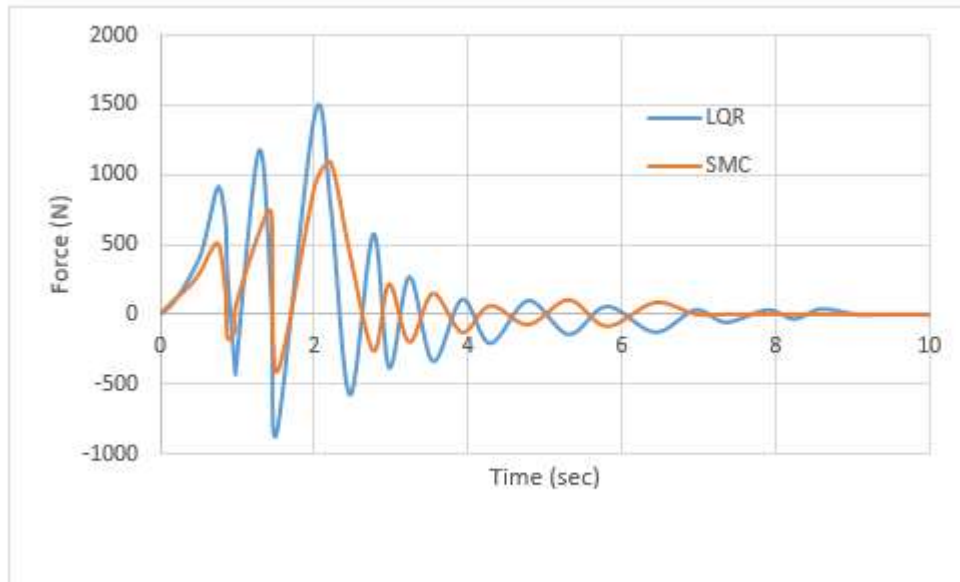


Figure 81: Comparison of Forces in Operating Cylinders Based on SMC and LQR Controllers while Carrying a Load of 10 kg

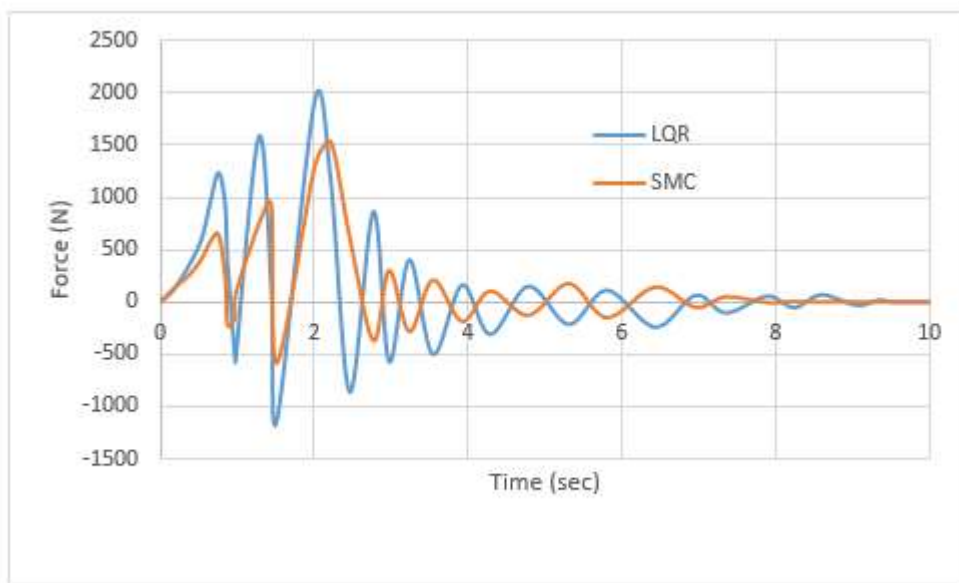


Figure 82: Comparison of Forces in Operating Cylinders Based on SMC and LQR Controllers while Carrying a Load of 30 kg

Analysing the results of the numerical model, it is clear that the increase in load can cause increases in acceleration domain and angular displacement range of forklift mast system. On the other hand, implementing various controllers lead to an improvement in vibrational

behaviour of forklift mast unit as well as reducing the fluctuation time. It means that the presence of the LQR controller in the system with the load of 10 kg had declined acceleration domain and angular displacement by 28% and 26%, respectively; whilst these measures for SMC are 41% and 38%, respectively.

Furthermore, in SMC, the system stops oscillating after 7.5 secs while this time for LQR system is 8.5 secs. Also, the magnitude of cylinder's forces in the SMC system was lower compared to that in the LQR system. Accordingly, SMC showed a better performance in general, as by using it the amount and time of the mast vibrations can be decreased to a desirable level. This improvement implies a positive viewpoint toward reaching the goal of the current research.

In order to do a better evaluation of the proposed control methods based on the applied numerical model, maximum acceleration domain and angular displacement of the forklift mast unit based on different load weights are shown in table 9.

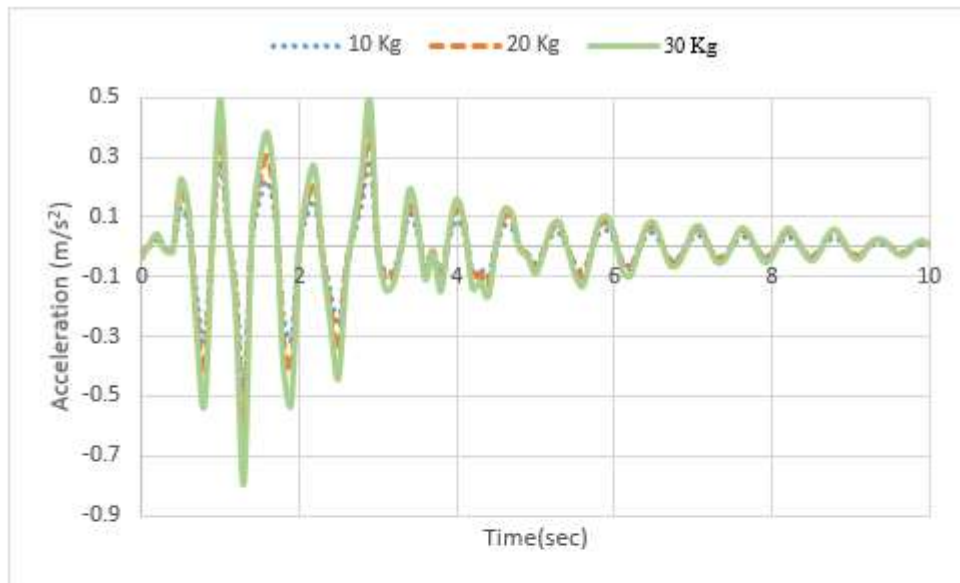
Table 10: Comparison of Maximum Acceleration Domain and Angular Displacement Variables Based on Different Weights in Numerical Model

Mass[Kg]	10		20		30	
	Accelerat ion (ms ⁻²)	Angular displaceme nt (deg)	Accelerati on (ms ⁻²)	Angular displaceme nt (deg)	Accelerati on (ms ⁻²)	Angular displaceme nt (deg)
Systems						
Passive	0.41	4.98	0.553	6.32	0.646	7.39
LQR	0.295	3.685	0.409	4.866	0.536	6.5
SMC	0.241	3.09	0.364	4.424	0.465	5.468

5.2) Experimental Results

After analysing the results of the numerical model without controller and with controller, these controlling methods were implemented on the platform model. In this section, the results of a realistic model of the forklift mast unit, which was implemented based on block diagrams in LabVIEW software, are presented. Then the results of the model with control would be discussed with different weights of the carried load. In figure 83, the results related to a mast mentioned in chapter 4 are presented. In part A and B of this figure, measured acceleration domain and displacement variations are presented for all three load weights of 10, 20, and 30

kg using LabVIEW software. Results are obtained using a first-order Low-pass filter.



A

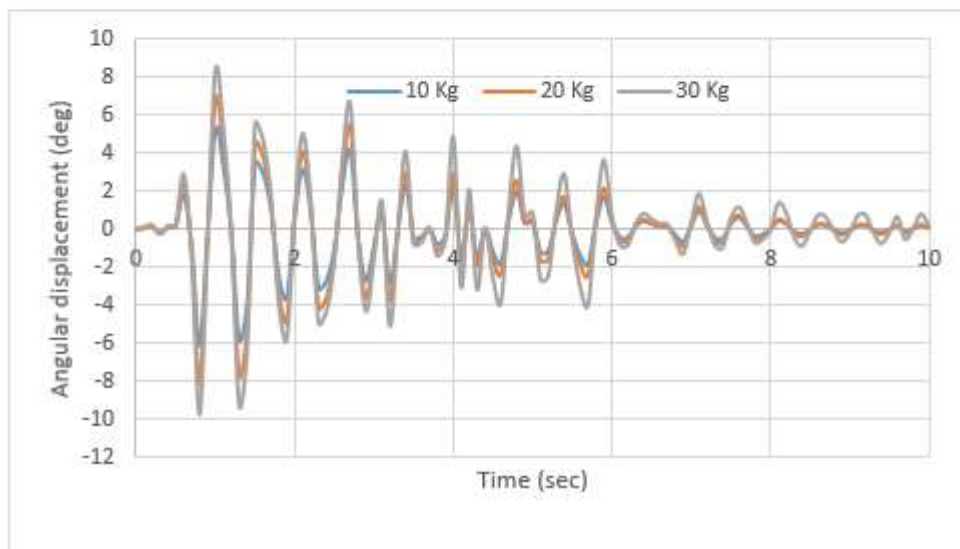


Figure 83: Vibrational Response of the Mast with Different Loads: A: Acceleration Domain B: Angular Displacement Range

In order to analyse and validate the results of the numerical model, result of the platform model and numerical model in the absence of controlling methods has been compared. Therefore, in the following table a comparison between the absolute maximum RMS values are presented for different weights and based on time variations chart of these variables.

Table 11: Comparison of RMS Value of Numerical Model Results and Experimental Test results for Weights of 10, 20 and 30 Kg

Mass	10 kg	20 kg	30 kg
Model			
Experimental	1.092	1.649	2.404
Numerical	1.130	1.706	2.484
Error (%)	3	3.4	3.5

By analysing the results presented in the table above, it can be concluded that the most significant level of error (3.5%) between the numerical and realistic model results occurred in the case of carrying a 30kg load. On this basis, it is confirmed that the numerical model results are in good agreement with the platform model results.

Also, by examining the response of the system based on the simulation tests, it can be found that by increasing the load weight from 10 kg to 30 kg, the maximum domain of vibrational acceleration and the angular displacement of the forklift mast system would reach from 0.5 (ms⁻²) and 6 degrees to 0.85 (ms⁻²) and 9 degrees, respectively. The RMS values of these responses are also 1.13 and 2.484 for acceleration and 13.52 and 21.63 for angular displacement, respectively; which means that an increase of 20 kg in the weight of the carried load, the maximum acceleration and displacement values increased by 0.35 (ms⁻²) and 3.6 degrees, respectively. The results of the control system based on LQR, SMC and PID controllers will also be discussed separately.

5.2.1) LQR_PID controller

In this section the results of the platform model equipped with LQR-PID controlling system is going to be analysed. Based on the descriptions presented in chapter 4 and controlling block diagram in LabVIEW software, this controlling system was implemented by controlling the input and output of cylinders on the forklift mast unit.

The system's performance will be studied based on the vibrations of the forklift mast unit in a platform model. Figure 83 shows the results related to cost function and control input voltage of platform model's valves with this controlling system and under the condition that a load of 10 kg is being carried. In figure 84, the changes in the cost function of the LQR controller are

illustrated when the controlling cylinders are being activated.

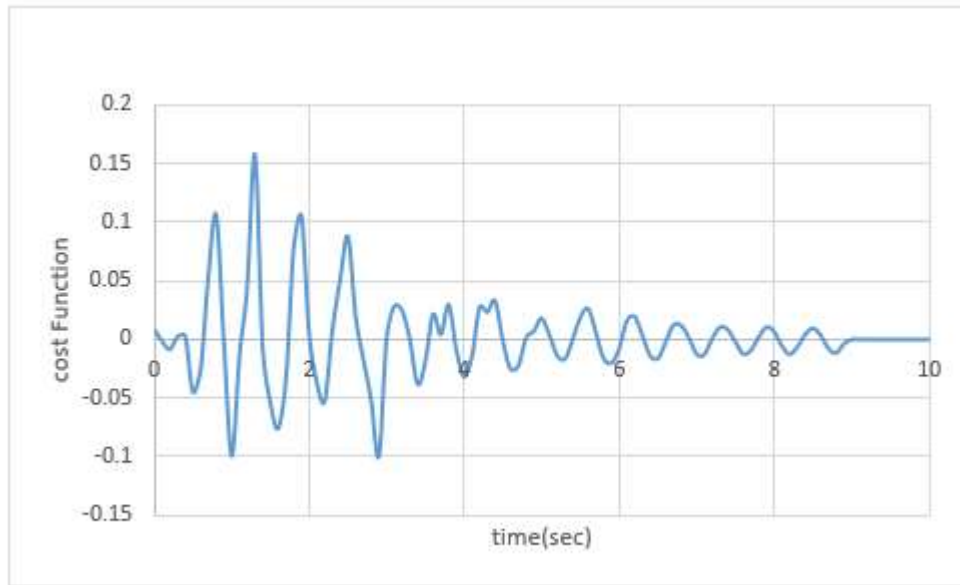


Figure 84:LQR Controller's Cost Function Changes While Carrying a Load of 10kg

The weight factor for the LQR controller was obtained as follow,

$$Q = \begin{bmatrix} 16650 & 0 \\ 0 & 74300 \end{bmatrix} \quad R = [32220]$$

PID controller's gain has been set to the following values.

Proportional gain (K_p) = 55

Integral gain (K_I) = 41

Derivative gain (K_d) = 22

5.2.2)SMC-PID controller

After implementing the SMC-PID method based on the block diagram presented in Chapter 4, the results of the performance of this control method are evaluated. Figures 85 to 88 exhibit the results related to the acceleration domain and angular displacement range of the forklift mast unit for loads of 10 and 30 kg while applying this control method

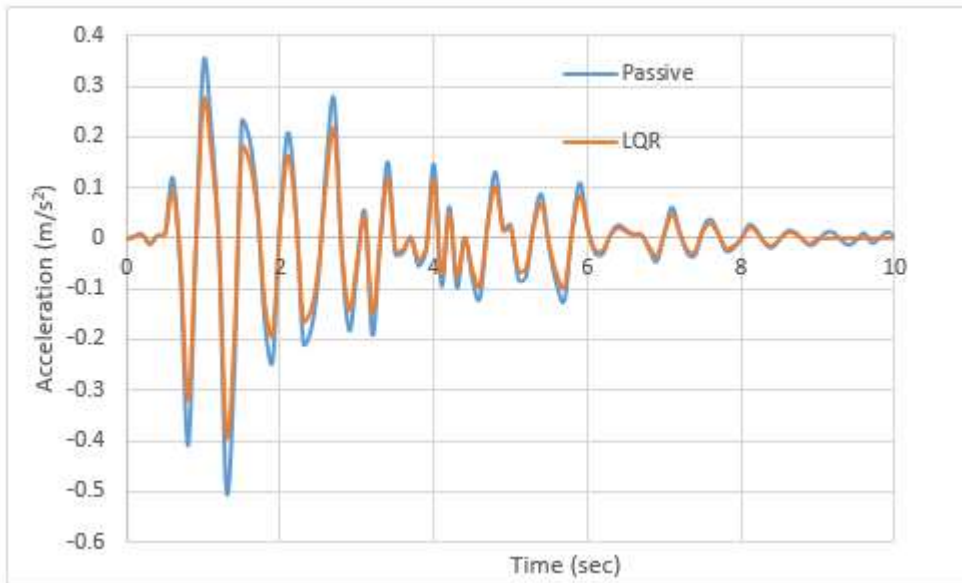


Figure 85: Acceleration Domain while Carrying a Load of 10kg

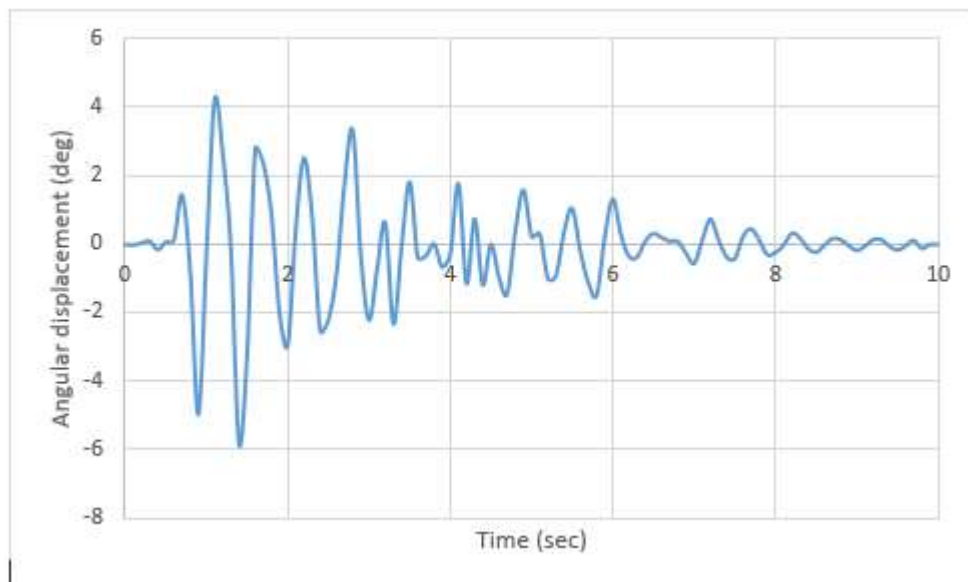


Figure 86: Angular Displacement while Carrying a Load of 10kg

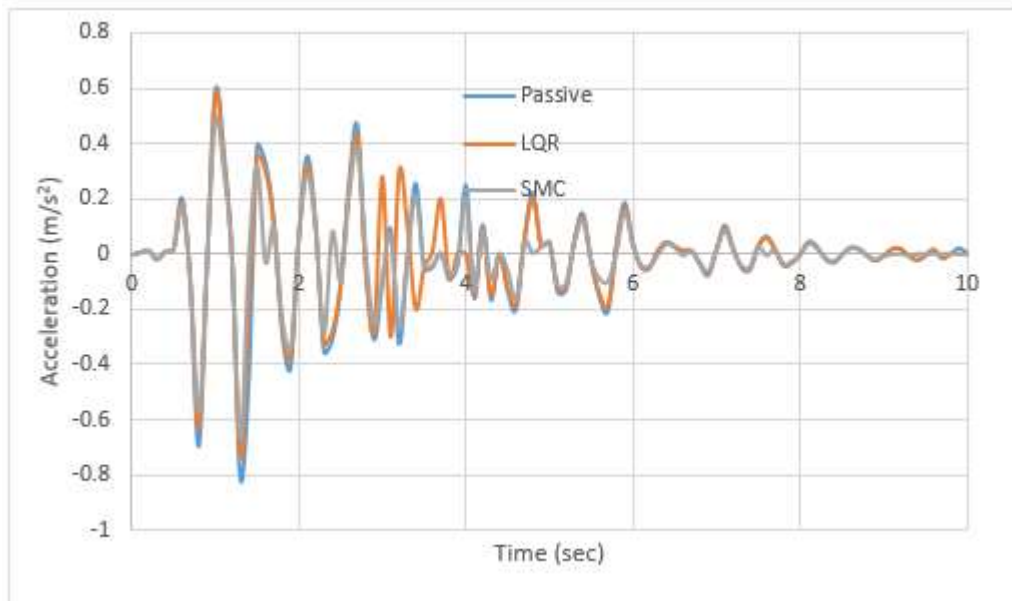


Figure 87: Acceleration domain while carrying a Load of 30kg

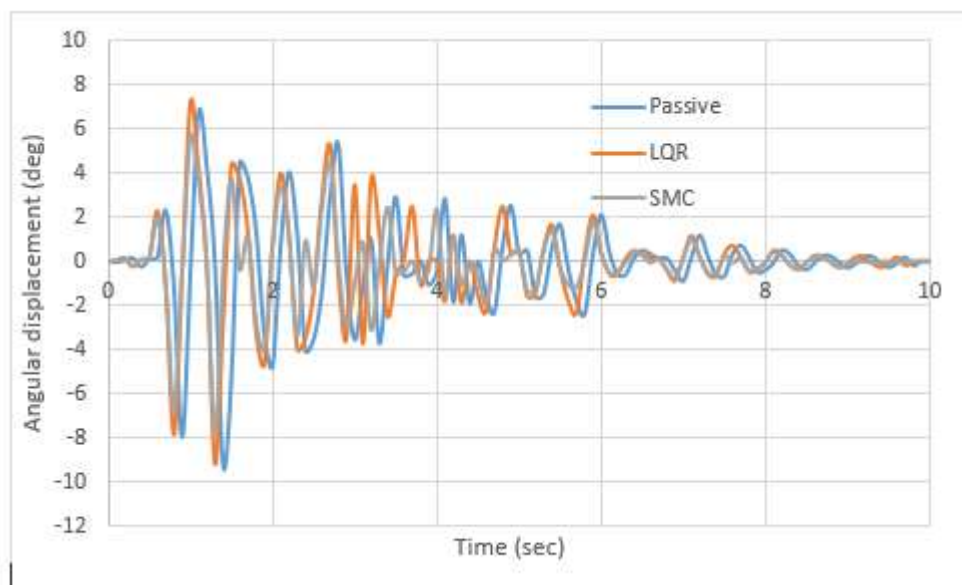


Figure 88: Angular displacement range while carrying a Load of 30kg

The weight factors for the SMC, based on implementing on platform model, are obtained as $\lambda = 24$ and $K = 8$. Furthermore, the PID gains were set as follows.

Proportional gain (K_p) = 62

Integral gain (K_I) = 26

Derivative gain (K_d) = 14

Figure 89 represents a comparison of time changes in voltage of controlling hydraulic servo valves during vibrations of forklift mast unit based on two controlling systems of LQR and SMC while carrying 30 kg weight of the load.

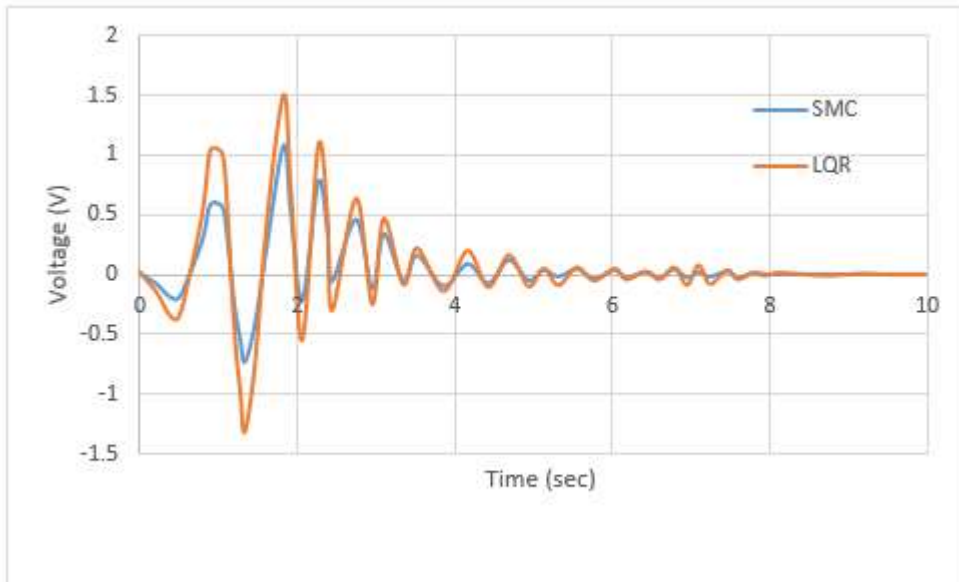


Figure 89: Comparison of Voltage Variations of Operating Cylinder Valves for Platform Model of Forklift Mast

As it is illustrated in the above figure, the controlling voltage applied on input and output valves is lower in the SMC system. Moreover, due to the faster damping of the controlled model through SMC, the applied voltage to the valves in this method would converge to zero more quickly, as opposed to the LQR controlling method where input voltage of valves are increased by 34% and are converged to zero in a longer time. This finding can be considered as an advantage to the SMC system in terms of both cost and time.

In the next section, a thorough analysis and comparison of results related to the controlled platform model by two controlling methods, namely LQR and SMC, as well as their pros and cons are presented

5.3) A Comparison of control methods

In this section, the performance of the control systems presented based on the vibrational behaviour of the actual model of the forklift system is compared. To achieve this, the maximum and RMS values of the acceleration domain and angular displacements of the forklift mast system are compared. In order to better compare the control methods presented, the results of the real model are discussed based on the effects of the model uncertainties. The results of controlled methods are discussed and evaluated by varying the height of the load carried in the

mast section from 1 meter to 2 meters. Further vibrational results of the system are compared and discussed with changes in load weight and the robustness of the control methods.

Figures 90 and 91 present the results of the acceleration domain and angular displacement for a load carrying condition of 10 located 2m above the level of the base

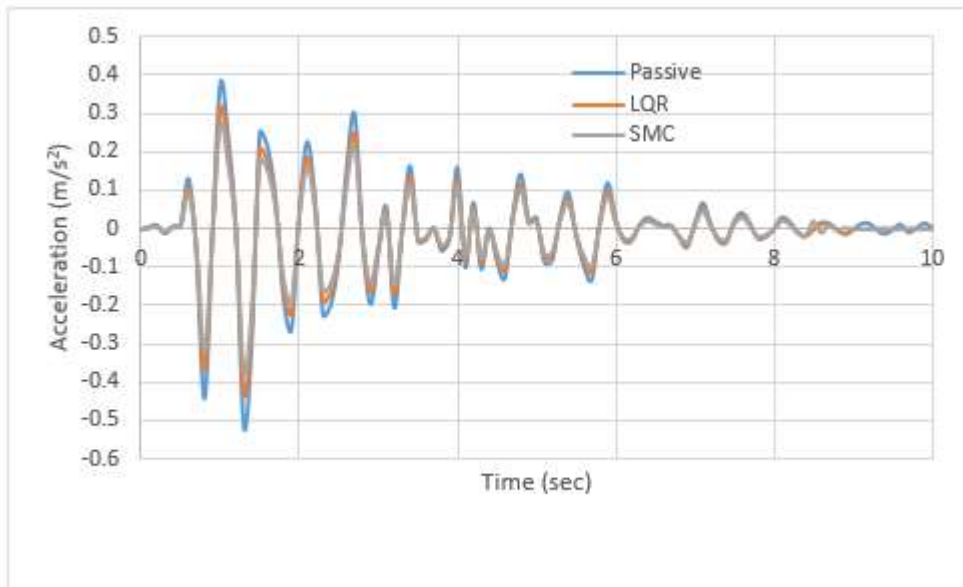


Figure 90: Acceleration domain while carrying a load of 10kg in 2m height

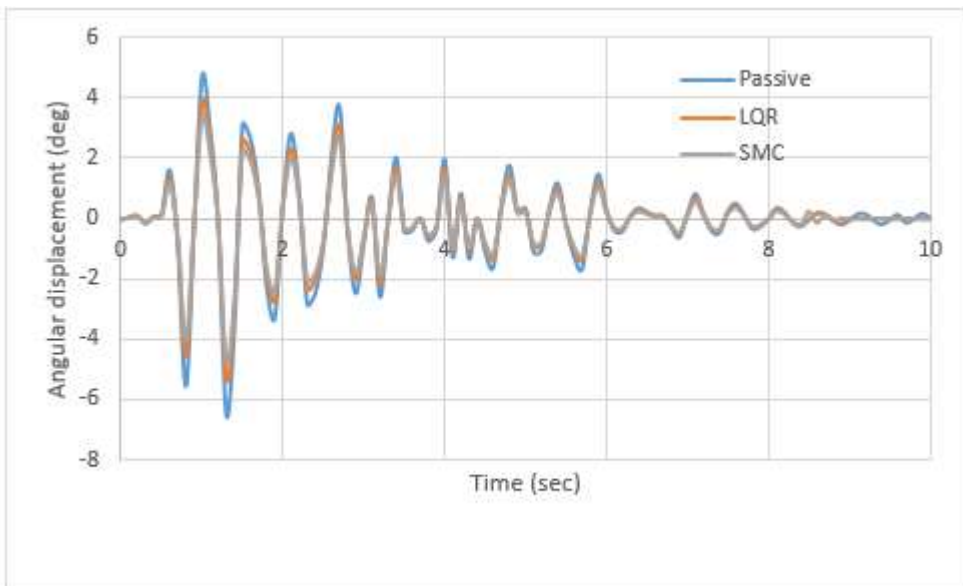


Figure 91: Angular displacement while carrying a load of 10kg in 2m height

Similarly, in figures 92 and 93, the results of acceleration domain and angular displacement for a load carrying condition of 30 kg, located 1m above the level of the forklift system are presented for the platform model.

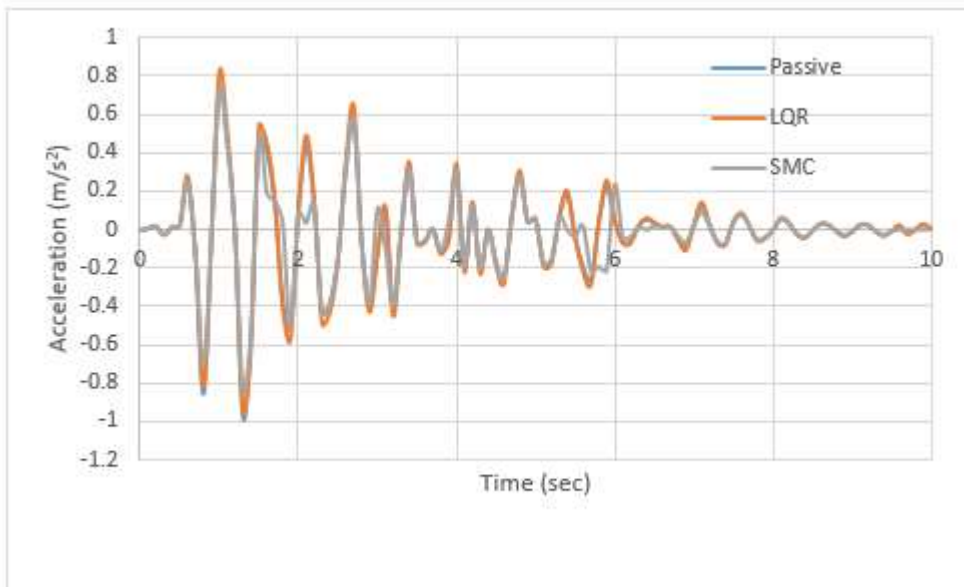


Figure 92: Acceleration Domain while Carrying a Load of 30kg in 1m Height

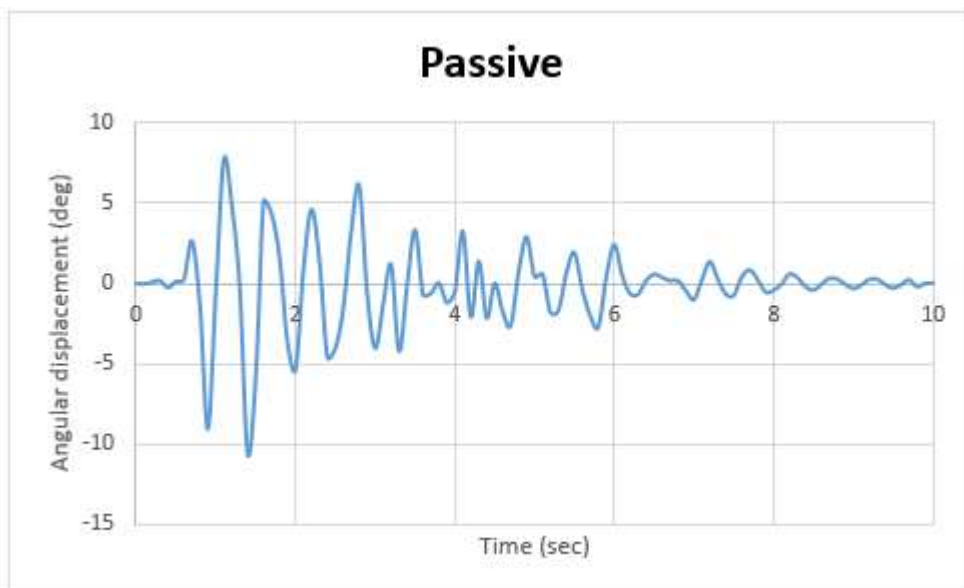


Figure 93: Angular displacement range while Carrying a Load of 30kg in 1m Height

Also, figure 94 represents a comparison of time changes in voltage of controlling hydraulic servo valves during vibrations of forklift mast unit based on two controlling systems of LQR and SMC while carrying 30 kg weight of the load in 1m Height.

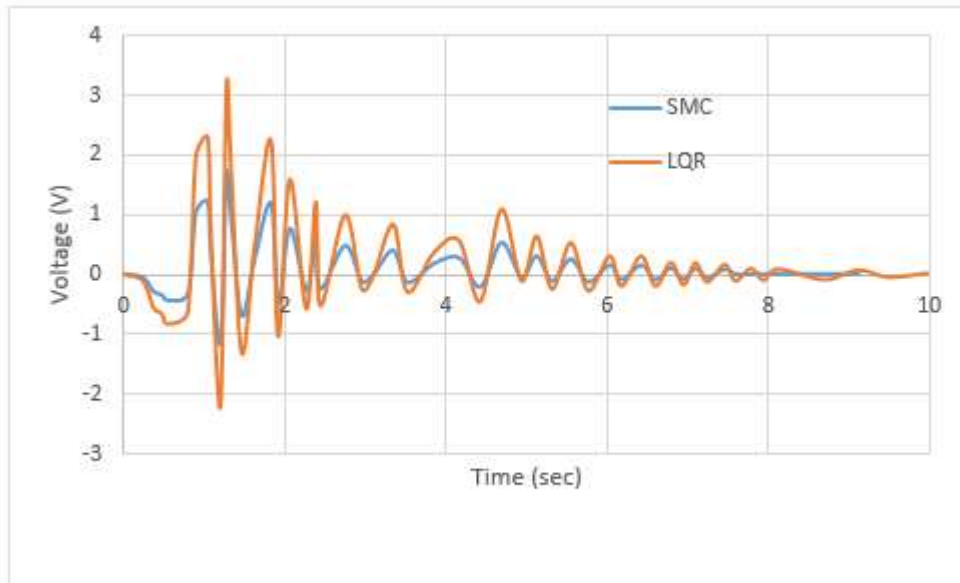


Figure 94: Comparison of Input Voltage of Dual- Cylinder Valves 2m Height

By comparing the above chart, it can be concluded that changing the placement of weights from 1m to 2m can have an adverse effect on controllers performance. On the other hand, this decrease in performance level was lower for the LQR controller in comparison with SMC, which shows the superiority of the former method. That is, when the system carries a load of 10kg, with increasing the height of the load and using the LQR controller method, vibrational behaviour of the forklift mast unit improves by 16.7% as compared to the platform model without the controller.

When using the SMC controller, this amount goes up to 28%, which in comparison with the similar situation placing the load in 2m height, 8% of the positive performance would be decreased for both controllers. Accordingly, with 30 kg of weight, this would reach nearly 7% in LQR controller, and 3.5% for SMC controller.

Thus, it can be concluded that in the most critical situation (30kg in 2m height), SMC shows a better performance giving this controlling method an edge and turning it to the final option to control the vibrations of the forklift mast systems.

Tables 11 and 12 present the comparative results associated with three controlling options, namely passive, LQR, and SMC systems under different loads of 10kg, 20kg, and 30kg at 1m height.

Table 12: Maximum acceleration domain based on positioning at 1 meter

Mass [Kg] \ Systems	10	20	30
Passive	0.5	0.7	0.85
LQR Controller	0.39	0.59	0.77
SM Controller	0.32	0.51	0.7

Table 13: Maximum angular displacement based on positioning at 1 meter

Mass [Kg] \ Systems	10	20	30
Passive	6	7.9	9.6
LQR Controller	4.7	6.5	8.7
SM Controller	3.9	5.7	7.9

Similarly, tables 13 and 14 compare the same results but at 2m height.

Table 14: Maximum acceleration domain based on positioning at 2 meters

Mass [Kg] \ Systems	10	20	30
Passive	0.54	0.78	0.98
LQR Controller	0.45	0.72	0.95
SM Controller	0.39	0.6	0.83

Table 15: Maximum angular displacement based on positioning at 2 meters height

Mass [Kg] \ Systems	10	20	30
Passive	6.8	8.7	11
LQR Controller	5.57	7.9	10.7
SM Controller	4.9	6.8	9.5

5.4)Chapter Conclusion

The aim of the current research was to control vibrations of the forklift's mast system based on a Semi-active controlling system related to the cylinders. In fact, in this thesis, for the first time, semi-active controller for cylinders in the forklift's mast unit was designed.

Accordingly, by using the components of the forklift's mast system and based on controlling the flow to inlet and outlet valves, vibrations of the mast unit was reduced.

Consequently, it was observed that the results related to SMC were acceptable due to high levels of robustness in various situations.

The magnitude of absolute maximums for acceleration and angular displacement variables for the system's body was extracted in the most critical situations of the system (i.e. carrying a load of 30 kg in 2m height).

Amount of angular displacement for the mast unit was 9.5 degrees while this amount was 11 degrees for the same situation in the uncontrolled system. Such a difference represents the robustness of controlling method to the positioning of the load while moving. However, the LQR controller showed some below-expectation results when carrying a load of 30 kg at a 2m height in controlled and uncontrolled situations; the angular displacement was 10.7 and 11 degrees, respectively. It shows the weakness of the LQR controlling method in comparison with SMC under critical conditions.

In order to make a better comparison of these two control methods with respect to the uncontrolled system, the results related to the maximum reduction rate for acceleration domain and angular displacement variables were discussed. Table 15 presents the results of the platform model based on different load weights at 1m height.

Table 16: Results for Maximum Reduction Rate of Acceleration Domain and Angular Displacement Variables Based on Placing The Load in 1 m Height in Platform Model.

Mass[Kg]	10		20		30	
	Acceleration (%)	Angular displacement (%)	Acceleration (%)	Angular displacement (%)	Acceleration (%)	Angular displacement (%)
Systems						
LQR	22	21.4	15.7	17	9.4	9.3
SMC	36	35	28.5	27.8	17.6	17.7

Moreover, table 16 includes the results related to the maximum reduction rates of acceleration domain and angular displacement variables associated with the platform model based on different load weights in 2m height.

Table 17: Results for Maximum Reduction Rate of Acceleration Domain and Angular Displacement Variables Based on Placing The Load in 2 m Height in Platform Model.

Mass[Kg] Systems	10		20		30	
	Acceleration (%)	Angular displacement (%)	Acceleration (%)	Angular displacement (%)	Acceleration (%)	Angular displacement (%)
LQR	16.7	18	7.7	9	3	2.7
SMC	27.7	28	23	21.8	15	13.6

the voltage diagram of inlet and outlet servo-hydraulic valves of the dual-cylinders in SMC system shows a lower maximum rate and higher damping ratio, which also has a positive effect on the performance of the operators and it led to their superior performance compared to the LQR controller.

Therefore, the SMC-PID control method has a better performance in controlling and reducing the vibrations of the forklift's mast system, indicating a relative advantage of this method over the LQR-PID method.

Chapter 6 Conclusion

Highlights:

- ❖ Discussion of results between controllers
- ❖ Research Conclusions
- ❖ Limitations and Future work

This chapter is dedicated to the discussion of results associated with numerical and experimental tests with different control systems, extending to the final concluding remarks. This thesis is concluded with short summary of limitations and future works.

In this research a novel strategy for controlling is presented to reduce vibrations of forklift's mast unit based on controlling forces of dual-cylinders, which are used for lifting loads. To reach this aim, a new method was proposed based on controlling system's cylinders and controlling the flow of input and output in servo hydraulic valves.

In order to better investigate the purpose of this research, two controlling methods, namely LQR and SMC systems were used. Firstly, the LQR system was implemented as a cylinder controller and PID method was used as a valve controller. Then, the SMC system was implemented as a cylinder controller and a PID method to control the inlet and outlet valves. Summary of the analysis and evaluation of the control methods in different situations are discussed in this chapter.

6.1) LQR-PID controller

This controlling method was implemented based on an optimal linear controlling method for upper-level of the system and a PID controller for a lower level of the system. The results of this controlling method caused a particular vibrational behaviour of the forklift's mast unit. That is the amount of angular displacement for the forklift's mast body was improved by 21.4% in the controlled situation; in other words, carrying a load of 10 kg produced the maximum angular displacement of 6deg in the uncontrolled case coming down to 4.7deg in a controlled case. It should be mentioned that this amount for a load of 30 kg reached 9.3deg. Also, the results obtained from the platform model, for the 30 kg load, when the height changes from 1 to 2m, showed the maximum increase from 7.9 to 10.7 degrees (a 35% increase). The problem of the current controlling method can be traced back to its lack of resistance for uncertainties. Thus, the best performance for this method was observed when the load is 10 kg and it is located in 1m height while the most oscillation in the controlled system happens when it is carrying a load of 30 kg in 2m height. The reason for this issue can also be analysed considering the increase in torque distance related to the load weight force in the mast unit.

6.2) SMC-PID controller

After implementing this controlling method, the results showed an improvement in maximum angular displacement variable, decreased from 6 to 3.9 degrees (a 35% improvement) while carrying a load of 10 kg in 1m height. On the other hand, the amount of maximum decrease for this variable while carrying a load of 30 kg in 2 m height is 17.7. Furthermore, with changing the height from 1 to 2 m the maximum angular displacement for the mast unit decreased from 11 to 9.5 degrees (a 14% improvement). It means that the height of load had an adverse effect

on the positive performance of this controlling method too, but it still managed to decrease the maximum angular displacement by 14%. Therefore, the increase in the height of load in the worst situation, i.e. carrying a load of 30 kg, had a less smoothing effect on oscillations of forklift's mast unit. This observation can be explained by the resistance of SMC in a way that uncertainties in model parameters cannot have noticeable effects on the results of the system. That is, with a 100% increase in the height of the load, this controlling method still managed to decrease the maximum angular displacement variable in forklift's mast unit by 14%. This reduction reflects the superiority of this method in critical situations, and this can encourage designers to select these controllers for systems with uncertainties and work environments with noise.

6.4) Overall outcome

The aim of the current research was to control vibrations of the forklift's mast system based on a Semi-active controlling system related to the cylinders. In fact, in this thesis, for the first time, semi-active controller for cylinders in the forklift's mast unit was designed.

Accordingly, by using the components of the forklift's mast system and based on controlling the flow to inlet and outlet valves, vibrations of the mast unit was reduced. In the current research, it has been strived to control the vibrations of the forklift's mast unit with a novel strategy that dampens the vibration of the mast with the semi-active control system and without adding any extra mechanical component to the system. This has been achieved by, draw a numerical model based on a simplified system and the degree of freedom associated with the mast unit oscillations. This research introduced and implemented two methods of second-order linear control (i.e. LQR and SMC) to control the cylinders of the forklift. Then, in order to achieve the maximum force for the cylinders, a PID control method is presented based on flow control of servo-hydraulic valves of the forklift. By comparison with real results, the newly designed controllers have been successful to achieve between 13.6% to 36 % reduction in vibration of forklift's mast with different loads on the mast unit.

6.5) Future work

The current research aimed to reproduce the vibrations experienced on the forklift mast as they would occur on the full size forklift mast; however there were restrictions that limited the scope of this investigation and have been noted for further investigation.

A key factor that predominantly limited the depth of this investigation was the absence of a Software Engineer to provide the readily available support service when problems occurred

during the use of the LabVIEW software. As a novice in programming, all the LabVIEW knowledge was gained during a brief efficient period. The final execution of the VI, at its finest, may still be a generally intermediate code and could be improved to account for a greater range of factors or better at governing autonomous activity. A study into a diverse range of LabVIEW code with different output control methods could be examined to ascertain the optimum method for control and even possible reduction of mast vibrations.

The following list provides new possible solutions to the vibration control of the forklift's mast system providing a more accurate dynamic model based on the simultaneous movement of the forklift system:

- Presenting a new model of vibration for the forklift's mast unit based on the effect of vertical displacement of axes and movement path.
- Providing a comprehensive model for longitudinal, transverse and vertical dynamics of the forklift system based on the flexural vibrations of the forklift.
- Investigating the effects of forklift's mast vibrations on the noise and vibrations of driver's cabin.
- Providing a robust adaptive control method to increase the stability and control of oscillations in the system under critical conditions.
- Using hydraulic system called Magneto-Rheological (MR) dampers non-linear control system.
- Further investigation of the virtual sensing technique to reduce the initial delay given by the hydraulic pump. Since the type of nonlinearity is piecewise linear, it can cause numerical problems during the linearisation .
- A comparison of the performance of the combined SMC-LQR-PID loop with th single VFC loop in terms of structural vibration reduction, when the structure is subject to a broadband excitation

References

- [1] Hartford, "Forklift Safety Awareness," 2008. [Online]. Available: http://www.naw.org/nawnews/news_article.php?articleid=530.
- [2] T. Sellick, "A potted history of the forklift truck," 2012. [Online]. Available: <http://www.fork-lift-training.co.uk/history.html>.
- [3] Yale, "Our History," 2013. [Online]. Available: <http://www.yale.com/emea/en-gb/about-us/history/>
- [4] Q. Government, "What are forklift trucks," 2011. [Online]. Available: <http://www.deir.qld.gov.au/workplace/subjects/forklift/trucks/index.htm>.
- [5] W. D. Knowledge, "Life Trucks Explained - A Materials Handling Primer," 2011. [Online]. Available: <http://warehouseiq.com/what-is-a-forklift/>.
- [6] Harringt, "Forklift Classes and Lift Codes," Bnl.gov, USA, 2003.
- [7] Yale, "VL Series - Electric Forklift trucks with AC Technology," Yale Europe Materials Handling, England, 2011
- [8] T. Sellick, "Forklift truck longitudinal stability considerations," 2012. [Online]. Available: <http://www.fork-lift-training.co.uk/technical/forklift-stability-1.html>.
- [9] Toyota, "SAS - System of Active Stability," 2013. [Online]. Available: http://www.toyotaforklifts.co.uk/EN/Products/innovations/Pages/innovation_sas.aspx.
- [10] T. Sellick, "Forklift truck traction control - older system," 2012. [Online]. Available: <http://www.fork-lift-training.co.uk/technical/forklift-traction-systems-2.html>.
- [11] T. Crompton, "Battery Reference Book," Third, Ed., Oxford, Reed Educational and Professional Publishing Ltd, 2000, pp. 326-328
- [12] C.C.Power, "DC Motor Controller," 2011. [Online]. Available: <http://www.ccpowerltd.co.uk/tractioncontrollers.htm>.
- [13] Q. Government, "Forklift safety - reducing the risks," SafeWork, South Australia, 2010.
- [14] W. John, "Chapter 1 - Introduction to Mechanical Vibrations," London, 2011.
- [15] W. T. Thomson, Theory of Vibration With Applications, 4th ed., London: Chapman & Hall, 1993

- [16] W. T. Thomson, *Theory of Vibration With Applications*, 4th ed., London: Chapman & Hall, 1993
- [17] F. F. Ehrich, "Chapter 5 - Self-Excited Vibration," Prepress, 2005
- [18] Hyster, "WHole-Body Vibration," 2013. Available: [http://www.hyster-bigtrucks.com/Legislation/Whole-Body Vibration/](http://www.hyster-bigtrucks.com/Legislation/Whole-Body-Vibration/).<https://www.socotec.co.uk/news/blog/archive/make-reducing-health-and-safety-risks-your-new-year-s-resolution>
- [19] CESAB, "Intelligent mast design means greater productivity," 2011. [Online]. Available: <http://www.cesab-forklifts.co.uk/Uk/News/NewsPages/Pages/intelligent-mast-design.aspx>
- [20] NACCO, "Pluck Test on Mast Vibration," NACCO Material Handling Group, England, 2012
- [21] CESAB, "Industry leading mast technology," CESAS Mast Technology, 2011.
- [22] Franchek, M. A., M. W. Ryan, and R. J. Bernhard. "Adaptive passive vibration control." *Journal of Sound and Vibration* 189, no. 5 (1996): 565-585
- [23] Fuller, Christopher C., Sharon Elliott, and Philip A. Nelson. *Active control of vibration*. Academic Press, 1996
- [24] Balas, Mark J. "Active control of flexible systems." *Journal of Optimization theory and Applications* 25, no. 3 (1978): 415-436
- [25] Icmomega, https://micromega-dynamics.com/products/building_blocks/active-damper/
- [26] Goodwin, Graham C., Stefan F. Graebe, and Mario E. Salgado. *Control system design*. Upper Saddle River, NJ: Prentice Hall, 2001
- [27] Karnopp, Dean, Michael J. Crosby, and R. A. Harwood. "Vibration control using semi-active force generators." *Journal of engineering for industry* 96, no. 2 (1974): 619-626.
- [28] Marzocchi, <http://www.moto-choice.com/en/Press-Releases/430/marzocchi-introduces-a-complete-semi-active-suspension-system-for-motorcycles.html>
- [29] Marzocchi, <http://www.moto-choice.com/en/Press-Releases/430/marzocchi-introduces-a-complete-semi-active-suspension-system-for-motorcycles.html>
- [30] Z. Shuo, *Active Control Theory*, Taipei (Taiwan): Ting Mao, 2001
- [31] N. Instruments, "LabVIEW for Real-Time Control in Measurement and Automation," NI, 2002

- [32]Levant, Arie. "Principles of 2-sliding mode design." *automatica*43, no. 4 (2007): 576-586.
- [33]Levant, Arie. "Principles of 2-sliding mode design." *automatica*43, no. 4 (2007): 576-586
- [34]Tamba, Tua Agustinus, Bonghee Hong, and Keum-Shik Hong. "A path following control of an unmanned autonomous forklift." *International Journal of Control, Automation and Systems* 7, no. 1 (2009): 113-122.
- [35]Minav, Tatiana, L. Laurila, and J. Pyrhönen. "Relative position control in an electrohydraulic forklift." *International Review of Automatic Control (1974-6059)* 6, no. 1 (2010): 54-61
- [36]Ventura, Leonardo, Giovanni Paolo Bonelli, and Alberto Martini. "Development and experimental validation of a numerical multibody model for the dynamic analysis of a counterbalance forklift truck."
- [37]Blood, Ryan P., James D. Ploger, and Peter W. Johnson. "Whole body vibration exposures in forklift operators: comparison of a mechanical and air suspension seat." *Ergonomics* 53, no. 11 (2010): 1385-1394.
- [38]Myriad, Dean, Michael J. Crosby, and R. A. Harwood. "Vibration control using semi-active force generators." *Journal of engineering for industry* 96, no. 2 (1974): 619-626.
- [39]Marur, SR & Kant , T 1996, Free vibration analysis of fiber reinforced composite beams using higher order theories and finite element modelling ,, *journal of sound vibration*, vol.194, no.3, pp. 337-351
- [40]Peng , XQ, Lam, KY & Liu, GR 1998, ,,A vibration control of Composite Beams with Piezoelectrics: A Finite Element Model with third order theory ,, *Journal of Sound and Vibration*, vol.209, no.4, pp. 635 - 650.
- [41]Liu, GR., Peng , XQ ,Lam, KY & Tani, J 1999, ,, vibration control simulation of laminated composite plates with integrated piezoelectrics ,,*journal of sound and vibration*, vol. 220, no. 5, pp. 827-846.
- [42]Lin, Chien-Chang & Huang, HN 1999, ,,vibration control of beam- plates with bonded piezoelectric sensors and actuators ,, *composites and Structures*, vol. 73, no.1-5, pp. 239-248.

- [43] Valoor, manish , T Chandrasheakara , k, agarwal & sanjeev, 2001, „self adaptive vibration control of smart composite structure beams using recurrent neural architecture „, international journal of solids and structures, vol. 38, pp. 7857-7874
- [44] Moita S , jose, M, cristovao, M , Soares, M & Carlos, A 2005, „ Active control of forced vibration in adaptive structures using a higher order model“, Composite structures , vol.71 , no.3., pp. 349-355
- [45] Xinke & Gou 2007, „ Active vibration control of a cantileaver beam using bonded piezoelectric sensors and actuators „, The eighth international Conference on Electronic Measurement and Instruments, pp.186 -191
- [46] Umesh, K, Ranjan G 2009, „shape and vibration control of smart composite plate with matrix cracks,“ smart materials and structures , vol 18, no.2,pp.25-36
- [47] Irschik 2002, A Review on Static and Dynamic Shape Control of Structures by Piezoelectric Actuation , Article *in* Engineering Structures 24(1):5-11 · January 2002 Thermodynamics Flashcards
- [48] Fung, Eric, H.K., Chen, S.M., and Leung T.P., “Roundness Control in Taper Turning using FCC Technique”, Proceedings of the American Control Conference, Albuquerque, New Mexico, pp.1068-1069, 1997
- [49] Sun, B & Huang, D 2001 , „ vibration suppression of laminated composite beam with a piezo – electric damping layer „, composite structures, vol.53,no.4,pp.437-447
- [50] Kermani, MR, Moallem, M & Patel, RV 2002, „optimizing the performance of piezoelectric actuators for active vibration control“, Proceedings of the 2002 IEEE Conference on Robotics and Automation, Washington DC. pp. 87-92
- [51] Baillargeon, BP & Vel, SS 2004, „Active vibration suppression of smart structures using piezoelectric shear actuators „,“proceedings of the fifteenth International Conference on Adaptive Structures and Technologies, Bar Harbor, Maine. pp. 141-148
- [52] Hu & Vukovich, G 2005, „Active robust shape control of flexible structures „, Mechatronics , vol .15,pp.807-820
- [53] lin E, Brennam MJ & Mac BR 2005 , „A shape memory alloy adaptive tuned vibration absorber : design and implementation „, smart materials & structures , vol.14,no.1.pp.19-28

- [54] Moita, JS 2008, „ optimal dynamic control of laminated adaptive structures using a higher order modal and a genetic algorithm“, *Computers and Structures*, vol.86, no. pp.198-206.
- [55] Donoso, A & Sigmund, O 2008, „optimization of bimorph actuators with active damping for static and dynamic loads „, *struct multidisc optim*, Springer Verlag. vol. 38, no. 4, pp. 171-183
- [56] Zhang, wenming , meng , guang, Li & Hongguang 2006 , „Adaptive vibration control of micro-cantilever beam with piezoelectric actuator in MEMS“, *International journal of advanced manufacturing technology*, vol.28, no.3, pp.321-327.
- [57] Kiral, zeki, malgaca, levent, akdag, & Murat 2008, „Active control of residual vibrations of a cantilever smart beam“, *turkish Journal of Engineering and Environmental Sciences*, vol.32, no. pp. 51 – 57
- [58] Baz, A, Imamand, K & Mc Coy, J 1990, „Active vibration control of flexible beams using shape memory actuators „, *journal of sound and Vibration*, vol.140, no.3, pp. 437 -456
- [59] Song, G, Qiao, PZ, Binienda, WK & Zou, GP 2002, „Active vibration damping of composite beam using smart sensors and actuators“, *journal of aerospace engineering* , vol .15.no.3, pp .97-103
- [60] Active vibration control of smart piezoelectric beams: Comparison of classical and optimal feedback control strategies Article in *Computers & Structures* 84(22):1402-1414 · September 2006
- [61] J. Fei Active Vibration Control of a Flexible Structure Using Piezoceramic Actuators March 2008
- [62] Chen, SH, Lien-Wen, Lin, Chung-Yi & Wang, CC 2002, „Dynamic stability analysis and control of a composite beam with piezoelectric layers, composite structures“, vol.56, no.1, pp.97-109
- [63] Youn, SH, Han, JH & Lee, I 2000, „ Neuro- -adaptive vibration control of composite beams beams subjected to sudden delamination „, *journal of Sound and Vibration*, vol.238, no.2, pp. 215- 231
- [64] Kumagai et al Control of shape memory alloy actuators with a neuro-fuzzy feedforward model element AKIHIKO KUMAGAI1, *, TIEN-I. LIU1 and PAUL

HOZ IAN2 1Department of Mechanical Engineering, California State University,
Sacramento, 6000 J Street, Sacramento, CA 95819-6031, USA

- [65] Youn, SH, Han, JH & Lee, I 2000, „ Neuro- -adaptive vibration control of composite beams beams subjected to sudden delamination „, journal of Sound and Vibration, vol.238, no.2, pp. 215- 231
- [66] Zhi-cheng et al (2007) Qiu, Zhi-cheng, et al. "Active vibration control of a flexible beam using a non-collocated acceleration sensor and piezoelectric patch actuator." *Journal of sound and vibration* 326.3 (2009): 438-455
- [67] Nguyen, Tuan, Nicholas Haritos, Emad F. Gad, and John L. Wilson. "Simplified Assessment of Forklift-Induced Floor Vibrations." (2014).
- [68] Baroudi, Mariam, Mohamad Saad, and Walid Ghie. "State-feedback and linear quadratic regulator applied to a single-link flexible manipulator." In *2009 IEEE International Conference on Robotics and Biomimetics (ROBIO)*, pp. 1381-1386. IEEE, 2009.
- [69] Zimmert, Nico, and Oliver Sawodny. "Active damping control for bending oscillations of a forklift mast using flatness based techniques." In *Proceedings of the 2010 American Control Conference*, pp. 1538-1543. IEEE, 2010
- [70] Zhang, Ke Jun, and Jian Chen. "Research on Dynamic Optimization Principles for Forklift Truck Mast." In *Applied Mechanics and Materials*, vol. 556, pp. 1147-1150. Trans Tech Publications, 2014
- [71] Lehtonen, Lasse, Kyösti Sarkkinen, and Janne Polvilampi. "Method and an arrangement for dampening vibrations in a mast structure." U.S. Patent Application 12/309,127, filed December 17, 2009
- [72] Jungheinrich AG, Lift truck with a movably arranged lift mast, European patent EP 0427001A1
- [73] Rainer Dr Ing Bruns, Friedrich Wilhelm Dipl I Groll, Fork lift truck for tall stacking ,European Patent DE4019075A1
- [74] Jungheinrich AG, mast vibration, European patent DE3617026C2
- [75] Larry Dean Friesen, Richard James Johannson, lift truck mast stabilizer patent registered US4082199A
- [76] Granta Design Limited, *CES EduPack software*, Cambridge: Granta Design Limited, 2009.

[77]Saginaw Valley State University, “Chapter 18 - Growth and Form,” [Online].

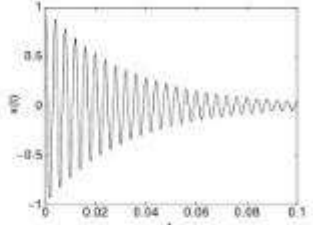
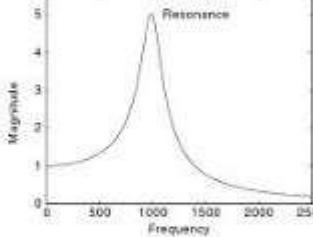
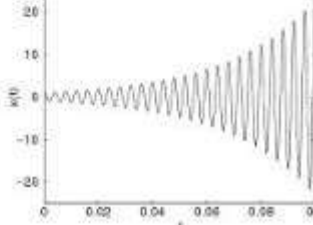
Available: <http://www8.svsu.edu/~nccolwel/125/class%20notes/Chap%2018.htm>.

[78]M. Mojahedi and M. H, “NONLINEAR FREE VIBRATION OF SIMPLY SUPPORTED BEAMS CONSIDERING THE EFFECTS OF SHEAR DEFORMATION AND ROTARY INERTIA, A HOMOTOPY PERTURBATION APPROACH,” *International Journal of Modern Physics B*, vol. 25, no. 3, pp. 441-455, 2011.

[79]Acroname Robotics, “Description of Pulse Width Modulation,” Acroname Inc, Boulder, 2007

Appendices

1) Different type of vibration

Vibration class	Excitation	Frequency of resulting motion	Characteristic
Free vibration	Initial conditions	(Damped) natural frequency	
Forced vibration	Persistent, periodic external source	Frequency of the external source	
Self-excited vibration	Persistent, steady external source	Self-selected and usually close to the natural frequency	

2) CESAB first two Cylinder design



3) Accelerometer calibration sheet



DJB Instruments
Vibration and dynamic pressure-measuring instruments.

DJB Instruments (UK) Ltd
Finchley Avenue, Mildenhall,
Suffolk IP28 7BG.

T: +44 (0) 1638 712288
F: +44 (0) 1638 717531
E: info@djbstruments.com
W: www.djbstruments.com

Accelerometer Calibration Sheet

THIS CALIBRATION IS TRACEABLE TO NATIONAL STANDARDS

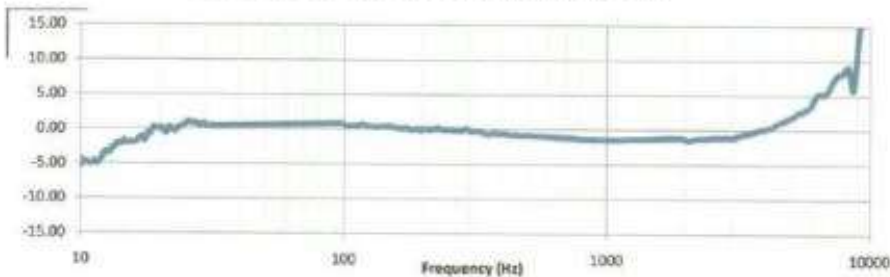
Type:	A/120/N-14
Serial No:	5402
Direction:	Uniaxial

Date:	10/08/2011
Tested by:	Debbie
Job No:	20535

Vibration		Accelerometer	
Level (g)	Freq (Hz)	Sensitivity (mV/g)	Deviation (%)
1	10	230.68	-5.4
1	20	243.80	0.1
10	40	247.19	0.6
10	60	248.32	0.7
10	80	249.33	0.8
10	100	249.92	0.7
10	200	249.56	0.1
10	400	249.67	-0.6
10	600	249.99	-1.0
10	800	249.96	-1.4

Vibration		Accelerometer	
Level (g)	Freq (Hz)	Sensitivity (mV/g)	Deviation (%)
10	1000	250.38	-1.4
10	2000	250.40	-1.4
10	3000	250.99	-1.1
10	4000	251.48	0.1
10	5000	252.81	1.8
10	6000	253.47	3.5
10	7000	252.79	5.9
10	8000	251.77	8.5
10	9000	255.67	11.6
10	10000	262.95	18.0

Measurements were made in ambient conditions of 22°C ± 3°C



Voltage Sensitivity @ 200Hz (mV/g)	249.56
Capacitance (pF)	
Insulation Resistance (Ω)	
Polar Cross-Axis @ 100Hz (max %)	5
Cable length (m)	

Reference Accelerometer Data	
Calibration Certificate No:	1.0261060002
A/20/N Serial No:	9817
Charge Sensitivity @ 200Hz (pC/g)	29.80

Temperature	± 2°C
Measurement Uncertainty	± 3%
Confidence Probability	95%

The test results refer to measurements made at the time of the test.
This certificate may not be reproduced other than in full.
This test does not demonstrate the instrument's ability to maintain calibration.

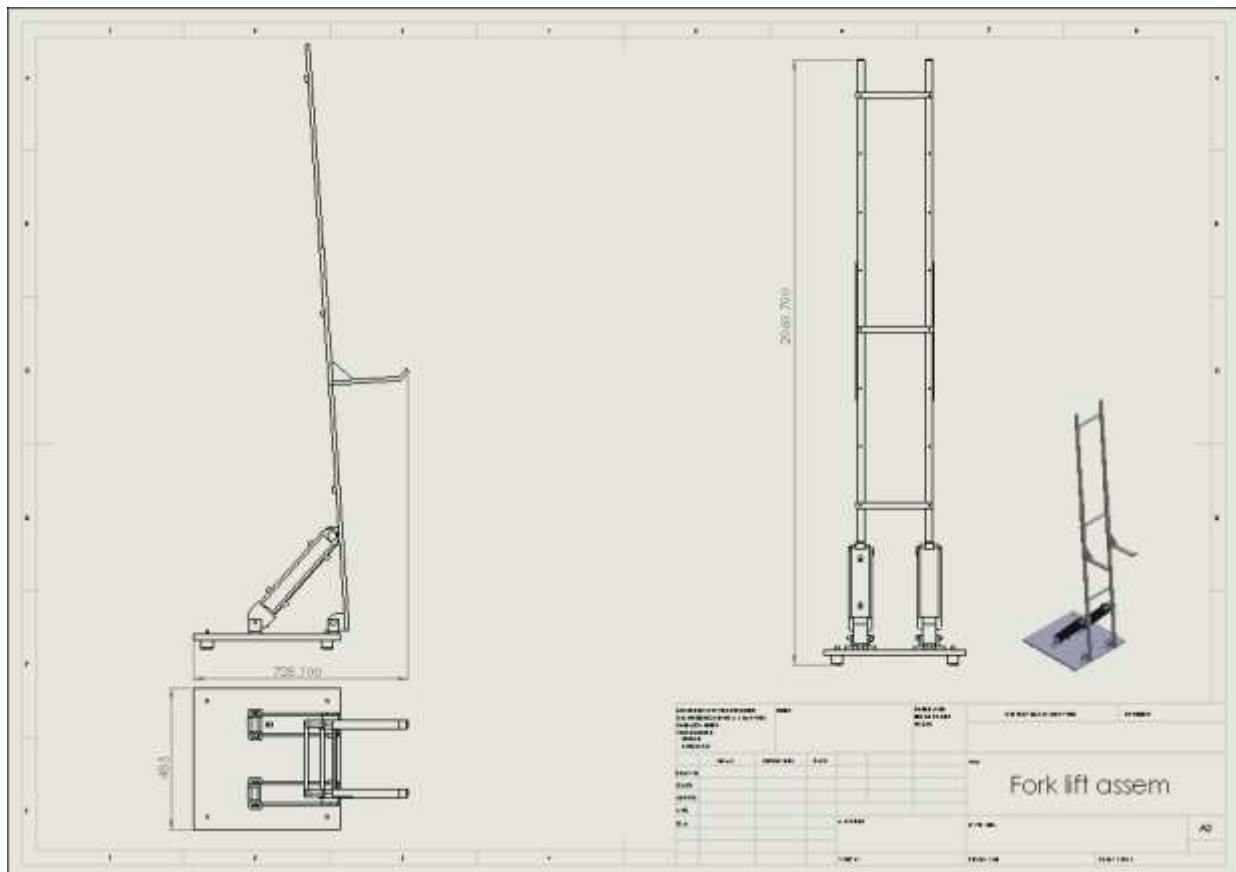
4)The centroid of mast and forklift details

Fork	mass [kg]	m1	1.758
	Centre point [m]	x1	0.255
	Centre point [m]	y1	1.8
Mast	Mass [kg]	m2	5.035
	Centre point [m]	x2	0.025
	Centre point [m]	y2	1.5
		Total mass	6.793
Centroid		x-bar	0.08452
		y-bar	1.57764

5)Fork and mast inertia

	Mass [Kg]	Moment of Inertia at centre [Kg/m ²]	moment of inertia about lug (pivot) point [Kg/m ²]
Fork	1.758	0.0078	105.28
Mast	5.035	1.678	
Total	≈ 6.79		

6)Optimised Design 2D Technical Drawing



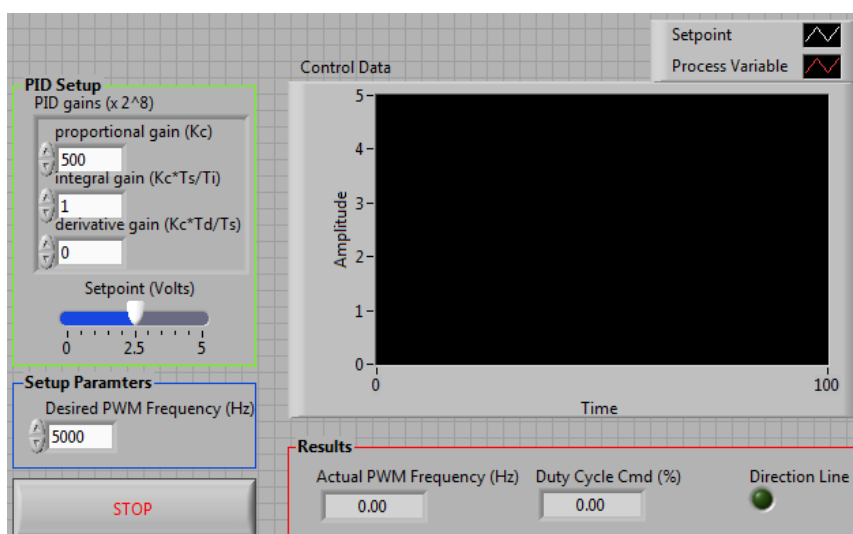
7) Hose Specification

Part Number	301SN-4
Hose Internal Diameter	¼ inch or 6.3 mm
Hose External Diameter	15 mm
Maximum Dynamic Pressure	40 MPa
Minimum Burst Pressure	160 MPa
Minimum Bend Radius	100 mm
Weight	0.39 kg/m
Temperature Range	-40°C up to 85°C

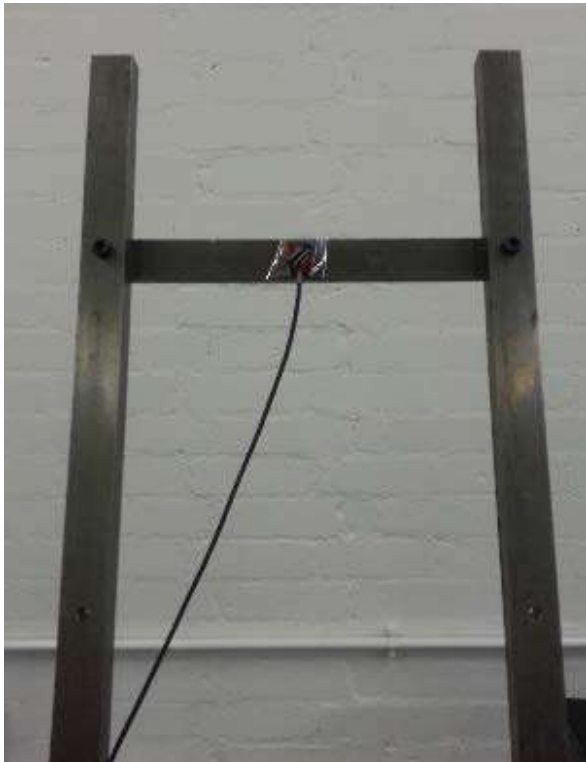
8) Hydraulic Connectors and Fittings



9) Project VI used to control Solenoid Valves and attain Accelerometer readings



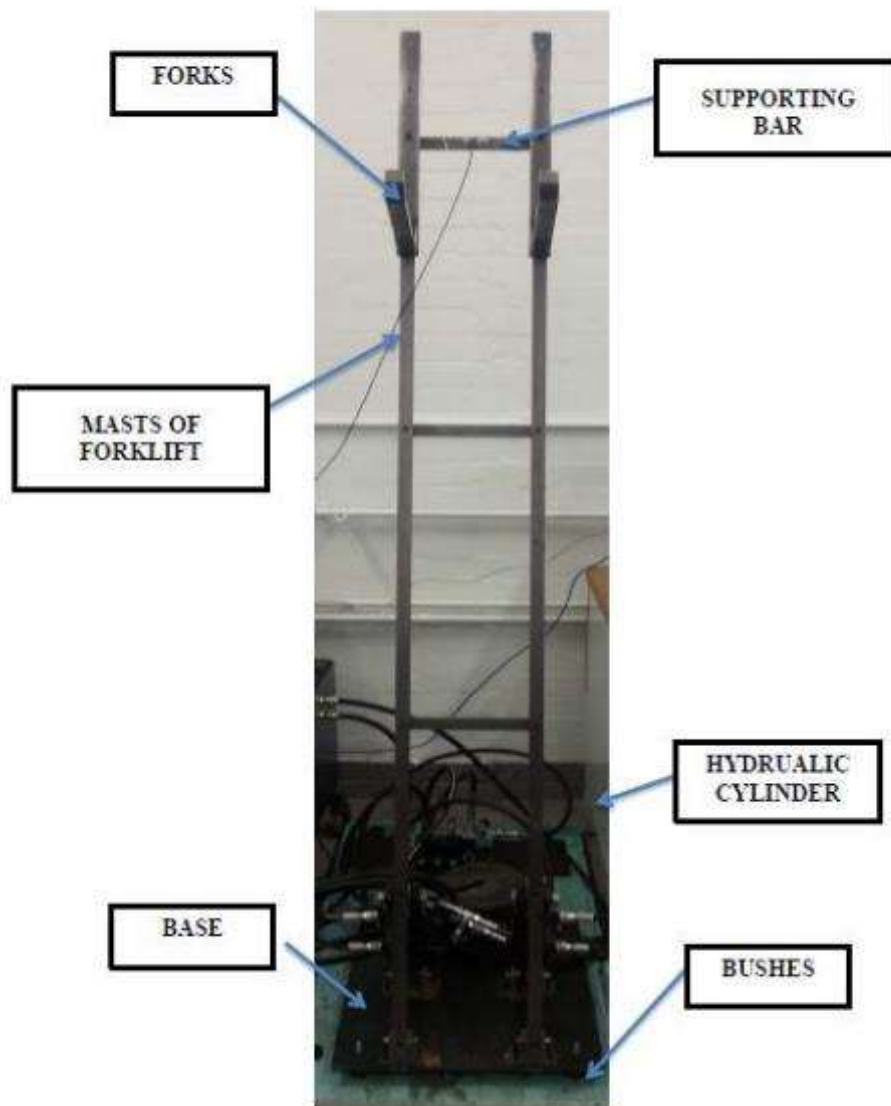
10) Illustration of the accelerometer connected to the rig



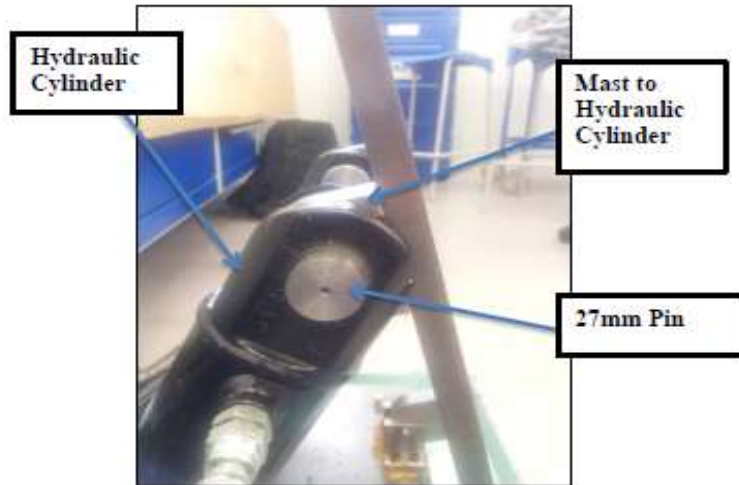
11) Loaded Mast



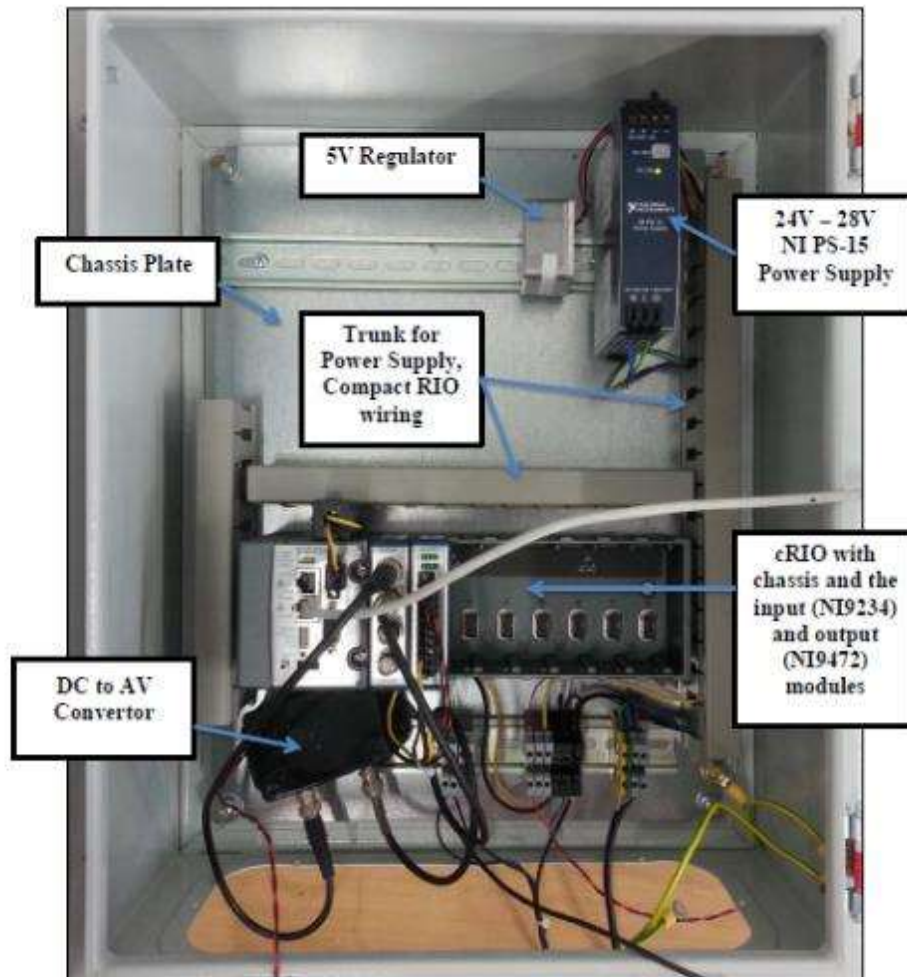
12) Assembly of tested forklift



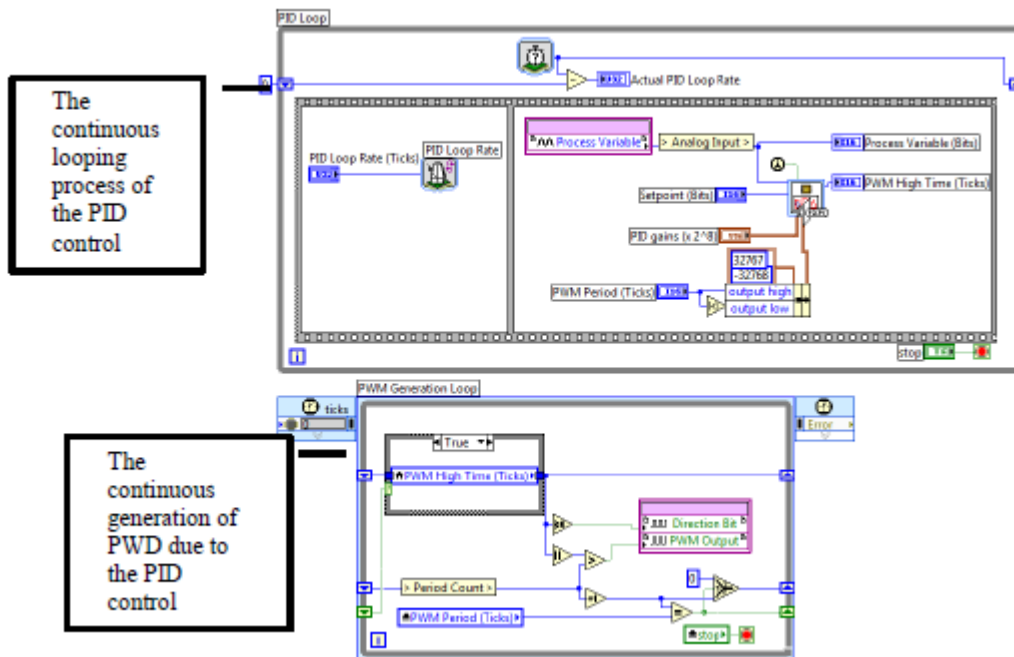
13) Hydraulic cylinder Pivot connecting to the Mast



14) Safety Cabinet for NI Equipment



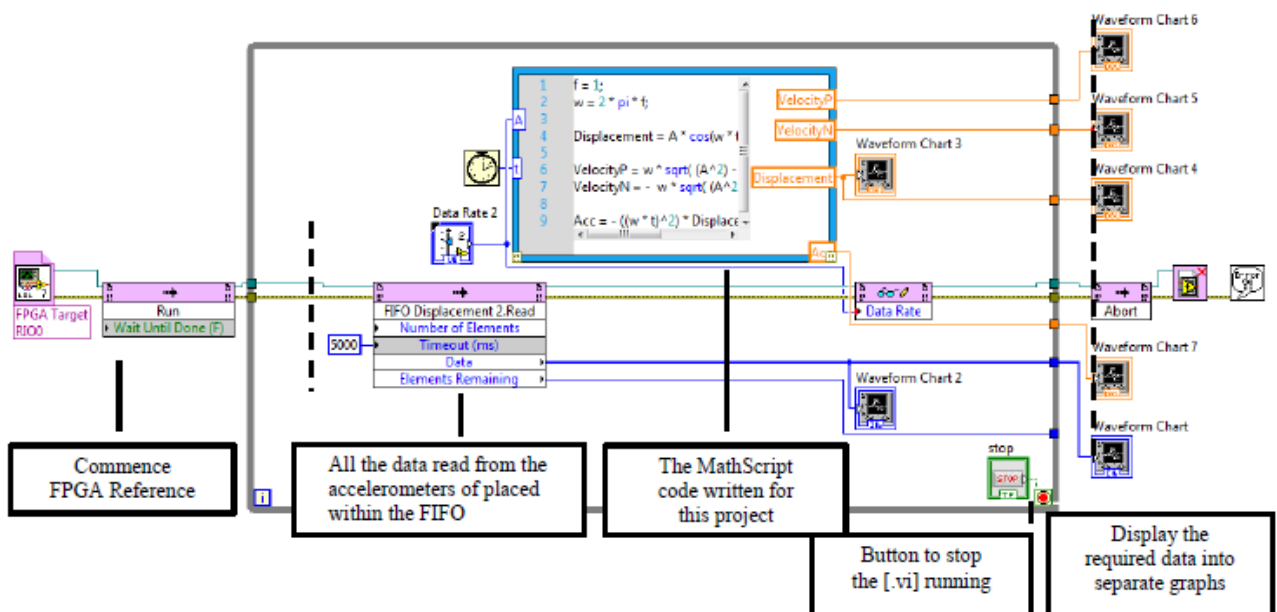
15) LabVIEW Output VI



The continuous looping process of the PID control

The continuous generation of PWD due to the PID control

16) LabVIEW Input VI



Hydraulic Dimensions / Specifications

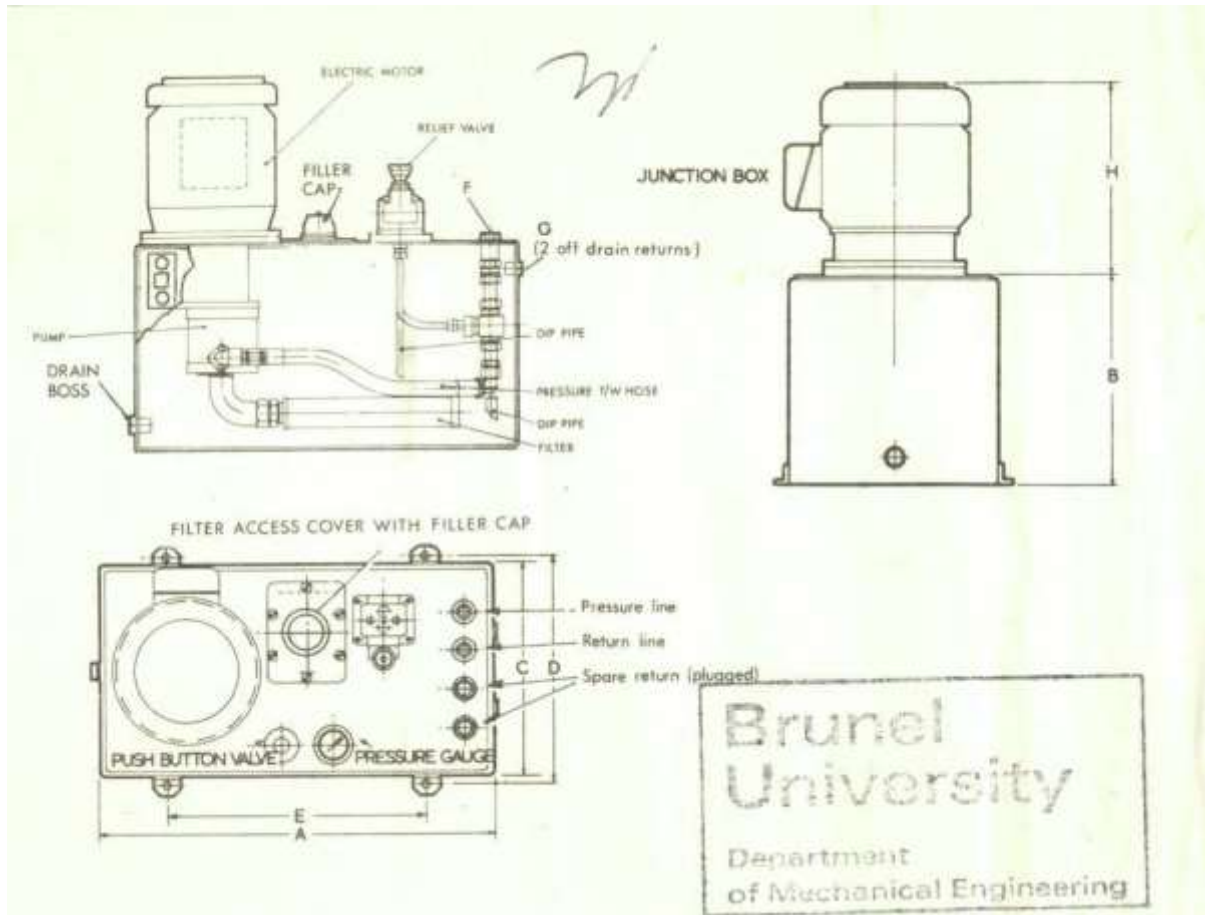
- Vertical ram will be lifting approx. 100KG + 10/15kg (weight of the fork itself so total of approx.120kg.)
- Maximum lifting speed will be 0.40m/sec with load.
- Maximum lifting speed will be 0.63m/sec without load.
- The horizontal two rams will be tilting the similar weight forwards and backwards.
- The speed will vary but the maximum 0.7 m/sec but will need to be controlled so we can vary it.
- Approximate duty cycle: We'll be working on it a few hours a day. 3/4 days a week.
- The horizontal stroke length does not need to be higher than 50cm.

Rams	Bore (mm)	Rod (mm)	Cylinder OD (mm)
1 x Vertical	40	25	50
2 x Horizontal	25	16	35

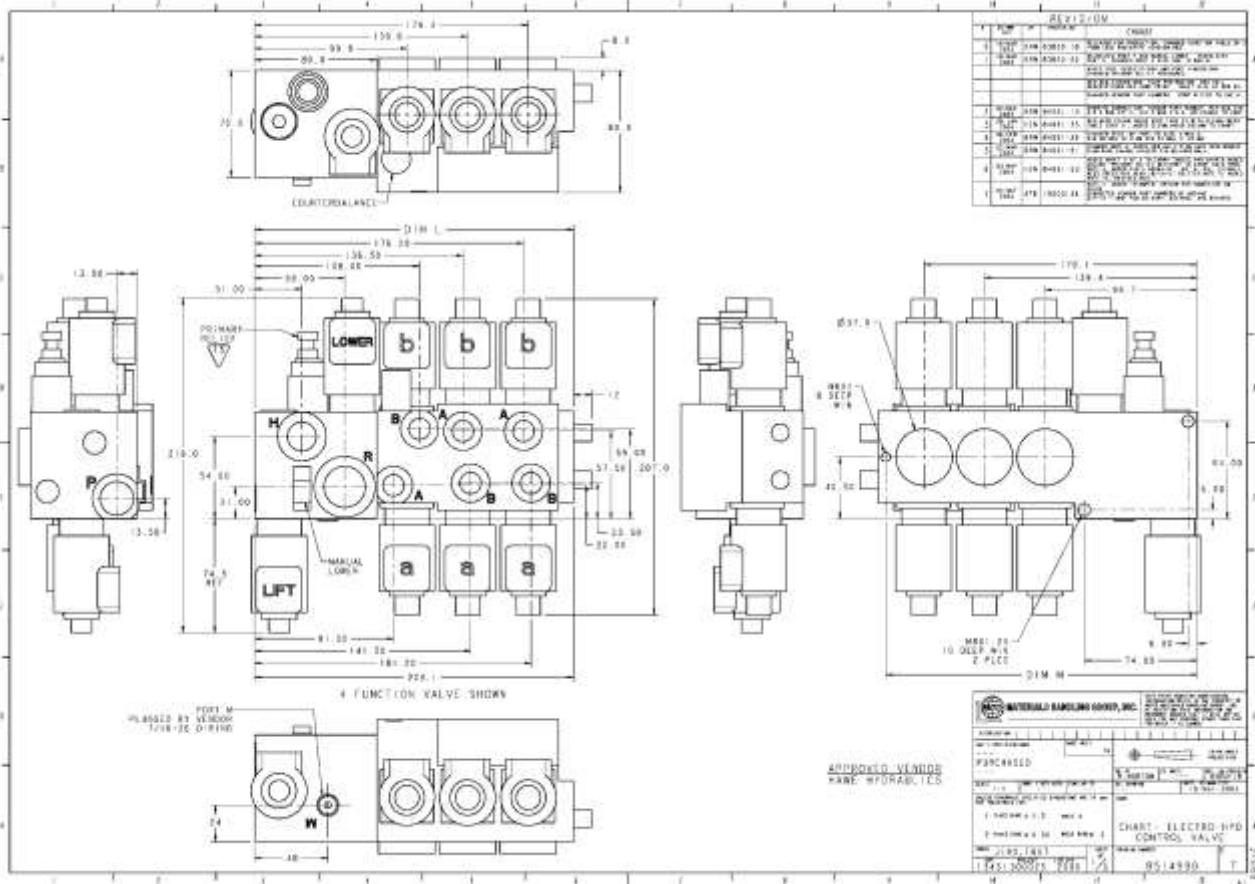
17) Overall Scale down Dimension of the Forklift Rig

Original Dimensions		Scaled Dimensions scale factor 4	
Height of Mast mm	2192	648.75	
Overall length of Mast mm	3960	1636.5	
Overall length of Truck mm	3321	830.25	
Seat Height mm	1007	251.75	
Overall width of truck mm	1173	293.25	
Fork Dimensions : Thickness mm	40	10	
Width mm	100	25	
Length mm	1000	250	
Free Lift/Moving mm	100	25	
Ground Clearance at Mast mm	98	24.5	
Ground Clearance mm	137	34.25	
Unladen Weight of Forklift kg	4465	67.65625	
Weight of Forks kg	1.825	0.45625	
Load capacity kg	2200	34.375	

18)Hydraulic Power Unit Schematic



19) Electro-Hydraulic Control Valve Schematic



20) Tilt Cylinder Schematic

